

PREPARATION OF GOLD DECORATED COBALT-SILICA CORE-SHELL  
NANOPARTICLES FOR SURFACE ENHANCED RAMAN SCATTERING  
APPLICATIONS

A THESIS SUBMITTED TO  
THE GRADUATE SCHOOL OF NATURAL AND APPLIED SCIENCES  
OF  
MIDDLE EAST TECHNICAL UNIVERSITY

BY

LÜTFİYE SEZEN KESER

IN PARTIAL FULFILLMENT OF THE REQUIREMENTS  
FOR  
THE DEGREE OF MASTER OF SCIENCE  
IN  
CHEMISTRY

SEPTEMBER 2010

Approval of the Thesis;

**PREPARATION OF GOLD DECORATED COBALT-SILICA CORE-SHELL  
NANOPARTICLES FOR SURFACE ENHANCED RAMAN SCATTERING  
APPLICATIONS**

submitted by **LÜTFİYE SEZEN KESER** in a partial fulfillment of the requirements  
for the degree of **Master of Science in Chemistry Department, Middle East  
Technical University** by

Prof. Dr. Canan Özgen  
Dean, Graduate School of **Natural and Applied Sciences** \_\_\_\_\_

Prof. Dr. İlker Özkan  
Head of Department, **Chemistry** \_\_\_\_\_

Prof. Dr. Mürvet Volkan  
Supervisor, **Chemistry Department, METU** \_\_\_\_\_

**Examining Committee Members:**

Prof. Dr. O. Yavuz Ataman  
Department of Chemistry, METU \_\_\_\_\_

Prof. Dr. Mürvet Volkan  
Department of Chemistry, METU \_\_\_\_\_

Prof. Dr. Macit Özenbaş  
Department of Metallurgical and Materials Eng, METU \_\_\_\_\_

Prof. Dr. Ceyhan Kayran  
Department of Chemistry, METU \_\_\_\_\_

Prof. Dr. Necati Özkan  
Department of Polymer Science and Techn, METU \_\_\_\_\_

Date: 16.09.2010

**I hereby declare that all information in this document has been obtained and presented in accordance with academic rules and ethical conduct. I also declare that, as required by these rules and conduct, I have fully cited and referenced all material and results that are not original to this work.**

Name, Last name: Lütfiye Sezen KESER

Signature

## **ABSTRACT**

### **PREPARATION OF GOLD DECORATED COBALT-SILICA CORE-SHELL NANOPARTICLES FOR SURFACE ENHANCED RAMAN SCATTERING APPLICATIONS**

Keser, Lütfiye Sezen

M.Sc., Department of Chemistry  
Supervisor: Prof. Dr. Mürvet Volkan

September 2010, 84 pages

Bringing together several materials into a single nanoparticle is an attractive way to design systems that exhibit diverse physical and chemical properties. Cobalt nanoparticles are extensively used in magnetic separation, ferrofluids, and magnetic storage media. The deposition of gold nanoparticles onto cobalt core significantly affects their optical properties due to the introduction of surface Plasmon.

Here the synthesis of gold nanoparticles decorated cobalt-silica nanoparticles are reported for the first time. Their optical and magnetic properties and capacity as a surface enhanced Raman scattering (SERS) substrate were investigated. This nano-material is of particular interest as a dual agent allowing both magnetic separation and SERS detection. The synthesis involves three steps: i) synthesis of Co nanoparticles; ii) deposition of a silica shell around the Co core and introduction of amine functional groups on the surface; iii) decoration of the surface with gold nanoparticles.

Co nanoparticles were prepared in an inert atmosphere in the presence of capping and reducing agents. Size of the cobalt nanoparticles was varied by changing the

concentration of the capping agent. Since cobalt particles are easily oxidized, they were coated with silica shell both to prevent oxidation and allow further functionalization. Silica coating of the particles were performed in water/ethanolic solution of tetraethyl orthosilicate (TEOS). Thickness of silica coating was controlled by varying the concentrations of TEOS. Besides, by adding 3-aminopropyl-triethoxysilane (APTS) to the reaction medium, primarily amine groups were introduced on the silica surface. For further modifications citrate stabilized gold nanoparticles were appended onto the surface of amine modified core-shell cobalt-silica nanoparticles. Gold decorated magnetic core-shell structures were used as SERS substrate with Raman dyes; brilliant cresyl blue (BCB) and rhodamine 6G (R6G). They were also utilized for preconcentration and SERS detection of 4-mercapto benzoic acid (4-MBA). Gold nanoparticles on the silica and thiol group on the 4-MBA were very selective to each other, thus, 4-MBA could be attached on to gold surface and it could be easily separated magnetically from the reaction medium and identified by Raman spectroscopy.

Characterization of the cobalt, cobalt-silica and gold modified cobalt-silica nanoparticles was done by Field Emission Scanning Electron Microscopy (FE-SEM), Scanning-Transmission Electron Microscopy (S-TEM), Energy-Dispersive X-ray Spectroscopy (EDX), UV-Vis spectrometry, and Raman microscope system.

**Keywords:** Magnetic nanoparticles, core-shell nanoparticles, silica coating, surface modification, magnetic separation, SERS

## ÖZ

### **YÜZEYDE GÜÇLENDİRİLMİŞ RAMAN SAÇILMASI UYGULAMALARI İÇİN ALTINLA BEZENMİŞ KOBALT-SİLİKA ÇEKİRDEK-KABUK NANOPARÇACIKLARIN HAZIRLANMASI**

Keser, Lütfiye Sezen

Yüksek Lisans, Kimya Bölümü

Tez Yöneticisi: Prof. Dr. Mürvet Volkan

Eylül 2010, 84 sayfa

Birden fazla malzemeyi tek bir nano parçacıkta bir araya getirmek, çeşitli fiziksel ve kimyasal özellikler gösteren sistemler tasarlamak için ilgi çekici bir yoldur. Kobalt nanoparçacıklar yaygın olarak manyetik ayırmada, ferro-akışkanlarda ve manyetik saklama alanlarında kullanılmaktadır. Altın nanoparçacıkların kobalt çekirdeği üzerinde birikimi yüzey plasmonlarının varlığı yüzünden parçacıkların optik özelliklerini önemli bir şekilde etkilemektedir.

Burada yüzeyine altın nanoparçacık tutturulmuş kobalt-silika çekirdek-kabuk nano yapıların sentezi ilk kez rapor edilmektedir. Optik ve manyetik özellikleri ile yüzeyde güçlendirilmiş Raman saçılımı (YGRS) yüzey kapasitesi araştırılmıştır. Bu nano malzeme hem manyetik ayırmaya hem de YGRS tespitine izin verdiği için dikkate değer bir ilgiye sahiptirler. Buradaki sentez üç basamağı içerir: i) Kobalt nanoparçacıkların sentezi; ii) Kobalt çekirdeği etrafında silika kabuk birikimi ve yüzeye amin fonksiyonel grubunun eklenmesi; iii) yüzeyine altın nanoparçacıkların tutturulması.

Kobalt nanoparçacıklar durağan ortamda indirgen ve sınırlandırıcı maddelerin varlığında hazırlanmıştır. Parçacıkların boyutu sınırlandırıcı maddelerin derişimi

değiştirilerek belirlenmiştir. Metal parçacıkların hava-hassasiyeti olduğundan parçacıklar hem yükseltgenmeyi engellemek hem de yüzeyi işlevsel hale getirmek için silica kabuk yapısıyla kaplanmıştır. Parçacıkların silika kaplaması su/etanol karışımında tetraetilortosilikat (TEOS) eklenmesiyle gerçekleştirilmiştir. Silika kaplamanın kalınlığı TEOS derişimindeki deęişiklikle belirlenmiştir.

Silika yüzeyini altın nano parçacık ile modifiye etmek için öncelikle 3-aminopropil-trietoksisilan (APTS) katılarak silika yüzeyine amin gruplarının tutunması sağlanmıştır. Daha fazla deęişiklik için sitrarla dengelenmiş altın nanoparçacıklar aminle yüzeyi deęiştirilmiş kobalt-silika nanoparçacıklara tutturulmuştur. Altın ile modifiye edilmiş manyetik çekirdek-kabuk yapıları parlak kresil mavisi (PKM) ve rodamin 6G (R6G) boyları ile YGRS substratı olarak kullanılmıştır. Ayrıca, bunlar 4-merkaptobenzoik asit (4-MBA) molekülü ile manyetik ayırma yönteminde kullanılmıştır. Altın parçacıklar tiol gruplarına karşı seçici davrandığından, 4-MBA altın yüzeyle etkileşime girmiş ve manyetik alan uygulayarak kolayca reaksiyon ortamından ayrılıp Raman spektrometriyle belirlenmiştir.

Sentezlenen kobalt, kobalt-silika ve altınla modifiye edilmiş kobalt-silika nano parçacıklarının karakterizasyonu Alan Emisyonlu Taramalı Alan Mikroskobu (AE-TEM), Taramalı-Geçirgen Elektron mikroskobu (T-GEM), Enerji Dağılımlı X-ışını spektrometre, (EDX), UV-Visible spektrometri ve Raman mikroskop sistemi kullanılarak yapılmıştır.

**Anahtar Kelimeler:** Manyetik nanoparçacıklar, çekirdek-kabuk nanoparçacıklar, silika kaplama, yüzey modifikasyonu, manyetik ayırma, YGRS

*To my parents and grandmother*

## ACKNOWLEDGEMENTS

I would like to express my sincere thanks to my supervisor Prof. Dr. Mürvet Volkan for her guidance, supports and encouragement.

I am deeply grateful to Murat Kaya for his endless help and trust. Whenever I need he is always there. I have learned lots of things from him.

I would like to thank all C-50 members; Gülfem Aygar, Recep Yüksel, Üzeyir Doğan, Taci Öztürk , Seher Karabıçak, Dilek Ünal, Tuğbanur Alp, Zehra Tatlıcı, Ümit Zengin, Seda Kibar for their help, support and friendship.

I should also thank Ataman's research group for their friendship, support and help.

I would like to thank to my big big home, dear home-mates and my friends; A.Şenay Dincer, Esra Debrelı, Emine Vardar, Erkan Koç. Whenever we are together, we are happier than before and every day we remembered with Şenay, "Chemistry Teacher can do everything".

Thanks God to give me a chance to be a daughter of Hayriye & Recai Keser. They are always with me. Thank you for life, patience, trust, and love.

I am very grateful to the day I met Emrah Yıldırım. *I know that he is always with me and never leaves me alone.* Thank you for your endless love, support, trust and patience.

Finally, my dear Grandmother, *Lütfiye*, I am deeply grateful to her. She not only gave me her name but also brought me up, gave endless love and I have a lot of memories with her. I miss you so much...

## TABLE OF CONTENTS

ABSTRACT .....	IV
ÖZ .....	VI
ACKNOWLEDGEMENTS .....	IX
TABLE OF CONTENTS .....	X
LIST OF TABLES .....	XIII
LIST OF FIGURES .....	XIV
CHAPTERS.....	1
1. INTRODUCTION.....	1
1.1 Nanoparticles .....	1
1.2 Magnetic Nanoparticles.....	2
1.2.1 Magnetic Parameters .....	3
1.2.2 Synthesis of Magnetic Nanoparticles .....	8
1.2.2.1 Synthesis of Magnetic Nanoparticles via Precipitation .....	10
1.2.2.2 Synthesis of Magnetic Nanoparticles via Hydride Reduction .....	11
1.3 Surface Modification of Magnetic Nanoparticles.....	11
1.3.1 Characterization Techniques of Magnetic Nanoparticles.....	12
1.4 Applications of Magnetic Nanoparticles.....	14
1.5 Raman Spectrometry.....	15
1.5.1 Principles of Raman Spectroscopy.....	15
1.5.2 Instrumentation of Raman Spectroscopy.....	17
1.5.3 Surface Enhanced Raman Spectrometry .....	19
1.6 Aim of This Study.....	19
2. EXPERIMENTAL .....	21
2.1 Materials .....	21
2.2 Instrumentation .....	21
2.3 Synthesis of Cobalt Nanoparticles .....	22
2.4 Synthesis of Silica Coated Cobalt Nanoparticles.....	23

2.5	Amine Functionalization of Cobalt-Silica Core-Shell Nanoparticles.....	24
2.6	Gold Nanoparticles.....	25
2.7	Gold Seeding on Amine Modified Core-Shell Nanoparticles. ....	25
2.8	Surface Enhanced Raman Scattering (SERS) Studies .....	25
2.9	Magnetic Collection and Identification Studies.....	26
3.	RESULTS AND DISCUSSION.....	28
3.1	Synthesis of Cobalt-Silica Core-Shell Nanoparticles .....	29
3.1.1	Cobalt Nanoparticle Synthesis .....	29
3.1.1.1	Effect of Citric Acid Concentration on Particle Size.....	31
3.1.2	Preparation of Silica Coated Cobalt Nanoparticles.....	33
3.1.2.1	Washing Optimization of Silica Coated Cobalt Nanoparticles .....	45
3.2	Addition of Amine Functional Groups on Silica Coated Cobalt Nanoparticles.....	48
3.3	Gold Deposition on Amine Modified Cobalt-Silica Nanoparticles.....	49
3.3.1	Preparation of Gold Nanoparticles .....	49
3.3.2	Preparation of Gold Modified Cobalt-Silica Nanoparticles .....	51
3.3.3	Optical Properties of Gold Nanoparticles Decorated Cobalt-Silica Core-Shell Nanoparticles .....	53
3.3.3.1	Effect of Au/Cobalt-Silica Volume Ratio on the Gold Decoration of Cobalt-Silica Nanoparticles .....	55
3.3.3.1.1	Gold Decoration of the Amine Coated Cobalt-Silica Particles at Low APTS/TEOS Volume Ratio .....	56
3.1.1.1.1	Gold Decoration of the Amine Coated Cobalt-Silica Particles at High APTS/TEOS Volume Ratio .....	60
3.2	Magnetic Behavior of the Prepared Particles .....	64
3.2.1	Magnetic Behavior of Cobalt Nanoparticles.....	64
3.2.2	Magnetic Behavior of Cobalt-Silica Nanoparticles.....	65
3.2.3	Magnetic Behavior of Gold Modified Cobalt-Silica Nanocomposites .....	67
3.3	Application of Gold Modified Cobalt-Silica as SERS Substrate .....	68
3.3.1	SERS Effect of Au Modified Cobalt-Silica Nanoparticles.....	69
3.3.2	The Performance of the Gold Modified Cobalt-Silica Nanoparticles both as a Magnetic Separator and SERS Substrate for the Preconcentration and the Detection of 4-MBA .....	73

CONCLUSION .....76

## LIST OF TABLES

### TABLES

<b>Table 1</b> Laser Sources for Raman System.....	18
<b>Table 2</b> Particle size distribution of Co nanoparticles as a function of citrate/Co <sup>2+</sup> molar ratio. ....	31
<b>Table 3</b> Concentration of reagents used in core-shell cobalt-silica nanoparticle synthesis in case of citrate/Co <sup>2+</sup> was 10 <sup>-2</sup> .....	35
<b>Table 4</b> Effect of TEOS/Co <sup>2+</sup> on shell thickness of the particles mentioned in Table 3. ....	35
<b>Table 5</b> The concentration of reagents used in the silica coating of cobalt nanoparticles. Citrate/Co <sup>2+</sup> molar ratio was 10 <sup>-3</sup> . ....	39
<b>Table 6</b> Effect of TEOS/Co <sup>2+</sup> on shell thickness of the particles mentioned in Table 5. ....	39
<b>Table 7</b> Concentration of reagents used in silica coating process. Citrate/Co <sup>2+</sup> molar ratio was 10 <sup>-3</sup> .....	41
<b>Table 8</b> Effect of [TEOS]/[Co <sup>2+</sup> ] on shell thickness of the particles mentioned in Table 7.....	41
<b>Table 9</b> Washing procedures of cobalt-silica nanoparticles. ....	45
<b>Table 10</b> Concentrations of reagents used in the preparation of the particles for the optimization of washing procedure.....	46
<b>Table 11</b> Change in APTS/TEOS volume ratio during silica and amine coating on the surface of cobalt-silica nanoparticles. ....	56

## LIST OF FIGURES

### FIGURES

<b>Figure 1</b> Nano-science is the study of matter at the dimension of 1-1000 nm (The University of Texas at Austin, 2008).....	1
<b>Figure 2</b> Magnetic state of elements in periodic table (Splung.com, 2010).....	3
<b>Figure 3</b> Representation of ferromagnetic behavior of electrons. ....	4
<b>Figure 4</b> Representation of Ferrimagnetic behaviour of a material. ....	5
<b>Figure 5</b> Representation of Anti-ferromagnetic behaviour of a material. ....	5
<b>Figure 6</b> Representation of paramagnetic behavior. ....	6
<b>Figure 7</b> General appearance of hysteresis loops.....	7
<b>Figure 8</b> Hysteresis loops of hard and soft ferromagnetic materials. ....	8
<b>Figure 9</b> Two concepts for the synthesis of nanoparticles; "top-down" and "bottom-up" approaches which refer to physical and chemical methods respectively (Hyeon, 2003) . ....	9
<b>Figure 10</b> Schematic diagram showing chemical synthesis techniques for magnetic nanoparticles in two different media; organic and aqueous.....	10
<b>Figure 11</b> Representation of Scanning Electron Microscope.....	13
<b>Figure 12</b> Schematic representation of VSM. ....	14
<b>Figure 13</b> Application of magnetic nanoparticles in various fields. ....	15
<b>Figure 14</b> Representation of elastic and inelastic scatterings: Stoke-Raman and Anti-stoke Raman Scattering.....	16
<b>Figure 15</b> Block diagram of Raman spectroscopy.....	17
<b>Figure 16</b> (a) Deoxygenation of citric acid added deionized water and (b) freshly prepared cobalt nanoparticles under N <sub>2</sub> atmosphere. ....	23
<b>Figure 17</b> The photograph of cobalt-silica nanoparticles' solution (After addition of TEOS/EtOH mixture). ....	24

<b>Figure 18</b> Preparation of sample for SERS measurements (a) Substrate: gold modified cobalt-silica nanocomposites, (b) mixture of Raman dye with gold modified cobalt-silica nanocomposites, (c) a drop of SERS substrate on glass slide. ....	26
<b>Figure 19</b> Steps of magnetic separation and identification with SERS technique. ...	27
<b>Figure 20</b> FE-SEM images of citrate stabilized Co nanoparticles having size range $46 \pm 4$ nm. ....	30
<b>Figure 21</b> EDX spectrum of Cobalt nanoparticles. ....	30
<b>Figure 22</b> FE-SEM images of citrate stabilized Co nanoparticles. Citrate/ $\text{Co}^{2+}$ molar ratio was $10^{-4}$ . Mean particle diameter was measured as $46 \pm 4$ nm. ....	32
<b>Figure 23</b> FE-SEM images of citrate stabilized Co nanoparticles. Citrate/ $\text{Co}^{2+}$ molar ratio was $10^{-2}$ . Mean particle diameter was measured as $34 \pm 4$ nm. ....	32
<b>Figure 24</b> FE-SEM images of citrate stabilized Co nanoparticles. Citrate/ $\text{Co}^{2+}$ molar ratio was $10^{-1}$ . Mean particle diameter was measured as $7 \pm 2$ nm. ....	33
<b>Figure 25</b> Schematic representation of cobalt- silica core-shell formation. ....	34
<b>Figure 26</b> FE-SEM images of the cobalt-silica core- shell particles, specified in Table 3, having $[\text{TEOS}]/[\text{Co}^{2+}]$ ratio (a) 5; (b) 10; (c) 20. ....	36
<b>Figure 27</b> EDX patterns of the cobalt-silica core- shell particles, specified in Table 5, having $[\text{TEOS}]/[\text{Co}^{2+}]$ ratio (a) 5; (b) 10; (c) 20. ....	38
<b>Figure 28</b> FE-SEM images of the cobalt-silica core- shell particles, specified in Table 5 having $[\text{TEOS}]/[\text{Co}^{2+}]$ ratio (a) 5; (b) 10; (c) 20. ....	40
<b>Figure 29</b> S-TEM images of the cobalt-silica core- shell particles, specified in Table 7, having $[\text{TEOS}]/[\text{Co}^{2+}]$ ratio (a) 5; (b) 10; (c) 20. ....	42
<b>Figure 30</b> FE-SEM images of core-shell cobalt-silica nanoparticles in case of $\text{TEOS}/\text{Co}^{2+}$ : 10 with different citrate/ $\text{Co}^{2+}$ in which (a) $10^{-2}$ , (b) $10^{-3}$ and (c) $10^{-5}$ . ....	44
<b>Figure 31</b> Washing procedures for cobalt-silica preparation: (a) Procedure 1 (3 washing steps) (b) Procedure 2 (5 washing steps) (c) Procedure 3 (11 washing steps). ....	47
<b>Figure 32</b> Water dispersed and dried core-shell cobalt-silica nanoparticles. ....	48
<b>Figure 33</b> Amine modification of core-shell cobalt-silica core-shell nanoparticles. ....	49
<b>Figure 34</b> UV-vis spectrum of Au nanoparticles. ....	50
<b>Figure 35</b> FE-SEM images of Au nanoparticles. ....	51
<b>Figure 36</b> EDX pattern of Au nanoparticles. ....	51

<b>Figure 37</b> A typical synthesis procedure of gold modified cobalt-silica nanocomposites. ....	52
<b>Figure 38</b> FE-SEM images of gold modified cobalt-silica nanocomposite. ....	52
<b>Figure 39</b> EDX spectrum of gold modified cobalt-silica nanocomposite. ....	53
<b>Figure 40</b> UV-Vis spectra of Au modified cobalt-silica nanocomposites, Au and Co colloids dispersed in distilled water. The insets show the photograph of the samples. ....	54
<b>Figure 41</b> Effect of reaction time on Au decoration on cobalt-silica nanoparticles surface, duration in minutes; (a) 1, (b) 5, (c) 15,(d) 30, (e) 45, (f) 60 and (g) 120. ...	55
<b>Figure 42</b> UV-Vis spectra of gold modified cobalt-silica nanoparticles prepared at various Au / cobalt-silica volume ratio. APTS /TEOS volume ratio was 1/3 (low amine deposition) and Au / cobalt-silica volume ratio: (a) 0.1, (b) 0.25, (c) 0.5, (d) 1 and (e) 2.....	57
<b>Figure 43</b> FE-SEM images of gold modified cobalt-silica nanoparticles prepared at various Au/cobalt-silica volume ratio. APTS /TEOS volume ratio was 1/3 (low amine deposition) Au / cobalt-silica volume ratio: (a) 0.1, (b) 0.25, (c) 0.5, (d) 1 and .....	58
<b>Figure 44</b> Larger scale FE-SEM images of gold modified cobalt-silica nanoparticles prepared at Au / cobalt-silica volume ratio of 1and 2 . APTS /TEOS volume ratio was 1/3 (low amine deposition) Au / cobalt-silica volume ratio: (a) 1, (b) 2 .....	59
<b>Figure 45</b> UV-Vis spectra of gold modified cobalt-silica nanoparticles prepared at various Au / cobalt-silica volume ratio. APTS /TEOS volume ratio was 1 (high amine deposition) and Au / cobalt-silica volume ratio: (a) 0.1, (b) 0.25, (c) 0.5,(d) 1 and (e) 2.....	61
<b>Figure 46</b> FE-SEM images of gold modified cobalt-silica nanoparticles prepared at various Au / cobalt-silica volume ratio. APTS /TEOS volume ratio was 1 (High amine deposition) Au / cobalt-silica volume ratio: (a) 0.1, (b) 0.25, (c) 0.5, (d) 1 and .....	62
<b>Figure 47</b> Larger scale FE-SEM images of gold modified cobalt-silica nanoparticles prepared at Au / cobalt-silica volume ratio of 1and 2 . APTS /TEOS volume ratio was 1 (high amine deposition) Au / cobalt-silica volume ratio: (a) 1, (b) 2. ....	63

<b>Figure 48</b> The collection kinetic of Co nanoparticles under the influence of external magnetic field (1.6 T) at various time intervals (5, 10, 20 seconds). .....	64
<b>Figure 49</b> Hysteresis curve of cobalt nanoparticles recorded at 300 K. ....	65
<b>Figure 50</b> Cobalt-silica nanoparticles under external magnetic field. ....	66
<b>Figure 51</b> The hysteresis curve for cobalt-silica core-shell nanostructures. ....	67
<b>Figure 52</b> Magnetization behavior of Au modified cobalt-silica nanoparticles. ....	68
<b>Figure 53</b> Raman spectrum of solid BCB. Insert is the molecular formula of BCB. ....	69
<b>Figure 54</b> Raman spectrum of solid R6G. Insert is the molecular formula of R6G. ....	70
<b>Figure 55</b> Raman spectrum of solid 4-MBA. Insert is the molecular formula of 4-MBA. ....	71
<b>Figure 56</b> SERS spectrum of $10^{-5}$ M BCB acquired by using Au modified cobalt-silica colloid as a substrate. ....	72
<b>Figure 57</b> SERS spectrum of $10^{-4}$ M R6G acquired by using Au modified cobalt-silica colloid as a substrate. ....	72
<b>Figure 58</b> SERS spectrum of $10^{-4}$ M 4-MBA acquired by using Au modified cobalt-silica colloid as a substrate. ....	73
<b>Figure 59</b> Illustration of magnetic separation procedure for biological molecules (Pankhurst, Connolly, Jones, & Dobson, 2003) .....	74
<b>Figure 60</b> SERS spectrum of (a) $10^{-5}$ M 4-MBA 1-hour incubated with gold modified cobalt-silica and magnetically collected by an external magnet and (b) $10^{-4}$ M 4-MBA on Au modified cobalt-silica. ....	75

# CHAPTER 1

## INTRODUCTION

### 1.1 Nanoparticles

Nano-science is an art of “making, manipulating, and imaging” materials having very tiny dimensions from 1 to 100 nm (Ozin & Arsenault, 2009; Nagarajan, 2008). Nano-science has a great potential at variety of areas due to unique optical, mechanical, electrical, physical and chemical properties of nanoparticles (Nanoparticles and their Applications, 2007).

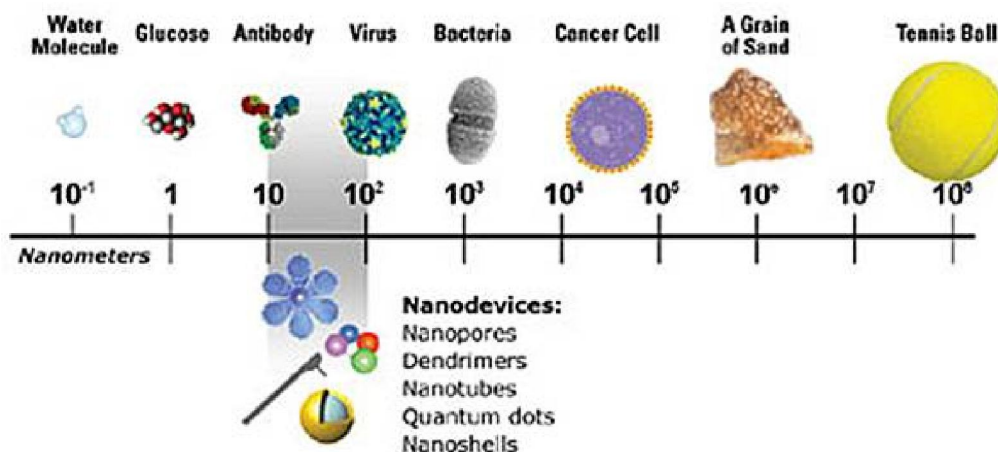


**Figure 1** Nano-science is the study of matter at the dimension of 1-100 nm (The University of Texas at Austin, 2008).

Nanoparticles are made of inorganic or organic materials, which have many novel properties compared with the bulk materials (Wu, He, & Jiang, 2008). Nanoparticles

are found in various chemical compositions such as metals (Chen, Sorensen, Klabunde, & Hadjipanayis, 1995), metal oxides (Sue, et al., 2006), semiconductors (Pickett & O'Brien, 2001), polymers (Bisht, et al., 2007), carbon materials (Harris, 1999), organics (Fu & Yao, 2001) or biological materials (Rozhkova, Ulasov, Lai, Dimitrijevic, Lesniak, & Rajh, 2009). Moreover, the particles can be found in different morphological shapes such as spheres, cylinders, disks, platelets, hollow spheres and tubes (Nagarajan, 2008).

## **1.2 Magnetic Nanoparticles**

Magnetic nanoparticles, also called as “smart particles”, constitute a very interesting class of nanoparticles (Safarik & Safarikova, 2009). They are very attractive for researchers because the particles have controllable size in the range of 1-100 nm which can be comparable with those of biologically important molecules such as virus, protein or gene (Tartaj, Morales, Gonzalez-Carreno, Veintemillas-Verdaguer, & Serna, 2005). In other words their sizes are close to the biologically important molecules, so they can interact with these molecules with proper surface modification. Moreover, the smart particles exhibit magnetic behavior that can be monitored and manipulated by an external magnetic field. In this way, they can be carried away or kept for intended job by the magnetic field (Pankhurst, Connolly, Jones, & Dobson, 2003).

In a specific way, magnetic nanoparticles are an important part of the nano-science, because they have many unique magnetic properties such as superparamagnetism, high coercivity, low Curie temperature, high magnetic susceptibility (Wu, He, & Jiang, 2008; Laurent, et al., 2008). In addition, they are of great interest for researchers from a broad range of disciplines, including magnetic fluids (Kima, Lee, Kwakb, & Kim, 2005), catalysis (An-Hui Lu, 2004), biotechnology/biomedicine (GuptaA. & Gupta, 200), magnetic resonance imaging (Li, Wei, Gao, & Lei, 2005), and data storage (Hyeon, 2003).

### 1.2.1 Magnetic Parameters

All materials are magnetic to some extent, with their response depending on their atomic structure and temperature (Pankhurst, Connolly, Jones, & Dobson, 2003). Magnetism originates from two motions of electrons in an atom. They are named as orbital motion around nucleus and spin motion around their axis. These motions separately take part in magnetic moment and act as a tiny magnet (Science Encyclopedia, 2010). However due to “Pauli Exclusion Principle”, mentioning as only two electrons of opposite spins can occupy one orbital, the magnetic moments of each electron cancels each other. Nevertheless, iron, cobalt and nickel whose magnetic moments are not annulled, are called magnetic metal as can be seen in Figure 2 (Klabunde, 2001).

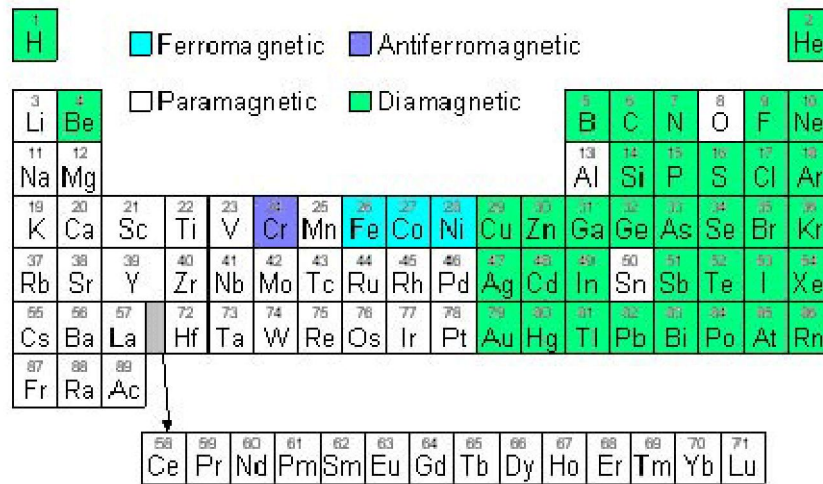


**Figure 2** Magnetic state of elements in periodic table (Splung.com, 2010).

Magnetization which results from these mentioned motions is represented by  $M$ ; the Magnetic field strength, i.e. intensity is expressed as  $H$ ; and a field due to both free and equivalent currents is known as magnetic induction,  $B$ . These three parameters are combined with each other in the field equation: (Pankhurst, Connolly, Jones, & Dobson, 2003; Jiles, 1998)

$$B = H + 4\chi M$$

The equation is expressed in different way by considering permeability ( $\mu$ ), which is the degree of magnetization of a material in response to a magnetic field.

$$B = \mu ( H + M )$$

Magnetization is expressed as  $M = m/V$  in which  $m$  is the magnetic moment of a material in a per unit volume. Magnetization of the materials is classified in terms of its volumetric magnetic susceptibility,  $\chi$ , where

$$M = \chi H$$

According to magnetic susceptibility of materials, six classification are present as “ferromagnetism”, “ferrimagnetism”, “antiferromagnetism”, “paramagnetism”, “superparamagnetism”, “diamagnetism” (Vollath, 2008; Klabunde, 2001).

Iron, cobalt and nickel are well known example of “*ferromagnetic*” materials. These materials show strong attraction towards external magnetic field due to dipoles of unpaired electrons of atoms. In Figure 3, dipoles of the electrons due to magnetic fields are represented (Klabunde, 2001; Vollath, 2008). Their magnetic susceptibility is positive and  $\chi \sim 50$  to 10000 (Jiles, 1998).

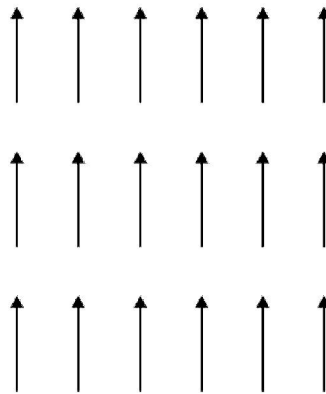


**Figure 3** Representation of ferromagnetic behavior of electrons.

In the case of  $\gamma\text{-Fe}_2\text{O}_3$  magnetic properties is different from the ferromagnetism; equal number of spins are aligned in two different arrangements, parallel and anti parallel. These two magnetic moments are not equal and a net magnetic moment is

observed (Vollath, 2008). These materials are called as “*ferrimagnetic*”. Behavior of magnetic moments in ferrimagnetic material is depicted in Figure 4.

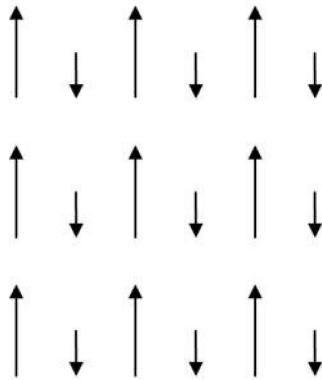


**Figure 4** Representation of Ferrimagnetic behaviour of a material.

In some cases, the magnetism from magnetic atoms or ions aligned in one direction is canceled out by the set of magnetic atoms or ions that are aligned in the reverse direction (Britannica, 2010) depicted as in Figure 5. This situation is called as “*antiferromagnetic*” materials.

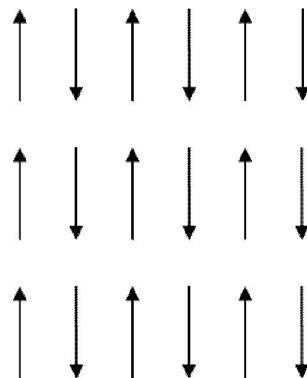


**Figure 5** Representation of Anti-ferromagnetic behaviour of a material.

“*Paramagnetism*” is weak interaction towards magnetic pole. If a magnetic field is applied to such a material, the dipole moments try to line up with the magnetic field, but are prevented from becoming perfectly aligned by their random thermal motion (Figure 6). When a paramagnetic material is placed in a strong magnetic field, it

becomes a magnet, and as long as the strong magnetic field is present, it will attract and repel other magnets in the usual way (Spencer, 1997). But when the strong magnetic field is removed, the net magnetic alignment is lost as the dipoles relax back to their normal random motion.  $\chi$  for paramagnetic materials is small and positive and between  $10^{-3}$  -  $10^{-5}$  (Jiles, 1998). W, Al, Pt and Mn are some examples of paramagnetic substances.

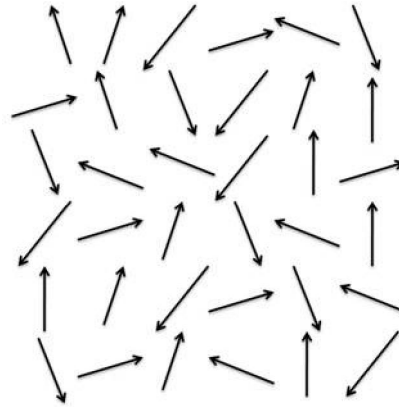


**Figure 6** Representation of paramagnetic behavior.

“*Superparamagnetism*” is a form of magnetism shows similar behavior with paramagnetism and observed in ferromagnetic and ferrimagnetic materials. By effect of temperature very small nanoparticles can randomly change its magnetic moments’ direction. This variation in magnetic moment is known as superparamagnetism. Although superparamagnetism is similar to the paramagnetism, magnetic susceptibility of superparamagnetic materials is higher than the one of paramagnetics ( Wikimedia Foundation, Inc., , 2010) .

*Diamagnetism* opposes to magnetic field and the diamagnetic materials have very small and negative susceptibility as listed in table 2. Bi, Be, Ag, Au, Ge and Cu are some of the diamagnetic materials (Jiles, 1998).

Magnetization of materials can be understood from the hysteresis curves. A hysteresis curve shows the relationship between the induced magnetic flux density

(B) and the magnetizing force (H). It is often called as the B-H loop. The loop is generated by measuring the magnetic flux of a ferromagnetic material while the magnetizing force is changed (NDT Resource center, 2001-2010).

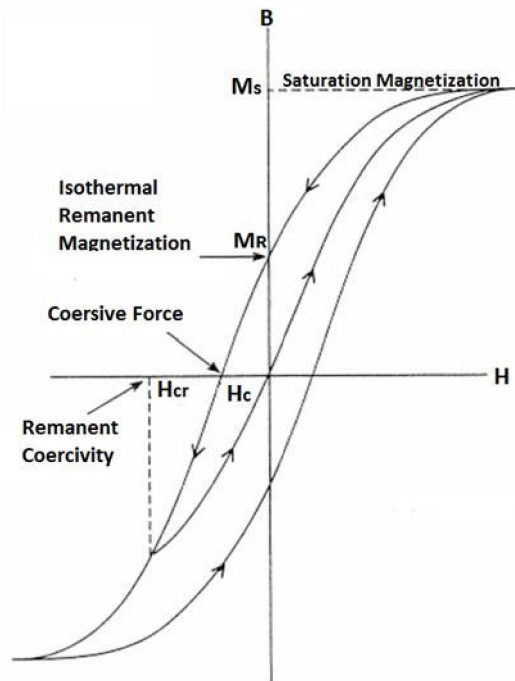


**Figure 7** General appearance of hysteresis loops.

According to the curve in Figure 7, the magnetization at which all the moments are aligned in both instances is referred to as the saturation magnetization ( $M_s$ ). The magnetization present after saturation and the subsequent removal of the field is referred to as the remanent magnetization ( $M_R$ ). The reversal of the field (in the direction opposite to the remanent magnetization) causes the magnetic moments to randomize again, and the field required to bring the net magnetization back to zero is called the coercivity,  $H_c$  (Willard, Kurihara, Carpenter, Calvin, & Harris, 2004). Coercivity is a structure-sensitive magnetic property, which means that it could be altered by subjecting the specimen to different thermal and mechanical treatments.

It has been noticed that iron and steel specimens which are mechanically hard have high coercivity, while those that are soft has low coercivity. Therefore the terms hard and soft are used to distinguish ferromagnets on the basis of their coercivity.

Magnetic materials with coercivity above  $10 \text{ kAm}^{-1}$  are called “hard” while the materials with coercivity below  $1 \text{ kAm}^{-1}$  are called “soft” (Jiles, 1998). In Figure 8, hysteresis loops of hard and soft ferromagnetic materials can be seen. While hard ferromagnets retain saturation field when driving force is removed, soft ferromagnets lose energy in repeatedly reversing the magnetization (Nave, 2010).

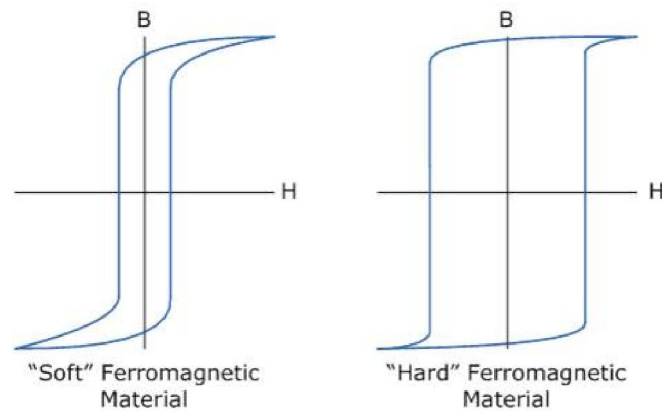


**Figure 8** Hysteresis loops of hard and soft ferromagnetic materials.

When ferromagnets are heated to sufficiently high temperatures, they become paramagnetic. The temperature which the materials transfer from ferromagnetic to paramagnetic is called *curie temperature*. At this temperature, the permeability of the material drops suddenly and both coercivity and remanence become zero (Jiles, 1998).

### 1.2.2 Synthesis of Magnetic Nanoparticles

Nanoparticles can be formed under two main methods, namely physical and chemical approaches. In chemical method nanoparticles are built from separate atoms, called “bottom-up” approach (Drexler & Peterson, 1989). Physical method is based on various dispersion and aggregation procedures, an approach from the “top-down” (Drexler & Peterson, 1989). Both physical and chemical approaches are illustrated basically in Figure 9 (Sergeev, 2006).

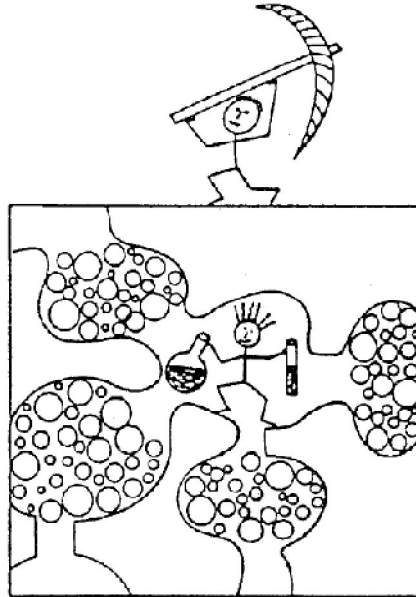


**Figure 9** Two concepts for the synthesis of nanoparticles; "top-down" and "bottom-up" approaches which refer to physical and chemical methods respectively (Hyeon, 2003) .

Between "top-down" and "bottom-up" approaches, in the literature physical vapor phase deposition (Yoshida, 1996) , mechanical attrition (Lam, Zhang, Tang, Lee, Bello, & Lee, 2000), and chemical methods (Jana, Gearheart, & Murphy, 2001; Hyeon, 2003) are the most common approaches used to produce magnetic nanoparticles. In both the vapor phase and solution routes, the particles are gathered together from individual atoms to form nanoparticles. Alternatively, mechanical attrition involves the breaking of larger coarse-grained materials to form nanoparticles (Lam, Zhang, Tang, Lee, Bello, & Lee, 2000). Because of straightforward nature and potential to produce large quantities of the final product, chemical methods have been widely used to produce magnetic nanoparticles (Hyeon, 2003). They usually accepted as the best method, because they provide homogeneity in design of the materials and low in price for production. Moreover, the methods allow researchers control particle size and size distribution, morphology, and agglomerate size through the individual manipulation of the parameters that determine nucleation, growth, and coalescence. Also, during synthesis or after synthesis, surface alteration of the particles is easily achieved, providing additional

functionality to the nanoparticles (Willard, Kurihara, Carpenter, Calvin, & Harris, 2004). The most commonly used chemical methods for magnetic nanoparticles synthesis are illustrated in Figure 10.

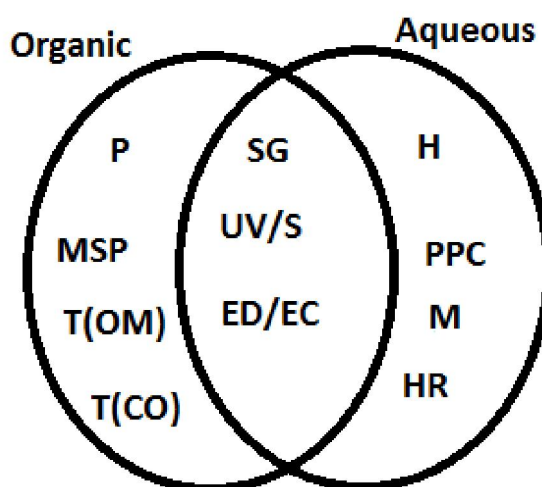


**Figure 10** Schematic diagram showing chemical synthesis techniques for magnetic nanoparticles in two different media; organic and aqueous.

*PPC: precipitation; H: hydrothermal; HR: hydride reduction; M: micellar or microemulsion; T(OM): thermolysis – organometallic decomposition; T(CO): thermolysis – carbonyl decomposition; UV: photolysis; S: sonolysis; SG: sol–gel; P: polyol; EC: electrochemical; ED: electrodeposition; MSP: multisynthesis processing.*

These methods are represented in Figure 10, are the most frequently used routes in the literature to produce magnetic nanoparticles. Herein, only precipitation and hydride reduction are going to be detailed.

### 1.2.2.1 Synthesis of Magnetic Nanoparticles via Precipitation

Chemical synthesis allows handling of matter at the molecular level. Good chemical homogeneity, better control of the particle size, shape and size distribution can be achieved in chemical synthesis (Edelstein & Cammarata, 1996).

Classical aqueous precipitation reactions are widely used method to prepare many magnetic nanoparticles having broad size distribution and irregular morphology. Generally, precipitation procedure is based on preparation of metal nanoparticles from their salt solution (Hernando, Crespo, & García, 2005). Those ions have a tendency to join, forming particles. During the growth of such particles when they are small, their growth is blocked in the nanometer range and thus nanoparticles are obtained. For blocking the particle growth, capping agents are used. Since the metal concentration must be very low to avoid the nucleation and growth of large nanoparticles, the final product mass is usually in the order of milligrams (Willard, Kurihara, Carpenter, Calvin, & Harris, 2004).

#### **1.2.2.2 Synthesis of Magnetic Nanoparticles via Hydride Reduction**

Uniform spherical nanoparticles can be formed by the reduction of metal salts using sodium borohydride. At room temperature by using  $\text{NaBH}_4$  in aqueous solutions, both homo- (Fe, Co, Ni) and heterometallic (Fe-Co, Fe-Cu, Co-Cu) nanoparticles were obtained as amorphous powders (Willard, Kurihara, Carpenter, Calvin, & Harris, 2004; Chaudret, 2003). Borohydride reduction of metal ions has been used extensively for the production of fine particles of metals in the nanoscale.

### **1.3 Surface Modification of Magnetic Nanoparticles**

Stability is a crucial requirement for almost any application of magnetic nanoparticles. Especially pure metals, Fe, Co, and Ni and their metal alloys, are very air-sensitive (Wu, He, & Jiang, 2008; Gubin, Yu Koksharov, Khomutov, & Yu Yurkov, 2005). Thus, the main difficulty for the use of pure metals or alloys arises from their instability towards oxidation. When the particles get smaller and smaller the susceptibility towards oxidation becomes higher (Faraji, Yamini, & Rezaee, 2010), and the particles produce aggregates resulting in bigger particle size (Ma & Liu, 2007). Therefore, it is crucial to develop efficient strategies to improve the effective chemical stability of magnetic nanoparticles.

Core-shell strategy is a type of protection method for the pure metal nanoparticles. The strategy includes coating of pure metal core with organic molecules, including small organic molecules or surfactants (Kim, Zhanga, Voith, Raob, & Muhammed, 2001), polymers (Ditsch, Laibinis, Wang, & Hatton, 2005), and biomolecules, or coating with an inorganic shell, such as silica (Ma, Zhang, Yu, Shen, Zhang, & Gu, 2003), metal (Kouassi & Irudayaraj, 2006) or nonmetal elementary substance (Majetich, Artman, McHenry, Nuhfer, & Staley, 1993), metal oxide or metal sulfide (Wu, He, & Jiang, 2008).

### **1.3.1 Characterization Techniques of Magnetic Nanoparticles**

The properties of magnetic nanoparticles are determined by several techniques. The following techniques are used; Transmission Electron Microscopy (TEM) and Scanning Electron Microscopy (SEM) for understanding the size, shape distribution and topology of particles; electron diffraction in order to get information on size, phases, structure and bond angles; scanning tunneling microscopy (STM) to determine size, shape and the internal structure of particles; photoelectron spectroscopy to determine the electronic structure (Edelstein & Cammarata, 1996).

SEM is an instrument (Figure 11) that produces a largely magnified image by using electrons instead of light to form an image. A beam of electrons is produced at the top of the microscope by an electron source. The electron beam follows a vertical path through the microscope, which is held within a vacuum. The beam travels through electromagnetic fields and lenses, which focus the beam down toward the sample. Once the beam hits the sample, electrons and X-rays are ejected from the sample (Rack, 2010).

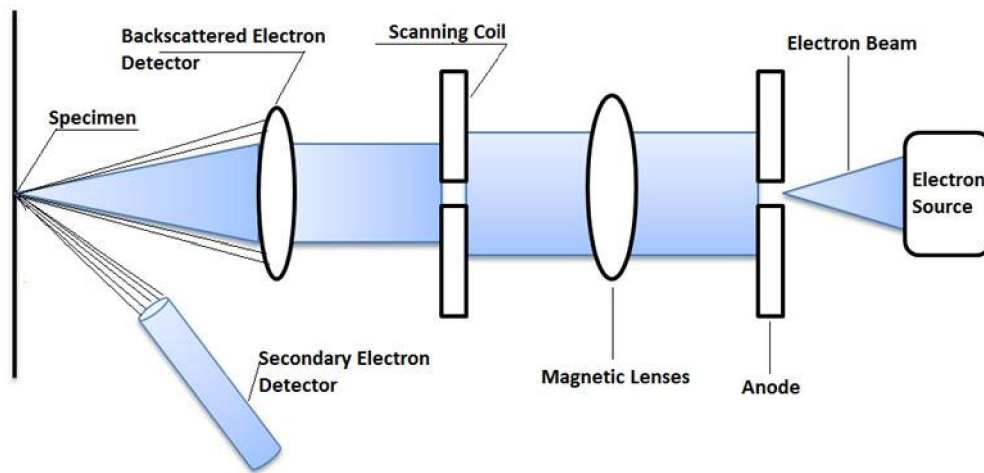


**Figure 11** Representation of Scanning Electron Microscope.

The instrument gives information about the surface features of an object (*topography*), the shape and size of the particles making up the object (*morphology*); the elements and compounds that the object is composed of and the relative amounts of them; direct relationship between composition and materials properties (*composition*), how the atoms are arranged in the object (*crystallographic information*) (Geochemical Instrumentation and Analysis, 2010).

In order to determine chemical composition of nano-material, the high energy electron beam of an electron microscope is employed to generate secondary electrons in the sample, which leads to the formation of holes and the subsequent emission of X-rays when the holes are filled. These X-rays are measured by energy dispersive spectroscopy (EDX). EDX can be used to find the chemical composition of materials and to create element composition maps over small area on the specimen. Usually EDX instrument is used in conjunction with SEM (Handbook of Analytical Methods for Materials, 2009).

Vibrating sample magnetometer (VSM) is an instrument which measures the magnetic behavior of substances. The device instrumentation is shown in Figure 12. As can be observed, there is magnetic field where a sample is placed inside. Then the sample is magnetizing by vibrating sinusoidally. The induced voltage is originated in the pickup coil which is proportional to the sample's magnetic moment. However, the

applied magnetic field does not affect the strength of the voltage ( Wikimedia Foundation, Inc., , 2010). The results of the magnetic measurements are shown with a *hysteresis curve*.

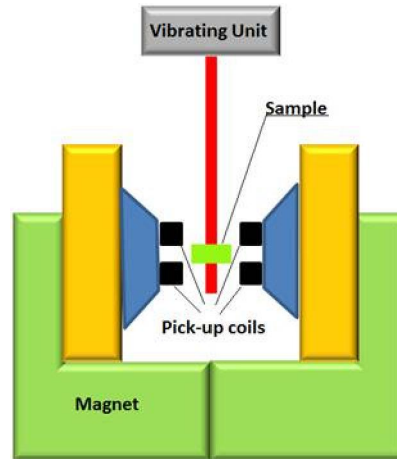


**Figure 12** Schematic representation of VSM.

#### **1.4 Applications of Magnetic Nanoparticles**

Magnetic nanoparticles have great importance in nanotechnology because they possess wide range applications. Magnetic materials can be controlled by magnetic field, so that they are usually used to catch the target in solution and concentrate them together with assistance of an external magnet (Zhai, Zhai, Wang, Guo, Ren, & Dong, 2009). They are studied mostly in ferro fluids, bio-separation (GuptaA. & Gupta, 200), drug delivery (Son, Reichel, He, Schuchman, & Lee, 2005), contrast agent in MRI (Jun, et al., 2005), hyperthermia, data storage media, and magneto resistive devices (Koch, 2007), which are summarized in Figure 13.

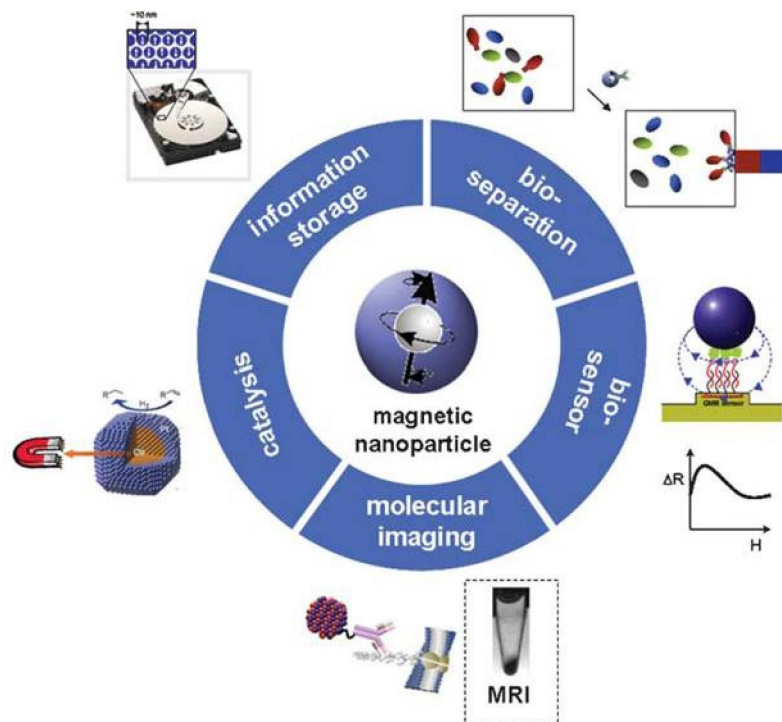


**Figure 13** Application of magnetic nanoparticles in various fields.

## 1.5 Raman Spectrometry

Raman spectroscopy is a spectroscopic technique based on inelastic scattering of monochromatic light (Princeton Instruments, 2010). In 1928 “Raman effect” was discovered and named by Sir C. V. Raman in 1928 and he was rewarded with Nobel Prize in 1930 (Venkata Raman - Biography, 2010). Raman spectroscopy has become an important analytical and research tool. It can be used for applications as wide ranging as pharmaceuticals, forensic science, polymers, thin films, semiconductors and even for the analysis of fullerene structures and carbon nano-materials (Horiba Scientific, 2010).

### 1.5.1 Principles of Raman Spectroscopy

When light is scattered from a molecule most photons are elastically scattered as shown in Figure 14. The scattered photons have the same energy (wavelength) as the incident photons which is called elastic (Rayleigh) scattering. However, a small

fraction of light (approximately 1 out of  $10^8$  photons) is scattered at optical frequencies different from the frequency of the incident photons. The process leading to inelastic scattering is called the Raman Effect (Petry, Schmitt, & Popp, 2003).

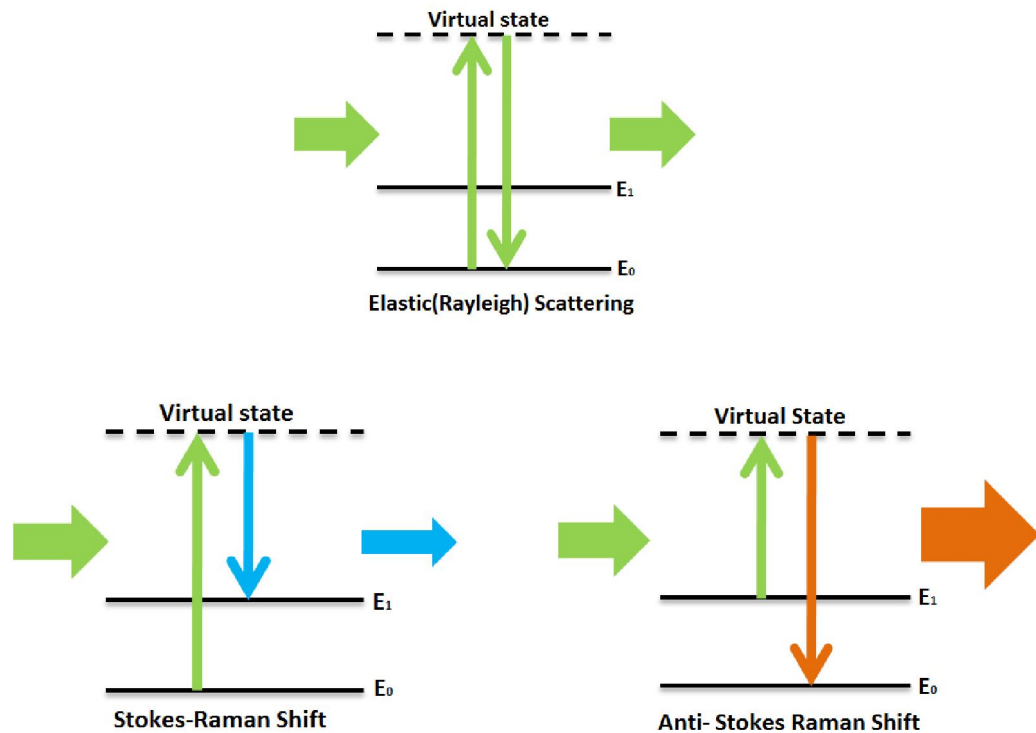


**Figure 14** Representation of elastic and inelastic scatterings: Stoke-Raman and Anti-stoke Raman Scattering.

As can be observed in Figure 14, there are two types of Raman scattering. If a transition from the lower energy level to a higher one, the Stokes- Raman effect occurs. In case of energy transfer from the system to the incident light wave, which corresponds to a transition from an higher energy level to a lower one the anti-Stokes effect is observed. The anti-Stokes intensity is less than the Stokes intensity because the anti-Stokes scattering occurs from an excited state, which is, according to the Boltzmann distribution, less populated than the ground state. Hence, in most cases the more intense lines of the Stokes -Raman spectrum are detected. (Petry, Schmitt, & Popp, 2003)

## 1.5.2 Instrumentation of Raman Spectroscopy

Raman system consists of three main components: (a) an excitation source, a laser; (b) sample illumination system; (c) a signal processing, a detector (Ferraro, Nakamoto, & Brown, 2003; Skoog, Holler, & Nieman, 1998).

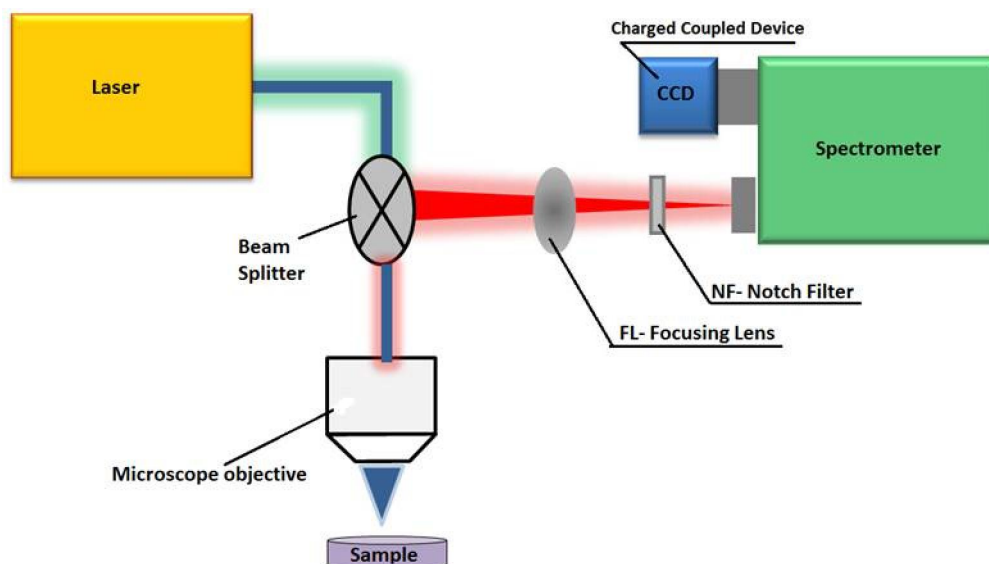


**Figure 15** Block diagram of Raman spectroscopy.

Usually Raman system uses laser sources because they have high intensity to produce Raman scattering. Laser sources can be applied in Raman system according to their intensity, which are listed in Table 1 (Skoog, Holler, & Nieman, 1998).

UV lasers, whose wavelengths are 224 and 325 nm, are generally used for biological, catalysts and wide band gap semiconductors. In case of visible region, Ar and Kr ion lasers are suitable for semiconductor, catalysts, biological, polymers and minerals. Also, He ion laser is usually applied for corrosion purpose. In the NIR region, laser sources are used for polymers, biological application of Raman Systems.

**Table 1** Laser Sources for Raman System.

<b>Laser Type</b>	<b>Wavelength, nm</b>
UV lasers	244 or 325
Argon ion ( <b>Visible</b> Laser)	488.0 or 514.5
Krypton ion ( <b>Visible</b> Laser)	530.9 or 647.1
Helium-neon ( <b>Visible</b> Laser)	632.8
Nd-YAG ( <b>NIR</b> Laser)	1064

In the Raman instrumentation, there is no need for inert atmosphere or unstable sample holder. In fact, sample handling for Raman spectroscopy is easy, since glass is a suitable material for windows, lenses and other optical components. Moreover, the laser source is effective for the Raman measurement because focusing on a small sample area and focusing of the emitted radiation on a slit is easy for laser source. As a result, very small samples can be analyzed with Raman systems (Skoog, Holler, & Nieman, 1998).

In order to determine the Raman signal a charge-coupled device (CCD) camera or photon-counting photomultiplier tube (PMT) were generally employed in Raman systems (Figure 15) (Baena & Lendl, 2004). Besides, a Fourier transform technique may be used in some cases (Wartewig & Neubert, 2005). The technique includes cooled germanium transducers or multichannel devices based on CCD. In contrast to PMT, because these detectors are sensitive to radiation at 782 nm, Raman excitation of many compounds are collected without fluorescence interference. Unlike conventional methods, the Fourier transform technique may only be used in the near-infrared spectrum in practise (Skoog, Holler, & Nieman, 1998; Ferraro, Nakamoto, & Brown, 2003).

### **1.5.3 Surface Enhanced Raman Spectrometry**

The enhancement of Raman signal was first observed by Fleischmann et al. (Fleischmann, Hendra, & McQuillan, 1974) with pyridine adsorbed on a silver electrode. The enhanced Raman signal, originally attributed to a high surface density produced by the roughening of the surface of electrodes, was later determined to be a result of a surface enhancement process, hence the term surface-enhanced Raman scattering (SERS) effect (Vo-Dinh, 1998).

SERS enhancement results from the product of two contributions: an electromagnetic enhancement and a chemical enhancement mechanism (Stiles, Dieringer, Shah, & Van Duyne, 2008). Electromagnetic enhancement known as field effect is produced near the surface of the metal. When an electromagnetic wave interacts with a metal surface, the fields at the surface are different than those observed in the far field. If the surface is rough, the wave may excite localized surface plasmons on the surface, resulting in amplification of the electromagnetic fields near the surface. Surface plasmons are collective excitation of conductive electrons in small metallic structures (Petry, Schmitt, & Popp, 2003; Stiles, Dieringer, Shah, & Van Duyne, 2008). Examples of such systems include metal colloids, metal island films and electrodes (Cotton, Kim, & Chumanov, 1991).

The chemical enhancement known as molecular effect is due to the molecular interaction between the molecule and the metal (Cotton, Kim, & Chumanov, 1991). The molecular polarizability is affected by interactions between the molecule and the metal surface. The electronic transitions of many charge transfer complexes are in the visible region, so that resonance enhancement occurs (Vo-Dinh, 1998; Stiles, Dieringer, Shah, & Van Duyne, 2008).

### **1.6 Aim of This Study**

In this study, gold decorated magnetic cobalt-silica core-shell nanoparticles were synthesized. Magnetic cobalt nanoparticles were prepared in the presence of strong

reducing agent and capping agent. The particles were protected with silica surface by addition of silicate reagent in ethanol/water medium. Silica surface was functionalized with amine groups for capturing gold nanoparticles. In order to modify silica surface with gold, gold nanoparticles were prepared by citrate reduction method and equilibrated with silica coated magnetic particles. Gold modified magnetic silica particles were utilized both as a solid phase for magnetic collection and substrate for the SERS detection of 4-mercaptobenzoic acid.

## CHAPTER 2

### EXPERIMENTAL

#### 2.1 Materials

The chemicals used in nanoparticle production and surface modification are Cobalt chloride hexahydrate ( $\text{CoCl}_2 \cdot 6\text{H}_2\text{O}$ , 99%), tetraethyl orthosilicate (TEOS, 98%), 3-aminopropyltriethoxysilane (APTS, 98%), 3-aminopropyltrimethoxysilane (APS, 98%), trisodium citrate ( $\text{Na}_3\text{C}_6\text{H}_5\text{O}_7$ , 99%), brilliant cresyl blue (BCB, 99%), rhodamine 6G (R6G, 99%), 4-mercaptobenzoic acid (4-MBA, 90%), chloroauric acid ( $\text{HAuCl}_4$ , 99%) were purchased from Sigma Aldrich; sodium borohydride ( $\text{NaBH}_4$ , 96%), ethanol ( $\text{C}_2\text{H}_5\text{OH}$ ), citric acid ( $\text{C}_6\text{H}_8\text{O}_7$ , 99,5%) were purchased from Merck. All reagents were in analytical grade and used without further purification.

All reagents used in this study were in analytical grade. Dilutions were made using 18 M $\Omega$ -cm deionized water obtained from a Millipore (Molsheim, France) Milli-Q water purification system.

#### 2.2 Instrumentation

The morphological, optical, and spectroscopic properties of prepared nanoparticles were examined using the following measurements. For SEM measurements, the obtained suspension solutions dropped on carbon-coated copper grids without metal coating. SEM was carried out with a QUANTA 400F Field Emission scanning electron microscope.

From the FE-SEM images arithmetic average particle diameter were determined for cobalt, cobalt-silica, and gold nanoparticles. From the FE-SEM images, randomly 10 particles were selected, their diameter measured and their arithmetic average diameter and standard deviations were calculated.

Energy-dispersive X-ray analysis (EDX) was performed with a scanning electron microscope equipped with energy-dispersive X-ray analyzer (EDAX) at the METU Central Laboratory.

UV-vis spectra were collected over the range 400-900 nm by using double beam instrument (Varian Cary 100). Plastic cells were used in all measurements.

SERS measurements were performed with Jobin Yvon LabRam confocal microscopy Raman spectrometer with a charge-coupled device (CCD) detector and a holographic notch filter. It was equipped with a 1800-grooves/mm grating and all measurement were done with a 200  $\mu\text{m}$  entrance slit. SERS excitation was provided by 632.8 nm radiation from a He-Ne laser with a total power of 20 mW.

Saturation magnetization was measured with ADE Magnetics Model EV9 Vibrating Sample Magnetometer having maximum field of 2.2 Tesla in METU Metallurgical and Materials Engineering Department.

For magnetic decantation of the particles  $\text{Nd}_2\text{Fe}_{14}\text{B}$  magnet was used, throughout the particle synthesis the ultrasonic water bath (Elma S40 H, Germany), magnetic stirrer were used.

### **2.3 Synthesis of Cobalt Nanoparticles**

Preparation of cobalt nanoparticles was began with  $\text{N}_2$  bubbling of 20 ml distilled water containing 2 ml citric acid for 15 minutes. The bubbling set-up was consisted of Schlenk flask which have two inlets; one is connected to  $\text{N}_2$  gas and the other was linked to vacuum pump (Figure 16-a). Then deaerated water was transfer into 3-necked round bottom flask, stirred with 400 rpm on magnetic stirrer and  $\text{N}_2$

atmosphere was provided by the help of N<sub>2</sub> filled balloon. After that, 0.2 ml of CoCl<sub>2</sub>.6H<sub>2</sub>O solution was added to the solution and reduction was performed by addition of NaBH<sub>4</sub>. At the end, black colored solution observed indicates of the presence freshly-prepared Co nanoparticles (Figure 16-b). The solution was stirred for 2 minutes in order to allow complete H<sub>2</sub> gas removal from the system.

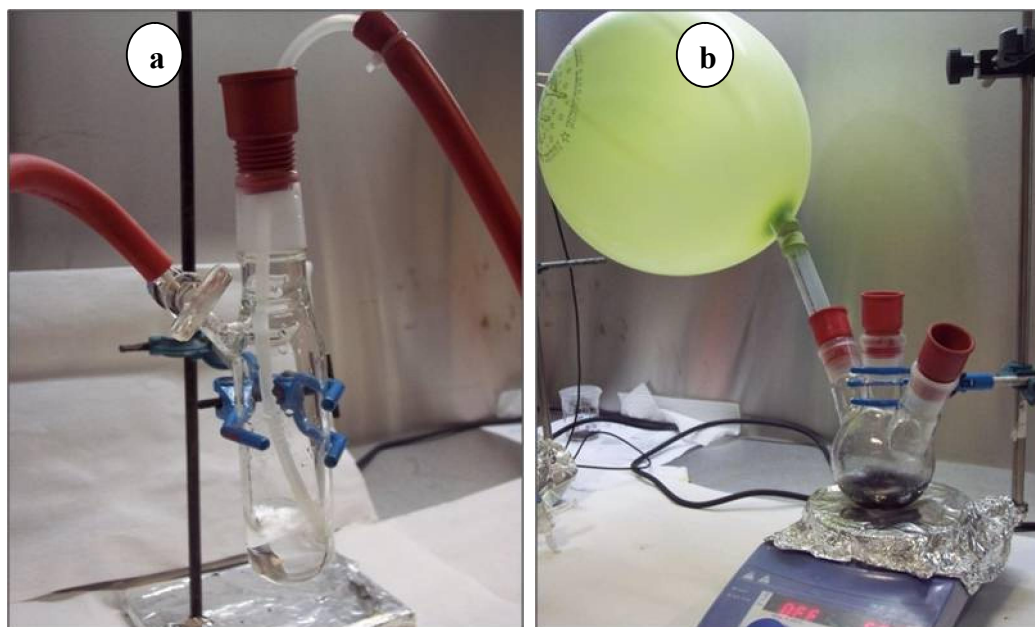


**Figure 16** (a) Deoxygenation of citric acid added deionized water and (b) freshly prepared cobalt nanoparticles under N<sub>2</sub> atmosphere.

To observe the change of size distribution of the particles different concentrations were used during the study.

#### **2.4 Synthesis of Silica Coated Cobalt Nanoparticles**

Co nanoparticles were coated with silica surface for protection against air oxidation and further functionalization. The well known Stöber method (Stöber, Fink, & Bohn, 1968) which is the hydrolysis of TEOS was applied. While the cobalt nanoparticles solution was stirring, 80 ml ethanol containing 17.0 μl of TEOS and 1.44 μl APS was added and allowed to stir for 3 hours (Figure 17).

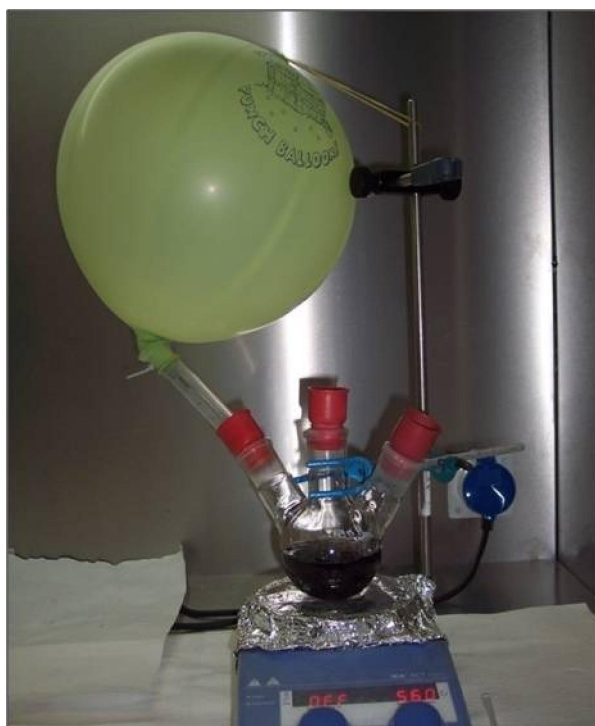


**Figure 17**, The photograph of cobalt-silica nanoparticles' solution (After addition of TEOS/Ethanol mixture).

## 2.5 Amine Functionalization of Cobalt-Silica Core-Shell Nanoparticles

After 3 hours of the Stober reaction (Mentioned in section 2.4), for amine modification of the surface, APTS was added to the cobalt nanoparticles-alcoholic TEOS mixture and allowed to stir at least 12 hours. At the end of 12 hours, the particles were collected by magnet and supernatant was removed. The collected particles were washed twice with ethanol, one time with water/ethanol mixture and three times with water using ultrasonic water bath (Elma S40 H, Germany). Finally they were dispersed in 100 ml of water, which were used as stock solution for further studies.

## **2.6 Gold Nanoparticles**

Gold nanoparticles were prepared according to citrate reduction method. Aqueous solution containing 144  $\mu\text{l}$  of  $\text{HAuCl}_4$  (0.1 M), in 50 ml beaker, was stirred and heated. When boiling was started, 2 mL of 1% (m/v) sodium citrate solution were added to the solution. Then, it was allowed stirring vigorously and boiling for one hour. After that, it was cooled to room temperature by continuous stirring. The prepared 50 ml gold colloid was used as stock solution for further applications.

## **2.7 Gold Seeding on Amine Modified Core-Shell Nanoparticles.**

Five milliliters of water dispersed amine modified silica coated magnetic nanoparticles were mixed with same volume of citrate stabilized gold nanoparticles and vigorously stirred for some time. All solutions were used from previously mentioned stock solutions of gold colloid and gold modified cobalt-silica nanocomposites. Reaction time was varied from one minutes to two hours and Au:cobalt-silica (v:v) ratios were varied from 1:2 to 0.1:1. Excess gold nanoparticles were removed by three repeated magnetic collection/wash cycles and the particles were redispersed in 10 ml water.

## **2.8 Surface Enhanced Raman Scattering (SERS) Studies**

In order to measure the enhancement effect of prepared nanoparticles on SERS process, BCB and R6G were chosen as Raman reporter molecules. Various fresh stock solutions of analytes were prepared in deionized water with different concentrations and used for serial dilutions. Gold modified cobalt-silica nanocomposites mixture (1:1 (v/v) ratio) was mixed with Raman dyes in eppendorf tubes (Figure 18) and vortexed respectively. Then, 15 $\mu\text{l}$  of the resulting mixture were dropped on the glass slide and allowed to dry at room temperature.

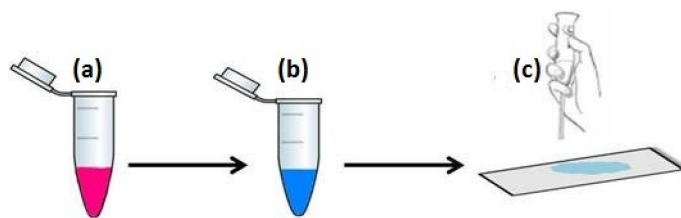


**Figure 18** Preparation of sample for SERS measurements (a) Substrate: gold modified cobalt-silica nanocomposites, (b) mixture of Raman dye with gold modified cobalt-silica nanocomposites, (c) a drop of SERS substrate on glass slide.

After drying was completed, Raman measurement were taken at a range of wave number with  $400-800\text{ cm}^{-1}$  for BCB, and  $1000-1800\text{ cm}^{-1}$  for R6G having acquisition times between 10-50 seconds.

## 2.9 Magnetic Collection and Identification Studies

Gold modified cobalt-silica nanoparticles were used with 4-MBA for magnetic collection and identification with SERS technique as summarized in Figure 19. Briefly, 50 ml of cobalt-silica was mixed with 100 ml of gold colloid; stock gold modified cobalt-silica nanoparticles were prepared and dispersed in 10 ml of deionized water. After the preparation of gold modified cobalt-silica particles,  $10^{-5}\text{M}$  4-MBA was prepared in water. Then, 5 ml of the 4-MBA and 1 ml of stock gold modified cobalt-silica particles were added to five different test tubes. The test tubes were shaken horizontally for 1 hour; afterwards the supernatant was removed by magnetic decantation process. At the end, magnetically collected particles were placed on glass slide and dried at room temperature. Raman measurement was taken at a range of  $1000-2000\text{ cm}^{-1}$  for 4-MBA and  $800-1600\text{ cm}^{-1}$  for detection of the dyes.

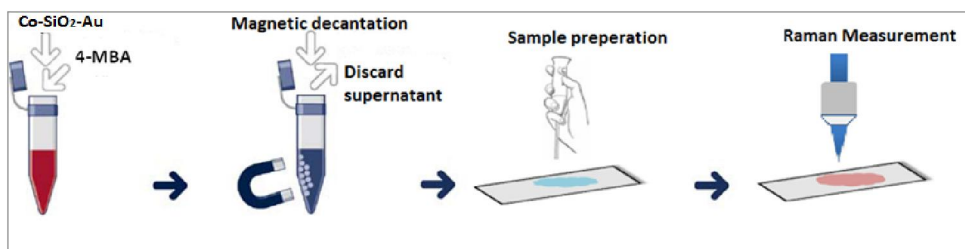


**Figure 19** Steps of magnetic separation and identification with SERS technique.

## CHAPTER 3

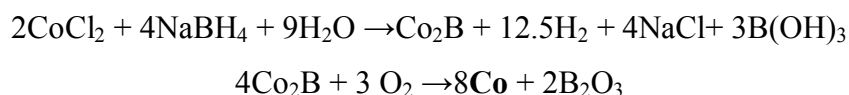
### RESULTS AND DISCUSSION

In this thesis, as the first time, the synthesis of gold modified cobalt-silica core-shell nanoparticles and their usage both as a solid sorbent and a SERS substrate for the detection of 4-MBA aqueous solution were reported. We have used a citrate-based approach to stabilize the cobalt particles. The molar ratio effect of reagents on the size of formed cobalt nanoparticles was investigated. After preparation of the cobalt nanoparticles the monolayer functionalization chemistry of APS molecules was applied, which reveals good linkage with Co layers, for further growth of TEOS through slow hydrolysis. Then amine modification was performed in order to add functional groups on silica shell. Different ratios of APTS/TEOS were tested to obtain different amount of amine groups on the surface of magnetic cobalt-silica core-shell nanoparticles. Afterwards gold decoration on amine modified cobalt-silica core-shell nanoparticles was performed by using gold nanoparticles prepared with citrate reduction. The amount of gold nanoparticles on the surface of silica shell was optimized by changing the amount of amine groups on the surface of silica shell and interaction times between gold nanoparticles and amine modified cobalt-silica core-shell nanoparticles. SERS efficiency of prepared nanoparticles was measured by using BCB, R6G dyes. Then magnetic separation and identification of 4-MBA was performed by using gold modified magnetic cobalt-silica nanocomposites. Their morphological, optical, chemical and magnetic properties were investigated using FE-SEM, EDX, UV-Vis spectroscopy and VSM.

### 3.1 Synthesis of Cobalt-Silica Core-Shell Nanoparticles

#### 3.1.1 Cobalt Nanoparticle Synthesis

It has been stated that (Lee & Fang, 1995), citric acid as a stabilizer provides a wider range of control on particle sizes and better stability. Co nanoparticles were prepared according to the conventional NaBH<sub>4</sub> reduction of CoCl<sub>2</sub> (Kobayashi, Horie, Konno, Rodríguez-González, & Liz-Marzán, 2003). Under inert atmosphere citrate containing CoCl<sub>2</sub> and reducing agent were rapidly mixed and a black color solution was observed. The steps of the reduction reaction of CoCl<sub>2</sub> with NaBH<sub>4</sub> are given below (Kobayashi, Horie, Konno, Rodríguez-González, & Liz-Marzán, 2003).



Co<sub>2</sub>B reacts with the dissolved oxygen; boron is oxidized while cobalt is reduced to Co(s) (Salgueirino-Maceira, Correa-Duarte, Farle, López-Quintela, Sieradzki, & Diaz, 2006). Thus prepared nanoparticles were found to be stable for several hours. The structure of the produced cobalt nanoparticles was characterized by FE-SEM and EDX. Representative FE-SEM images and EDX pattern of prepared Co nanoparticles are shown in Figure 20 and Figure 21 respectively.

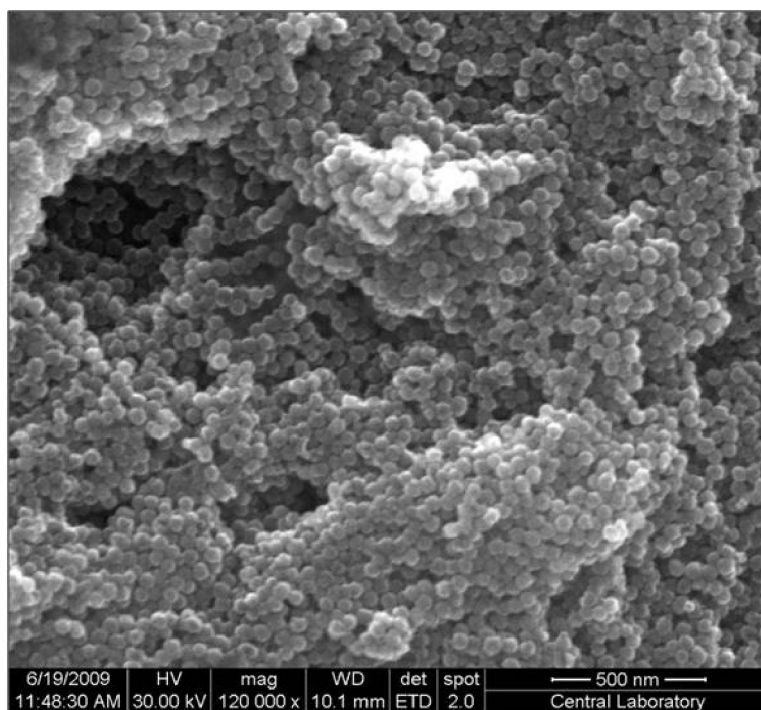


**Figure 20** FE-SEM images of citrate stabilized Co nanoparticles having size range  $46 \pm 4$  nm.

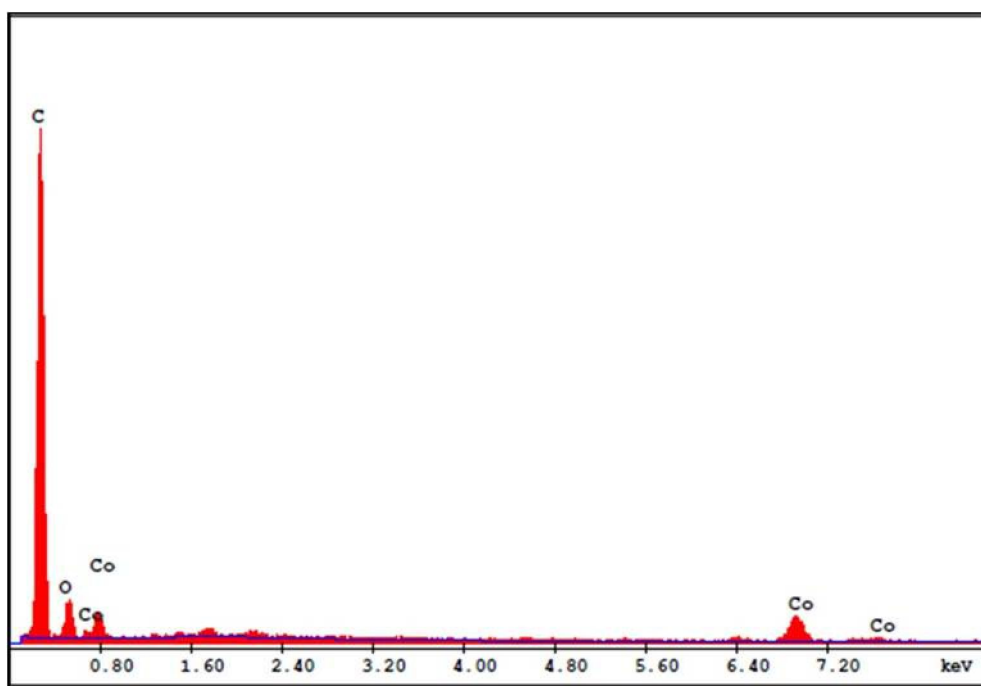


**Figure 21** EDX spectrum of Cobalt nanoparticles.

The size distribution of these particles was quite wide. The nano-sized cobalt particles distribution is highly affected by the amount of O<sub>2</sub> present in the aqueous solution and the citrate/Co<sup>2+</sup> molar ratio. Reduced environment was created only by a nitrogen filled balloon attached to the reactor and no further control over the inert gas concentration was done. However, citrate/Co<sup>2+</sup> molar ratio was optimized.

### 3.1.1.1 Effect of Citric Acid Concentration on Particle Size

The growth of the particles was tried to be controlled by altering the concentration of capping agent. The relation between citrate concentration and particle size distribution of the Co particles is given in Table 2.

**Table 2** Particle size distribution of Co nanoparticles as a function of citrate/Co<sup>2+</sup> molar ratio.

[Citrate], M	[CoCl <sub>2</sub> ], M	[Citrate]/[Co <sup>2+</sup> ]	Particle size, nm	Figure
4 x 10 <sup>-6</sup>	0.04	10 <sup>-4</sup>	46 ± 4	Figure 22
4 x 10 <sup>-4</sup>	0.04	10 <sup>-2</sup>	34 ± 4	Figure 23
4 x 10 <sup>-2</sup>	0.4	10 <sup>-1</sup>	7±2	Figure 24

As can be seen from the Table 2 the size of the particles was getting smaller as the ratios of citrate to cobalt concentration were increased. The dependence of the core size on the relative amount of citrate present during the formation of the Co nanoparticles is related to the adsorption of citrate ions on the cobalt particle surface, preventing further growth through double layer repulsion between negatively charged cobalt particles (Kobayashi, Horie, Konno, Rodri'guez-Gonza'lez, & Liz-Marza'n, 2003). The FE-SEM images of the prepared cobalt nanoparticles with different concentration of citrate were shown in Figure 22, Figure 23 and Figure 24.

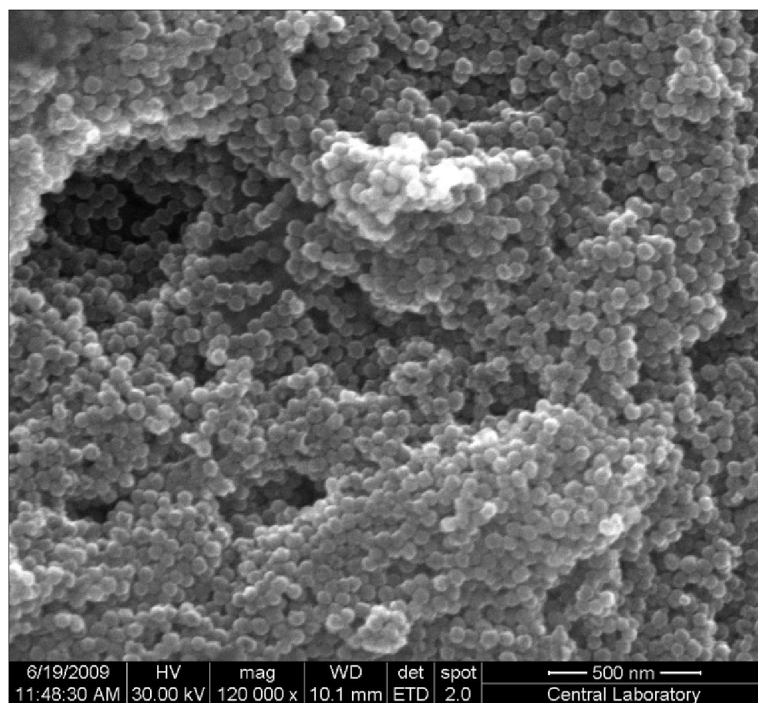


**Figure 22** FE-SEM images of citrate stabilized Co nanoparticles. Citrate/Co<sup>2+</sup> molar ratio was 10<sup>-4</sup>. Mean particle diameter was measured as 46 ± 4nm.

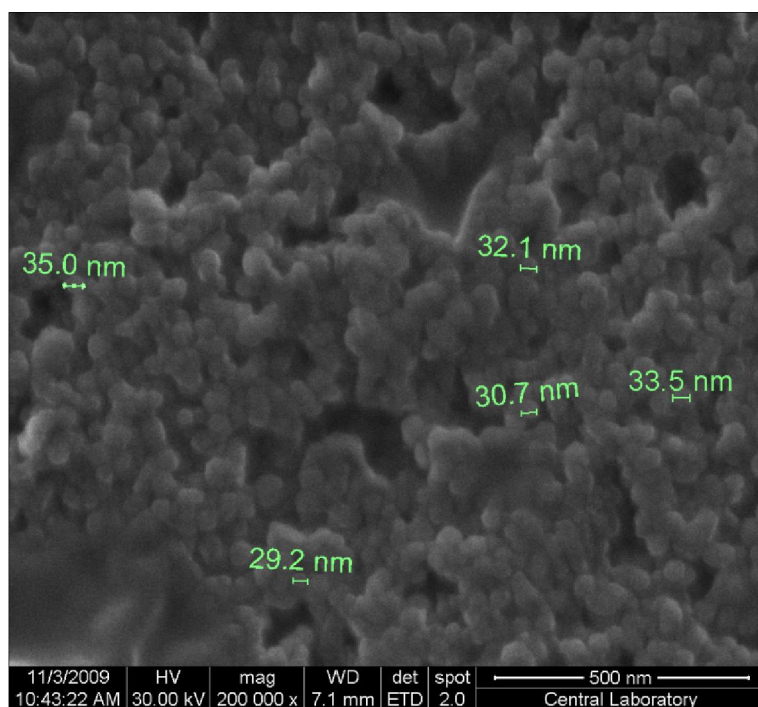


**Figure 23** FE-SEM images of citrate stabilized Co nanoparticles. Citrate/Co<sup>2+</sup> molar ratio was 10<sup>-2</sup>. Mean particle diameter was measured as 34 ± 4 nm.

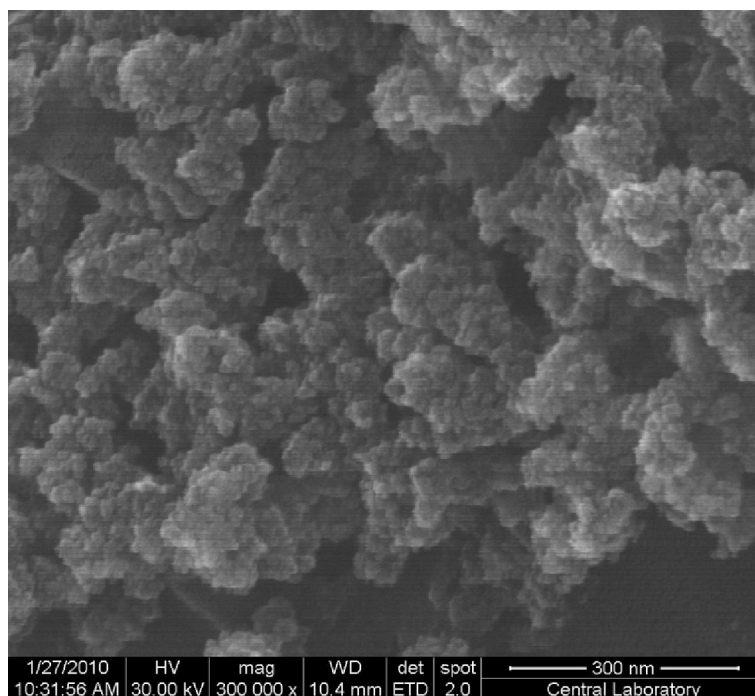


**Figure 24** FE-SEM images of citrate stabilized Co nanoparticles. Citrate/Co<sup>2+</sup> molar ratio was 10<sup>-1</sup>. Mean particle diameter was measured as 7±2 nm.

### 3.1.2 Preparation of Silica Coated Cobalt Nanoparticles

Non-toxic silica is most often used as the coating shell to provide magnetic nanoparticles with water solubility and biocompatibility in most applications (Lu, Yin, Mayers, & Xia, 2002). Besides, silica shell can also prevent the direct contact of the magnetic core with the environment thus avoiding undesired interactions (Gubin, Yu Koksharov, Khomutov, & Yu Yurkov, 2005). In addition silica can be functionalized to bind molecules. Consequently, silica coatings have been extensively studied and many synthetic methods have been developed for various applications. In our study Stöber method was used in order to achieve silica coating by application of which includes hydrolysis and condensation of an optimized amount of TEOS in water/ethanol solution to prevent the cobalt nanoparticles from air oxidation and further functionalization.

The schematic representation of the shell formation and the concentration of reagents used in the silica coating of cobalt nanoparticles have been shown in Figure 25 and Table 3 respectively.

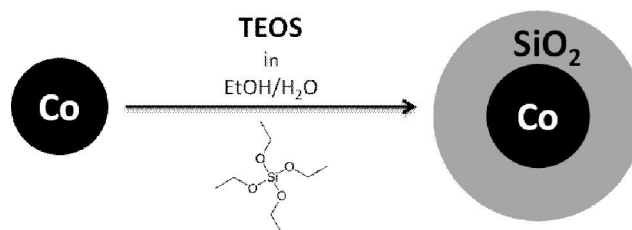


**Figure 25** Schematic representation of cobalt- silica core-shell formation.

The final size of the formed core-shell nanoparticle is related to the size of the core and thickness of the shell. In previous section we demonstrated how the size of core was changed by changing the citrate/Co<sup>2+</sup> ratio. In this section the monitoring of the thickness of the silica shell will be investigated by using different size of cobalt nanoparticles as core.

The thickness of the silica layer could be controlled by changing the amount of TEOS precursor. In the present study, different amounts of TEOS were added to synthesize silica-coated cobalt nanoparticles which are shown in Table 3. FE-SEM images shown in Figure 26 reveal that the thickness of silica coating on the surface of cobalt nanoparticles increases gradually with the increase of amount of TEOS. With the increase of the thickness of silica layer, silica-coated cobalt nanoparticles become more monodispersed.

**Table 3** Concentration of reagents used in core-shell cobalt-silica nanoparticle synthesis in case of citrate/Co<sup>2+</sup> was 10<sup>-2</sup>.

TEOS μL	NaBH <sub>4</sub> M	CoCl <sub>2</sub> M	[Citrate] M	Figure
8.5	4 x 10 <sup>-4</sup>	0.04	4 x 10 <sup>-4</sup>	Figure 26(a)
17.0	4 x 10 <sup>-4</sup>	0.04	4 x 10 <sup>-4</sup>	Figure 26(b)
34.0	4 x 10 <sup>-4</sup>	0.04	4x 10 <sup>-4</sup>	Figure 26(c)

**Table 4** Effect of TEOS/Co<sup>2+</sup> on shell thickness of the particles mentioned in Table 3.

[TEOS]/ [Co <sup>2+</sup> ]	[Citrate]/ [Co <sup>2+</sup> ]	Particle size, nm	Shell thickness, nm	Figure
5	0.01	34±4	-	Figure 26(a)
10	0.01	45±9	15-20	Figure 26(b)
20	0.01	83±17	40-50	Figure 26(c)

As can be seen from the Table 4, when [TEOS]/[Co<sup>2+</sup>] was equal to 5, the particle sizes were the same as the original size of the Co nanoparticles. Therefore, it was concluded that the amount of TEOS was not enough for complete silica shell formation. Conversely when [TEOS]/[Co<sup>2+</sup>] was increased from 10 to 20, the shell thickness of the core-shell nanoparticles were increased from 15-20 nm to 40-50 nm as expected. The FE-SEM images of the cobalt-silica core-shell particles specified in Table 4 have been given in Figure 26. The presence of Co, Si and O on the surface of Co nanoparticles were inspected by EDX, following the existence of silica peak on the spectrum. EDX patterns have been depicted in Figure 27.

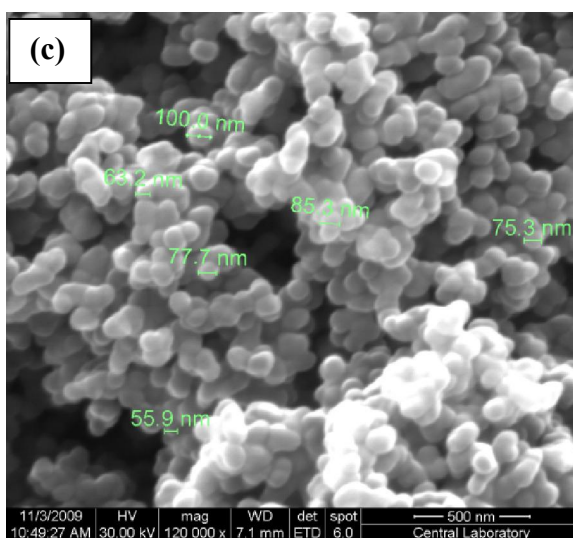
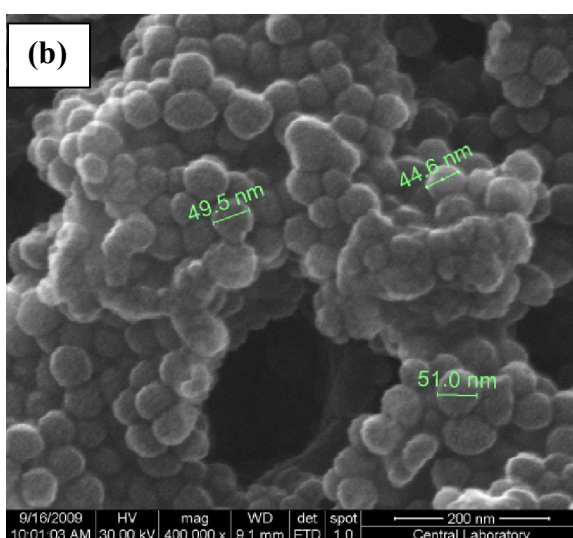
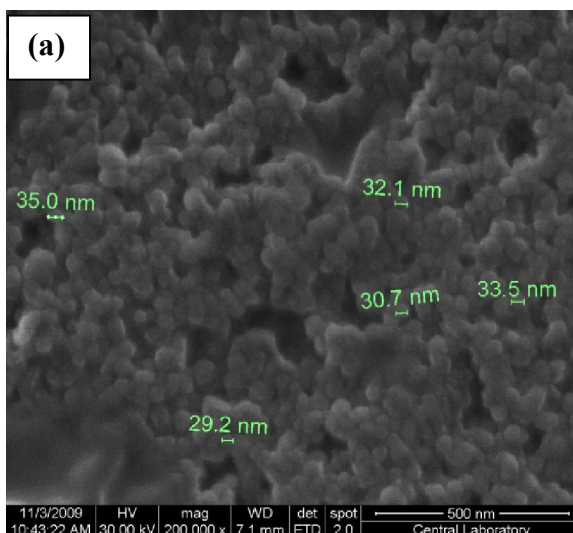


**Figure 26** FE-SEM images of the cobalt-silica core-shell particles, specified in Table 3, having  $[\text{TEOS}]/[\text{Co}^{2+}]$  ratio (a) 5; (b) 10; (c) 20.

Silica peak was observed for the particles having  $[\text{TEOS}]/[\text{Co}^{2+}]$  of 10 and 20 (Figure 27 b and c) whereas no Si peak was observed for the particles having  $[\text{TEOS}]/[\text{Co}^{2+}]$  of 5 (Figure 27-a). These results were confirming the out comes of FE-SEM evaluations regarding to the size of the coated Co nanoparticles. Therefore it was concluded that below a certain concentration of TEOS either indistinguishable or no silica deposition on Co surface was occurred.

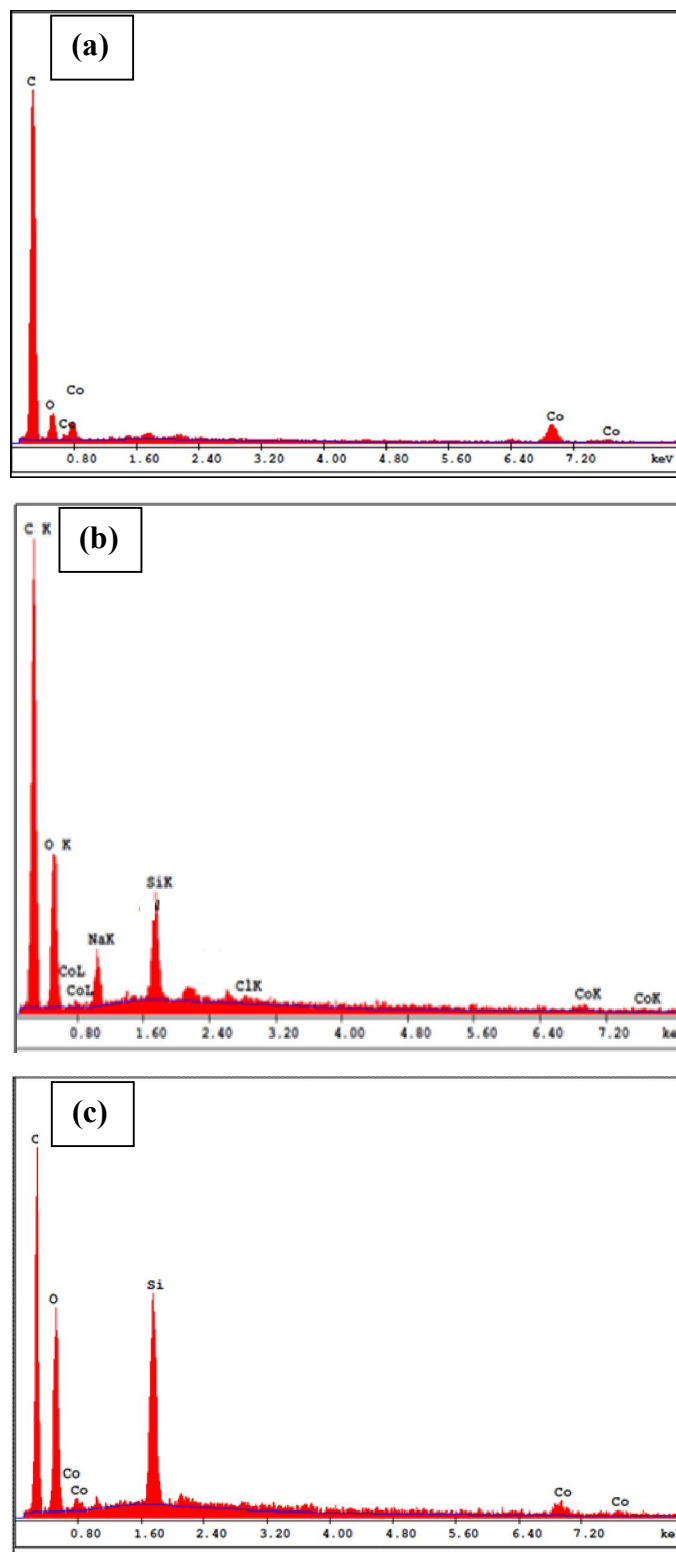


**Figure 27** EDX patterns of the cobalt-silica core- shell particles, specified in Table 5, having [TEOS]/[Co<sup>2+</sup>] ratio (a) 5; (b) 10; (c) 20.

Silica coating was also applied to greater Co particles having citrate/Co<sup>2+</sup> molar ratio of 10<sup>-3</sup> and 10<sup>-5</sup> and particle sizes in the range between 60-70nm and 80-90 respectively. The concentration of reagents used in the silica coating of cobalt nanoparticles and the effect of TEOS/Co<sup>2+</sup> molar ratio on shell thickness of the particles thus prepared have been shown respectively in Table 5 and Table 6 for 60-70 nm particles Table 7 and Table 8 for 80-90 nm particles. Their FE-SEM images have been presented in Figure 28 and Figure 29.

**Table 5** The concentration of reagents used in the silica coating of cobalt nanoparticles. Citrate/Co<sup>2+</sup> molar ratio was 10<sup>-3</sup>.

TEOS μL	NaBH <sub>4</sub> M	CoCl <sub>2</sub> M	[Citrate] M	Figure
85	4 x 10 <sup>-3</sup>	0.4	4 x 10 <sup>-4</sup>	Figure 28(a)
170	4 x 10 <sup>-3</sup>	0.4	4 x 10 <sup>-4</sup>	Figure 28(b)
340	4 x 10 <sup>-3</sup>	0.4	4x 10 <sup>-4</sup>	Figure 28(c)

**Table 6** Effect of TEOS/Co<sup>2+</sup> on shell thickness of the particles mentioned in Table 5.

[TEOS]/ [Co <sup>2+</sup> ]	[Citrate]/ [Co <sup>2+</sup> ]	Particle size, nm	Shell thickness, nm	Figure
5	10 <sup>-3</sup>	334±40	112-157	Figure 28(a)
10	10 <sup>-3</sup>	550±32	227-265	Figure 28(b)
20	10 <sup>-3</sup>	580±40	235-280	Figure 28(c)

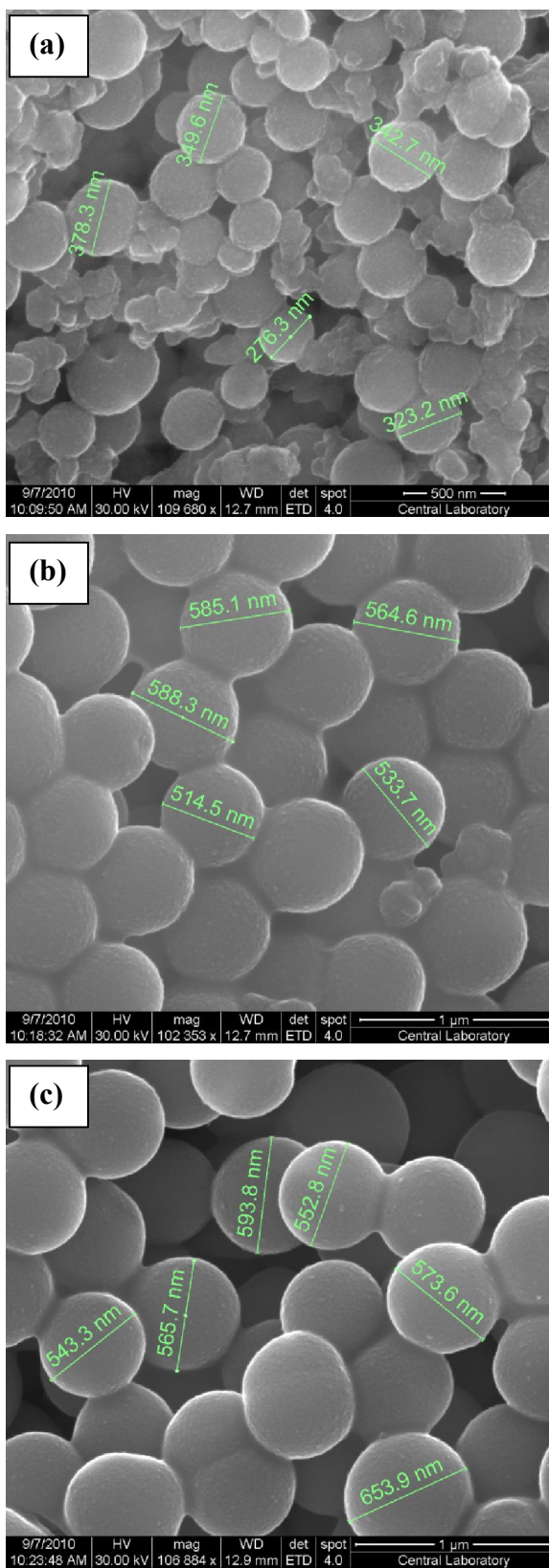


**Figure 28** FE-SEM images of the cobalt-silica core- shell particles, specified in Table 5 having  $[\text{TEOS}]/[\text{Co}^{2+}]$  ratio (a) 5; (b) 10; (c) 20.

**Table 7** Concentration of reagents used in silica coating process. Citrate/Co<sup>2+</sup> molar ratio was 10<sup>-3</sup>

TEOS μL	NaBH <sub>4</sub> M	CoCl <sub>2</sub> M	[Citrate] M	Figure
89	4 x 10 <sup>-3</sup>	0.4	4 x 10 <sup>-6</sup>	Figure 29(a)
170	4 x 10 <sup>-3</sup>	0.4	4 x 10 <sup>-6</sup>	Figure 29(b)
340	4 x 10 <sup>-3</sup>	0.4	4x 10 <sup>-6</sup>	Figure 29(c)

**Table 8** Effect of [TEOS]/[Co<sup>2+</sup>] on shell thickness of the particles mentioned in Table 7.

[TEOS]/ [Co <sup>2+</sup> ]	[Citrate]/ [Co <sup>2+</sup> ]	Particle size nm	Shell thickness, nm	Figure
5	10 <sup>-5</sup>	471 ± 64	160-320	Figure 29(a)
10	10 <sup>-5</sup>	657 ± 68	250-322	Figure 29(b)
20	10 <sup>-5</sup>	955 ± 123	351-500	Figure 29(c)

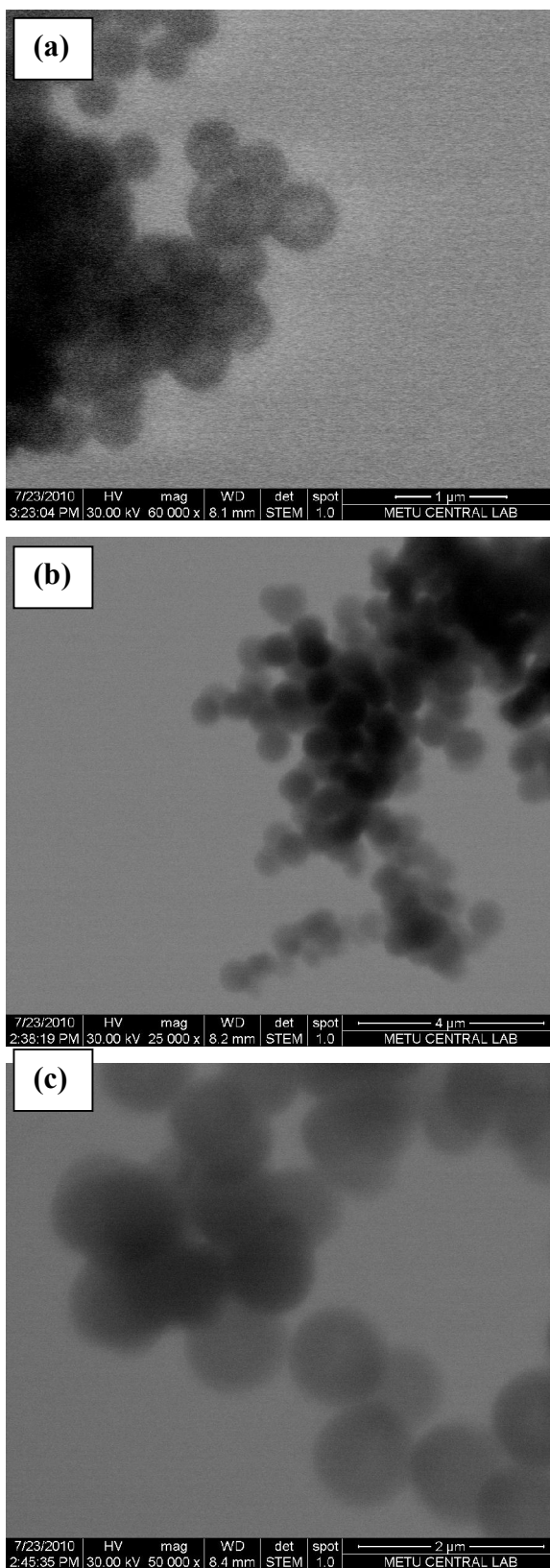


**Figure 29** S-TEM images of the cobalt-silica core-shell particles, specified in Table 7, having [TEOS]/[Co<sup>2+</sup>] ratio (a) 5; (b) 10; (c) 20.

Because lower citrate/Co<sup>2+</sup> ratio leads to more aggregated magnetic particles, size of core-shell particles were increased at citrate/Co<sup>2+</sup> molar ratio of 10<sup>-5</sup>, as observed in Figure 29.

As a result, while citrate/Co<sup>2+</sup> ratio determines the Co nanoparticles sizes, TEOS/Co ratio specifies shell thickness on core-particles. Throughout the silica coating processes, silica shell thickness was varied from 15 to 500 nm and the size of the cobalt particles were changed in between 30 to 90 nm. The FE-SEM images of the different size of core-shell cobalt-silica nanoparticles prepared by changing both TEOS/Co<sup>2+</sup> and citrate/Co<sup>2+</sup> molar ratio have been shown in Figure 30.

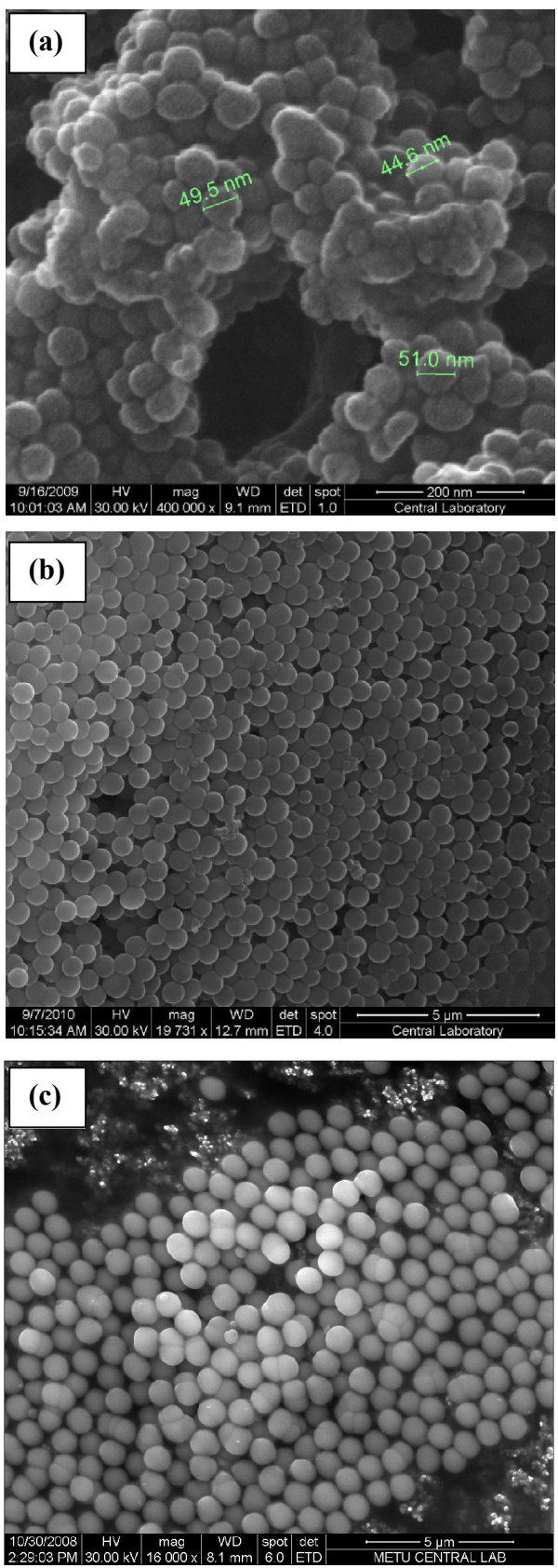


**Figure 30** FE-SEM images of core-shell cobalt-silica nanoparticles in case of  $[\text{TEOS}]/[\text{Co}^{2+}]$ : 10 with different citrate/ $\text{Co}^{2+}$  in which (a) $10^{-2}$ , (b) $10^{-3}$  and (c) $10^{-5}$ .

### 3.1.2.1 Washing Optimization of Silica Coated Cobalt Nanoparticles

Residual of reagents may affect the reaction condition, thus washing of the nanoparticles is necessary for further application. For optimization of washing procedure, three identical batches of cobalt-silica core-shell nanoparticles were prepared at [citrate]/[Co<sup>2+</sup>] ratio of 10<sup>-3</sup>. A different washing program was applied to each of them. Actually, the solvents used (ethanol, ethanol/water mixture and water alone) and their order of applications was the same. Only the number of washings with each solvent was different. Table 9 summarizes the steps followed in each case. At the end of washing steps, particles were dispersed in 100 ml water by the help of ultrasound agitation in order to separate particles homogenously. Subsequently their FE-SEM images were obtained, Table 10 states the preparation condition of the particles and the types of washing procedure applied.

**Table 9** Washing procedures of cobalt-silica nanoparticles.

<b>Washing procedure</b>	<b>Washing sequences</b>	<b>No.washing</b>	<b>Figure</b>
<b>1</b>	Ethanol ( <i>once</i> ) Ethanol and water mixture ( <i>once</i> ) Water ( <i>once</i> ) Ultrasound dispersion	<b>3</b>	Figure 31 (a)
<b>2</b>	Ethanol ( <i>twice</i> ) Ethanol and water mixture ( <i>once</i> ) Water ( <i>twice</i> ) Ultrasound dispersion	<b>5</b>	Figure 31 (b)
<b>3</b>	Ethanol ( <i>five times</i> ) Ethanol and water mixture ( <i>once</i> ) Water ( <i>five times</i> ) Ultrasound dispersion	<b>11</b>	Figure 31 (c)

**Table 10** Concentrations of reagents used in the preparation of the particles for the optimization of washing procedure.

<b>TEOS</b>	<b>CoCl<sub>2</sub></b>	<b>[Citrate]</b>	<b>[Citrate]/[Co<sup>2+</sup>]</b>	<b>Washing</b>	<b>Figure</b>
<b>μL</b>	<b>M</b>	<b>M</b>		<b>procedure</b>	
170	0.4	4 x 10 <sup>-4</sup>	10 <sup>-3</sup>	1	Figure 31(a)
170	0.4	4 x 10 <sup>-4</sup>	10 <sup>-3</sup>	2	Figure 31(b)
170	0.4	4x 10 <sup>-4</sup>	10 <sup>-3</sup>	3	Figure 31(c)

In Figure 31(a), shows FE-SEM images of the particles washed three times; they are detectable in general but some parts are cloudy. As can be seen in Figure 31(b), when the washing cycle was increased to five, the cloudiness disappeared and a clear image was obtained. Figure 31(c) illustrates the image of the particles that were washed eleven times. As can be understood from the last image, too much washing disturbed the particle morphology. Therefore, washing procedure 2 (Figure 31-b) was found optimum and it was applied to further studies.

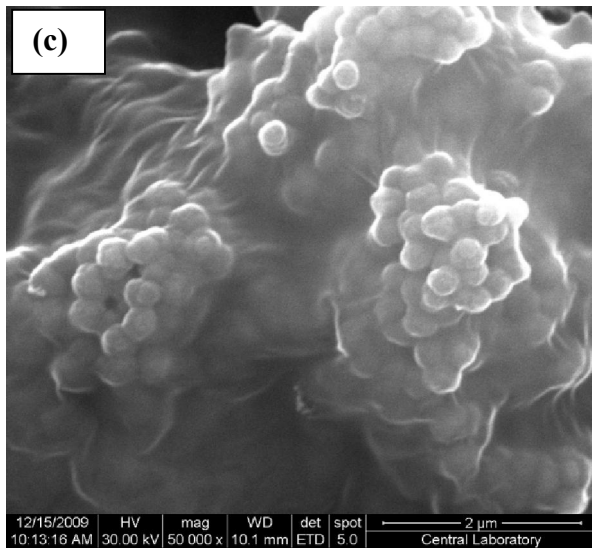
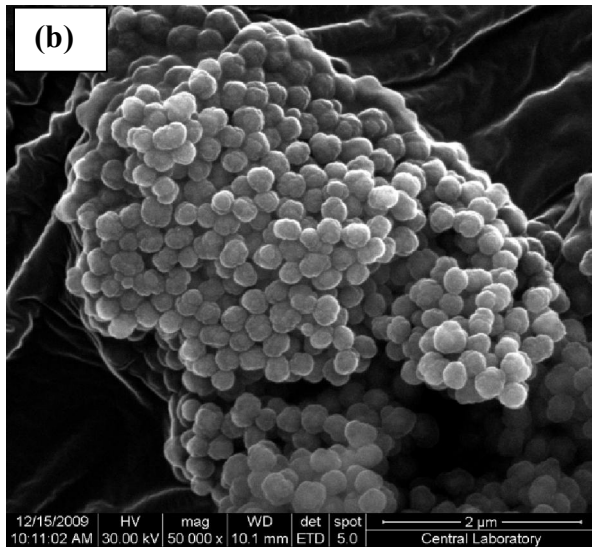
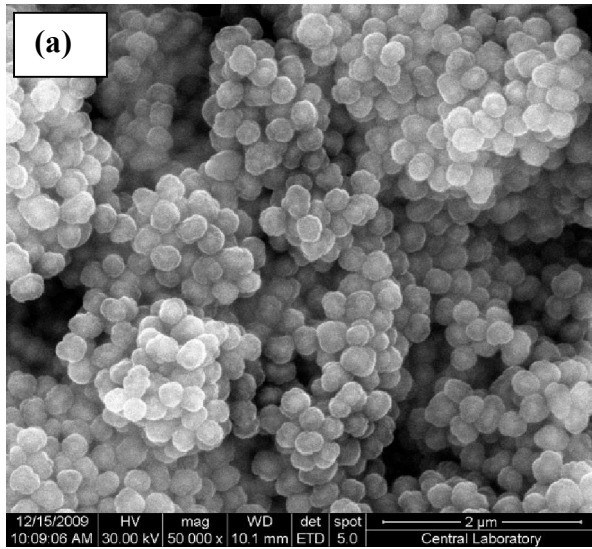


**Figure 31** Washing procedures for cobalt-silica preparation: (a) Procedure 1 (3 washing steps) (b) Procedure 2 (5 washing steps) (c) Procedure 3 (11 washing steps).

Drying makes particles more stable towards oxidation, since porous structure of silica shell gets thicker (Kobayashi, Horie, Konno, Rodríguez-González, & Liz-Marzán, 2003). In order to extend the shelf life, the optimized core-shell nanoparticles were dried and stored for several months. Powders displayed below had been prepared one year ago. As can be seen from Figure 32 they are still magnetic.



**Figure 32** Water dispersed and dried core-shell cobalt-silica nanoparticles.

### **3.2 Addition of Amine Functional Groups on Silica Coated Cobalt Nanoparticles**

Silica, not only protects the magnetic nanoparticles against degradation, but also provides a platform for further modification of the surface of the particles with various specific groups for the production of numerous functional nanocomposites. Amine functionalization also was carried out according to the Stöber reaction utilizing 3-aminopropyltriethoxy silane (APTS) as the sol-gel precursor (Figure 33). As given in the experimental section (2.5), silica coating was initiated with TEOS as precursor at basic condition. After three hours of aging, 3-aminopropyltriethoxy silane was added to the same reaction medium and thus, amine groups containing sol was

expected to deposit as a gel on the already formed silica sol-gel on the surface of Co nanoparticles. Two different [APTS] / [TEOS] ratio were used to adjust the amount of anchored amine groups on the surface for further modification with gold nanoparticles.

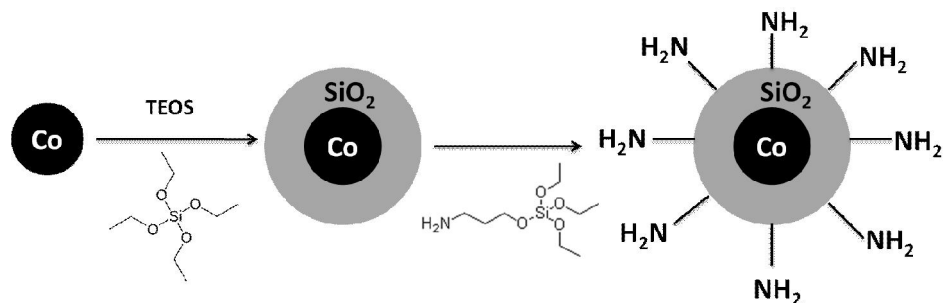


**Figure 33** Amine modification of core-shell cobalt-silica core-shell nanoparticles.

### 3.3 Gold Deposition on Amine Modified Cobalt-Silica Nanoparticles

Magnetic materials are usually used to collect the target in solution and concentrate them together under the influence of external magnetic field. Au nanoparticles, have wide applications in detection of the certain biomolecules due to their attractive electronic, optical, and catalytic properties. Therefore their combination will produce a multifunctional material having unique plasmonic and magnetic properties. Magnetic nanoparticles with Au shell are more stable in corrosive conditions and are easily functionalized through the strong interaction between Au and thiol groups. In this study gold particles coated magnetic cobalt-silica nanoparticles were prepared. Gold nanoparticles were prepared separately and attached to the surface of cobalt-silica nanoparticles through the amine anchor group. The plasmonic properties of the prepared composites were examined by utilizing Raman spectroscopy.

#### 3.3.1 Preparation of Gold Nanoparticles

Au nanoparticles were prepared through citrate reduction method and these particles were used without washing. Their characterization was done by using FE-SEM and Uv-vis spectrometry. As depicted in Figure 34, the gold colloid solution had bright

red color having absorbance at 520 nm. As can be seen from the Figure 35, the size of the particles was in the range of 10-15 nm. The EDX result, exhibited in Figure 36, shows the composition of the particles as pure gold.

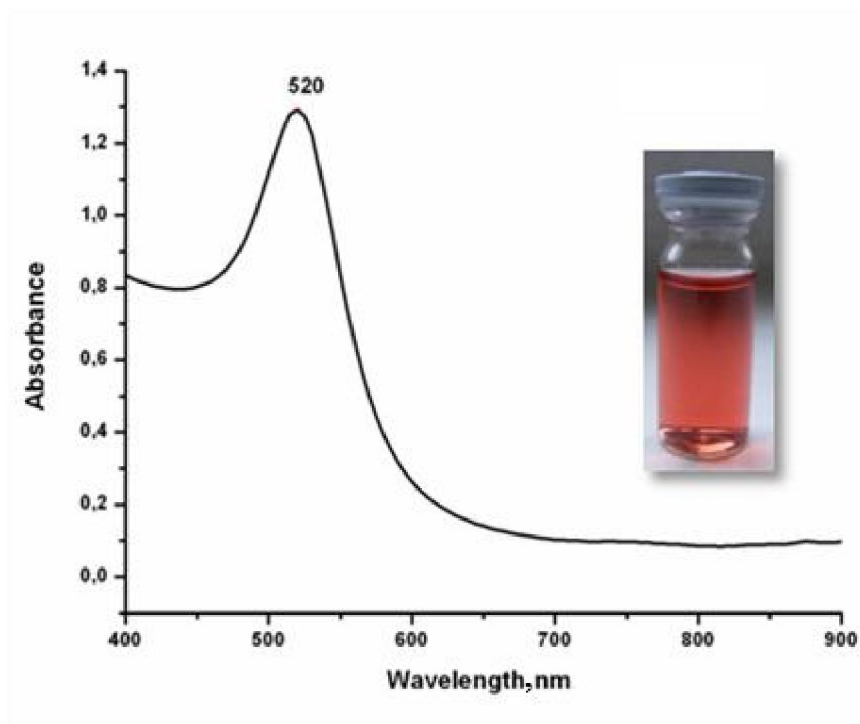


**Figure 34** UV-vis spectrum of Au nanoparticles.

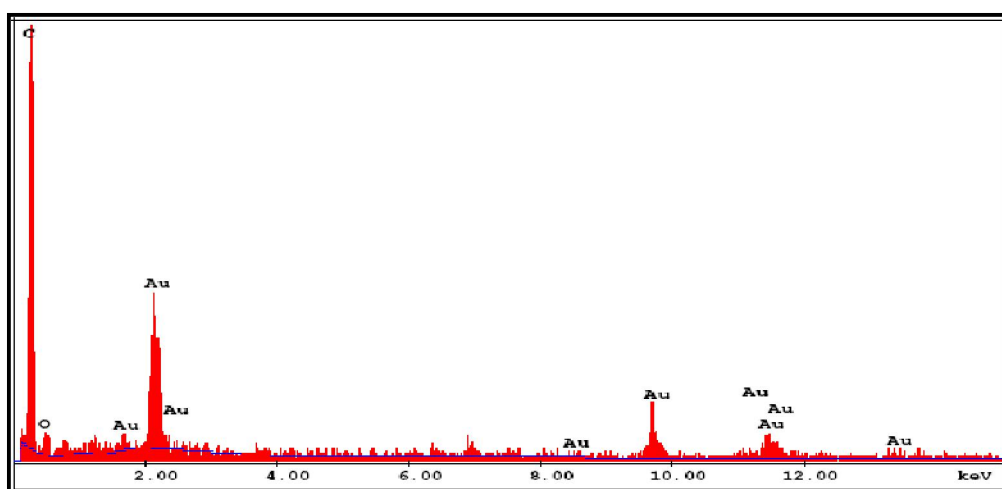
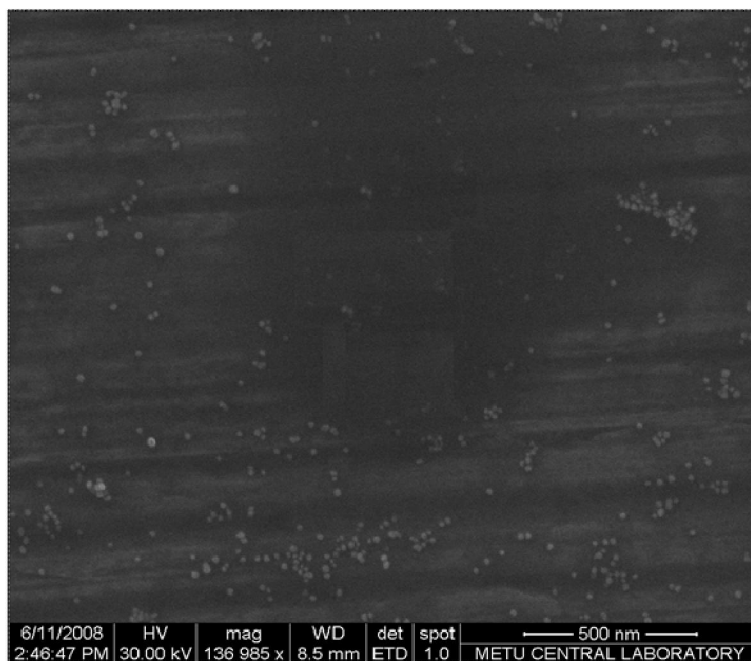


**Figure 36** EDX pattern of Au nanoparticles.

### 3.3.2 Preparation of Gold Modified Cobalt-Silica Nanoparticles

A typical procedure for the synthesis of the monodisperse Au nanoparticles decorated cobalt-silica nanocomposites is shown in Figure 37. Preparation and amine

modification of the Co nanoparticles were already discussed in the previous sections. For the decoration of thus prepared core-shell cobalt-silica nanoparticles with the citrate stabilized Au nanoparticles, two solutions were mixed. The amine groups ( $-NH_2$ ) present on the surface was expected to show strong affinity toward the gold nanoparticles and append them covalently onto the silica surface. The citrate coated Au seeds are negatively charged.

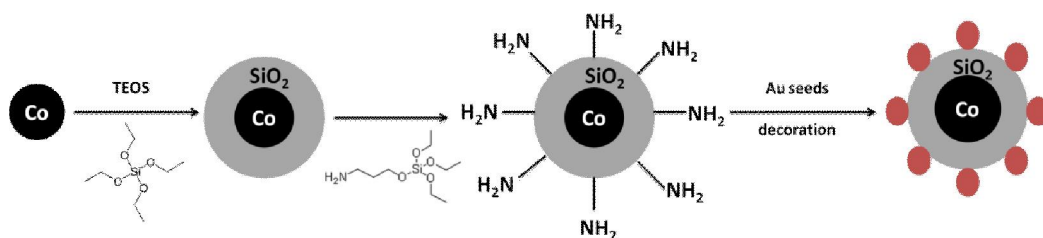


**Figure 37** A typical synthesis procedure of gold modified cobalt-silica nanocomposites.

The FE-SEM images of the nanoparticles at the stages of formation of Au decoration on amine modified cobalt-silica nanoparticles were illustrated in Figure 38. The average particle size of the resultant Au decorated core-shell cobalt-silica nanocomposites was about 400-500 nm.

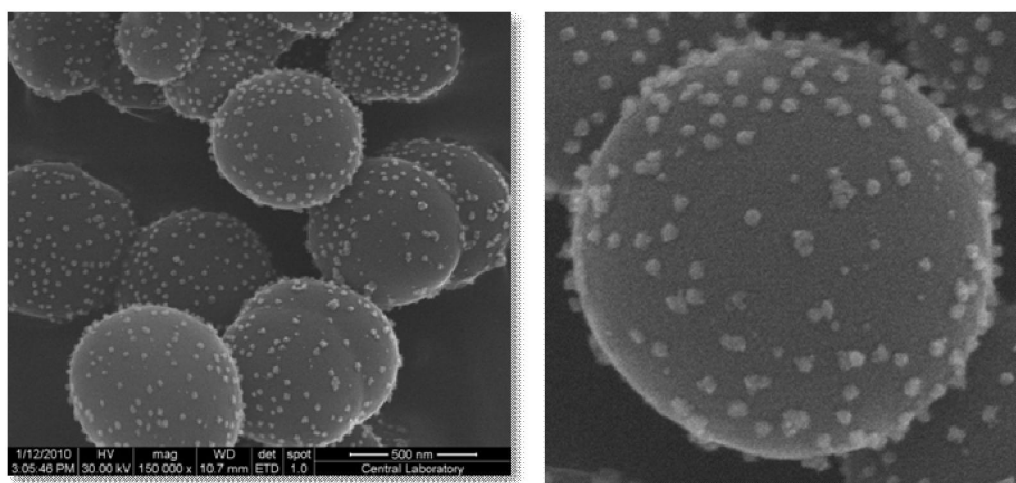


**Figure 38** FE-SEM images of gold modified cobalt-silica nanocomposite.

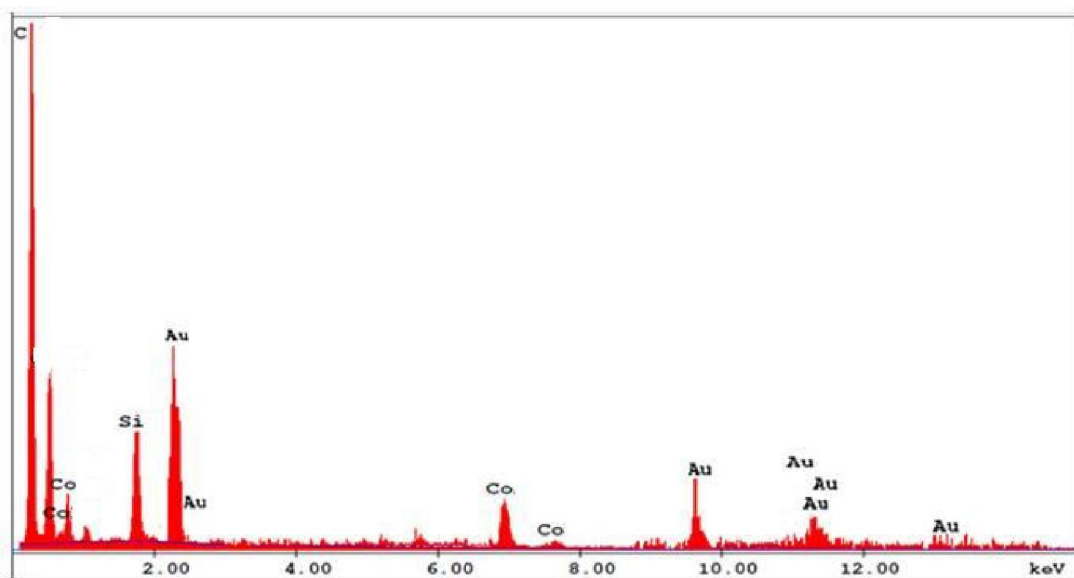


**Figure 39** EDX spectrum of gold modified cobalt-silica nanocomposite.

The components of the nanocomposite are Co, Si, O, Na and Au shown in EDX spectrum in Figure 39. The C signal is attributed to the FE-SEM grid while Na peak is coming from trisodiumtricitrate.

### **3.3.3 Optical Properties of Gold Nanoparticles Decorated Cobalt-Silica Core-Shell Nanoparticles**

UV-Vis spectra of Au decorated cobalt-silica, Co and Au nanoparticles all dispersed in distilled water are shown in Figure 40. The aqueous solutions of gold colloid have an at 520nm (Figure 34), whereas cobalt nanoparticles have no absorption peak. The strong optical extinction of Au nanoparticles is due to a collective oscillation of the free electrons at visible region known as the plasmon resonance. In addition to the dielectric functions of the metal and the embedding medium, the optical resonance is also a function of the size and the shape of the gold particle (Oldenburg, Westcott, Averitt, & Halas, 1998; Salgueirino-Maceira & Correa-Duarte, 2006) The gold modified cobalt-silica nanocomposites exhibited absorption peak at 540 nm. The

shifting in the optical spectra was probably due to the strong interparticle interaction and the coupling of the surface plasmon of neighboring particles (Oldenburg, Westcott, Averitt, & Halas, 1998)

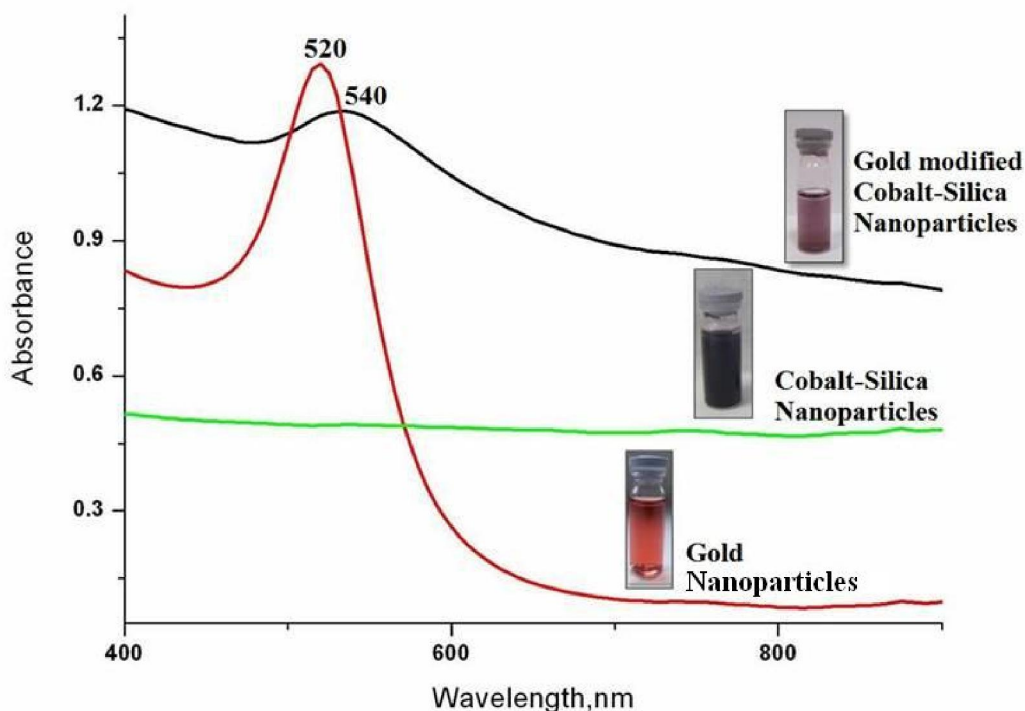


**Figure 40** UV-Vis spectra of Au modified cobalt-silica nanocomposites, Au and Co colloids dispersed in distilled water. The insets show the photograph of the samples.

The proper duration of mixing for amine coated cobalt-silica and gold nanoparticles were examined. Duration of mixing was changed from 1 to 120 minutes. The changes in the gold nanoparticle coating performance were followed by the absorption of surface plasmon at 540 nm, Figure 41.

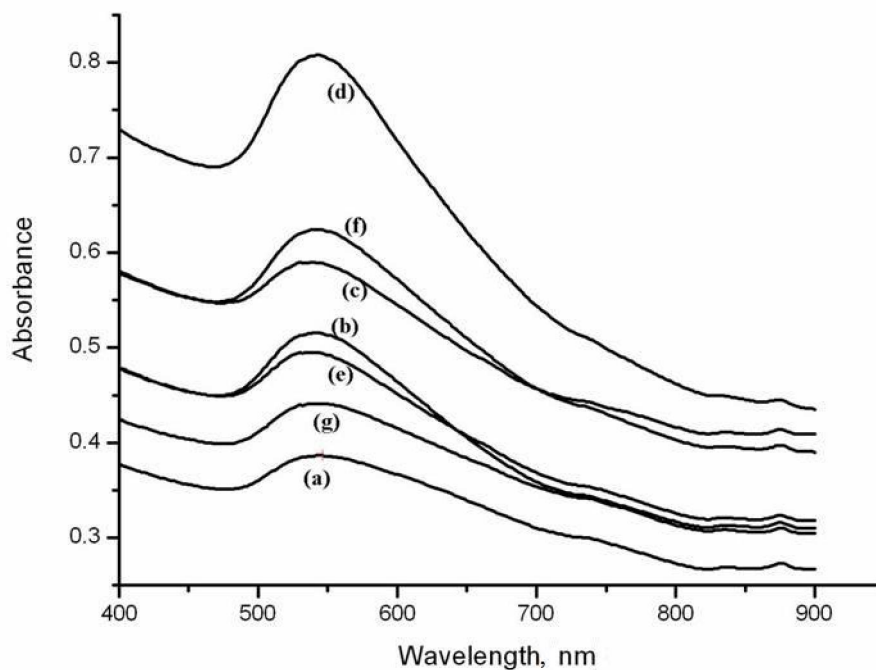


**Figure 41** Effect of reaction time on Au decoration on cobalt-silica nanoparticles surface, duration in minutes; (a) 1, (b) 5, (c) 15,(d) 30, (e) 45, (f) 60 and (g) 120.

As can be seen from the Figure, the highest Plasmon absorption was obtained when 30 minutes reaction time was applied. Hence, 30 minutes was selected as the optimum duration for mixing.

### 3.3.3.1 Effect of Au/Cobalt-Silica Volume Ratio on the Gold Decoration of Cobalt-Silica Nanoparticles

The effect of Au / cobalt-silica volume ratio on the coating of Au nanoparticles onto the surface of cobalt-silica nanoparticles was examined at two different TEOS/APTS (amine concentrations) as presented in Table 11.

**Table 11** Change in APTS/TEOS volume ratio during silica and amine coating on the surface of cobalt-silica nanoparticles.

	<b>APTS</b>	<b>TEOS</b>	<b>APTS/TEOS</b>	<b>[Citrate]</b>	<b>Figure</b>
	<b>μL</b>	<b>μL</b>		<b>M</b>	
<b>Low</b>	56	170	1/3	$4 \times 10^{-4}$	51
<b>High</b>	170	170	1	$4 \times 10^{-4}$	53

### 3.3.3.1.1 Gold Decoration of the Amine Coated Cobalt-Silica Particles at Low APTS/TEOS Volume Ratio

Au / cobalt-silica (v/v) volume ratio was changed in between 0.1 to 2 at APTS /TEOS volume ratio of 1/3 (low amine concentration on the surface), Table 11. Figure 42 illustrates UV-Vis spectra of the surface Plasmon of gold nanoparticles on the surface of amine coated cobalt-silica nanoparticles. As can be seen in the Figure 42, as the amount of Au nanoparticle increases the Plasmon absorption at 540 nm also increases.

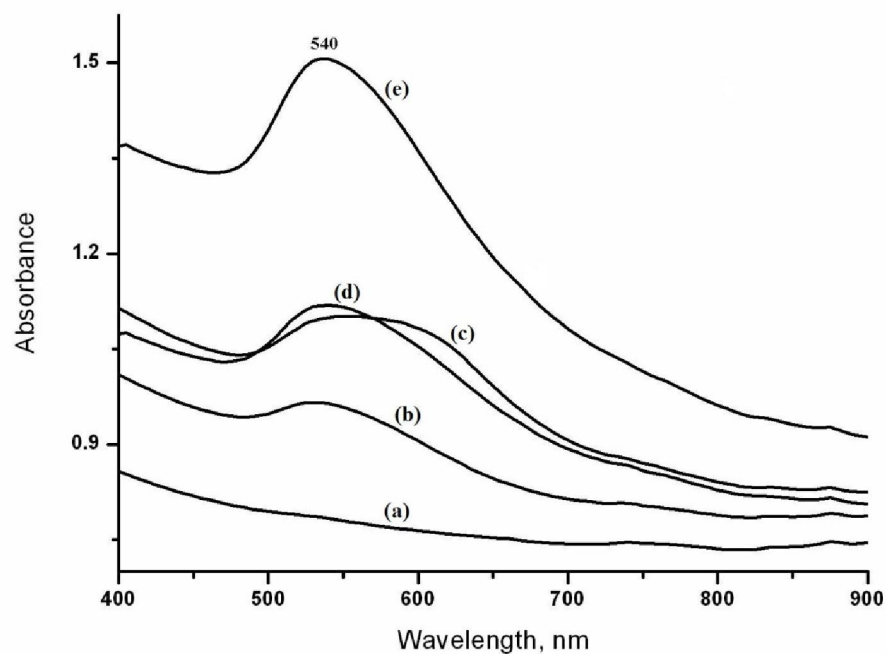


**Figure 42** UV-Vis spectra of gold modified cobalt-silica nanoparticles prepared at various Au / cobalt-silica volume ratio. APTS /TEOS volume ratio was 1/3 (low amine deposition) and Au / cobalt-silica volume ratio: (a) 0.1, (b) 0.25, (c) 0.5, (d) 1 and (e) 2.

Gold deposition on the surface was observed by FE-SEM as shown in Figure 43 (a,b,c,d,e).

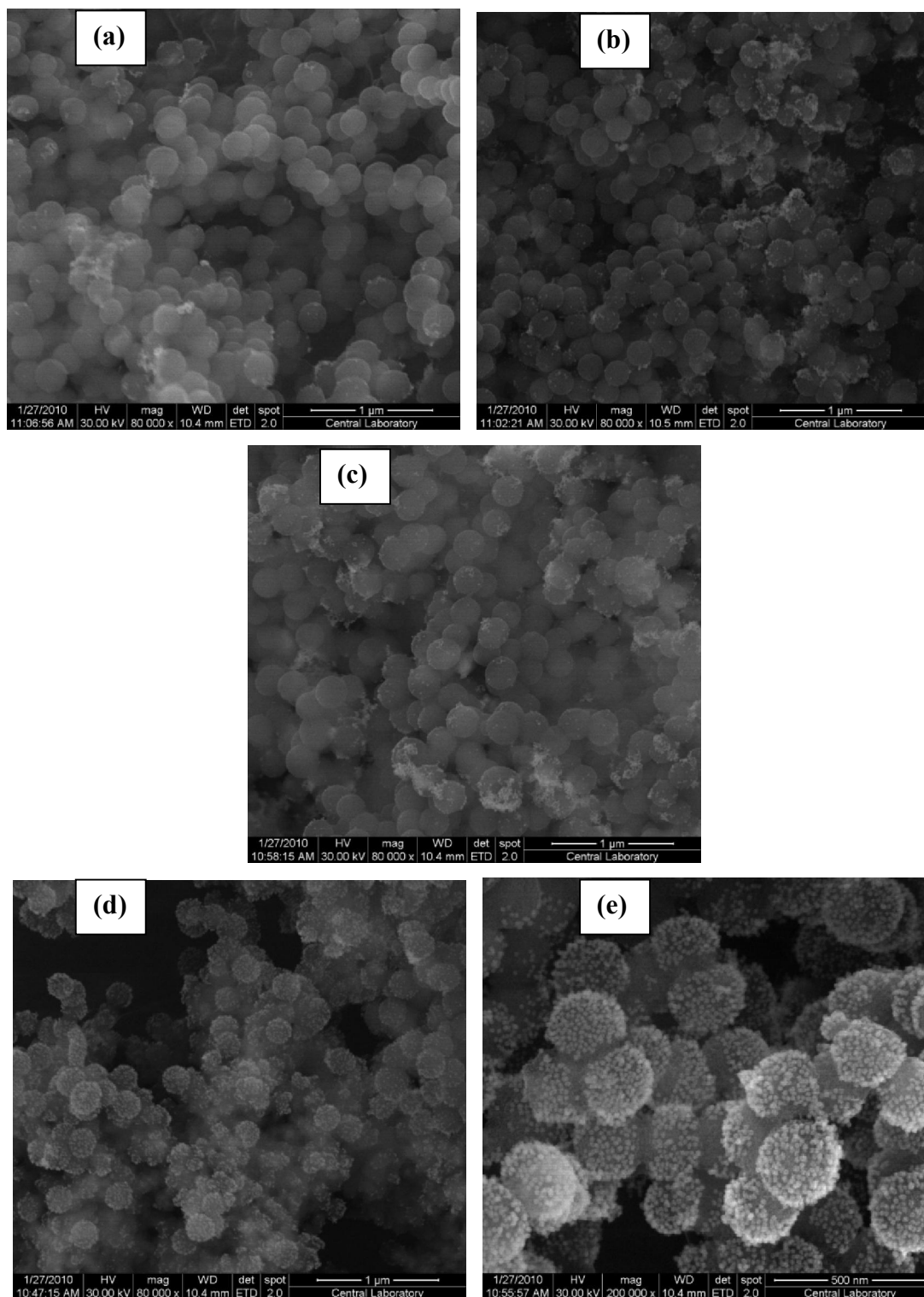


**Figure 43** FE-SEM images of gold modified cobalt-silica nanoparticles prepared at various Au/cobalt-silica volume ratio. APTS/TEOS volume ratio was 1/3 (low amine deposition) Au / cobalt-silica volume ratio: (a) 0.1, (b) 0.25, (c) 0.5, (d) 1 and (e) 2.

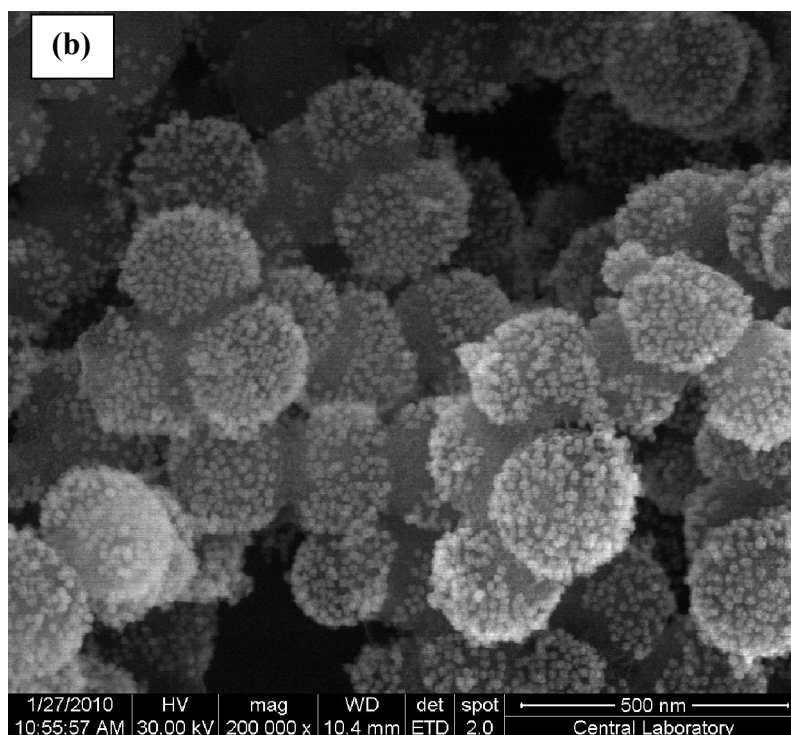
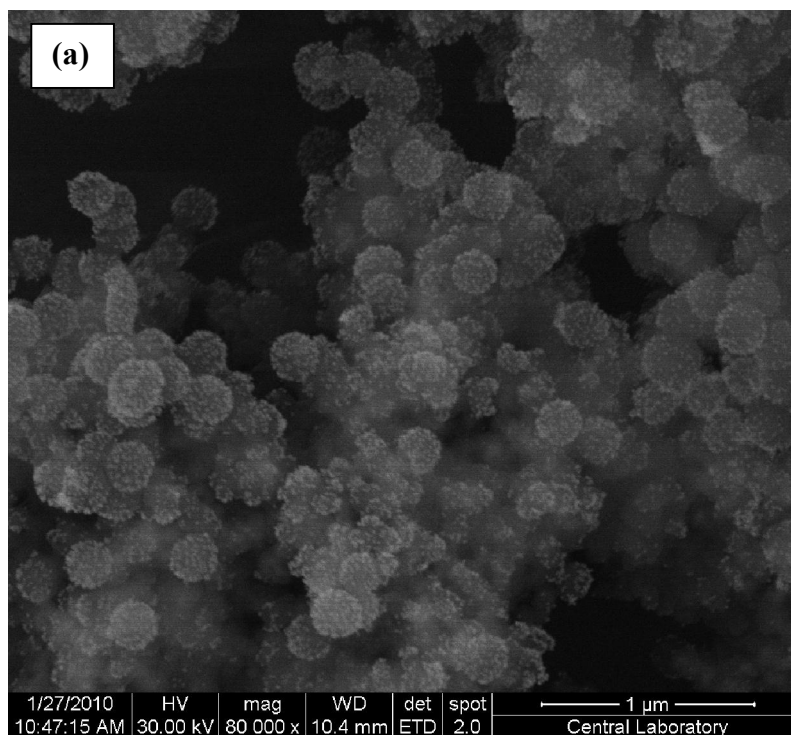


**Figure 44** Larger scale FE-SEM images of gold modified cobalt-silica nanoparticles prepared at Au / cobalt-silica volume ratio of 1 and 2 . APTS /TEOS volume ratio was 1/3 (low amine deposition) Au / cobalt-silica volume ratio: (a) 1, (b) 2

When Au/ cobalt-silica ratio was increased, gold deposition on the surface was also increased. Figure 44 (e) corresponds to Au / cobalt-silica volume ratio of 2. As can be seen clearly from Figure 44 (e), gold nanoparticles were arranged in an ordered way. These observations were supporting the results obtained by Uv-vis measurements. Hence Au / cobalt-silica volume ratio of 2 was chosen as the optimum ratio in the usage of low amine deposited cobalt-silica nanoparticles.

#### **3.1.1.1.1 Gold Decoration of the Amine Coated Cobalt-Silica Particles at High APTS/TEOS Volume Ratio**

In this case equal amounts of APTS and TEOS were used ( APTS/ TEOS was 1) and it was expected that on the silica surface more amine groups were deposited. The gold decoration efficiency at this condition were examined again by varying the Au / cobalt-silica volume ratio in the range of 0.1-2 and followed by Uv-vis and FE-SEM measurements.

When we analyze the UV-Vis results, Figure 45, Au / cobalt-silica volume ratio of 0.1 and 0.25, were slightly different than the ones at low amine coating. In the case of Au /cobalt-silica volume ratio of 0.5, 1 and 2, on the other hand, absorbance peaks were broadened and red shifted. This was indicating the accumulation of bigger Au nanoparticles or agglomerates on the surface. FE-SEM images, Figure 46 (d,e), were also confirming this observation. When the amount of gold nanoparticles was increased, high amount of Au nanoparticles were accumulated and formed large agglomerates on the surface and consequently caused deformation of the structure.

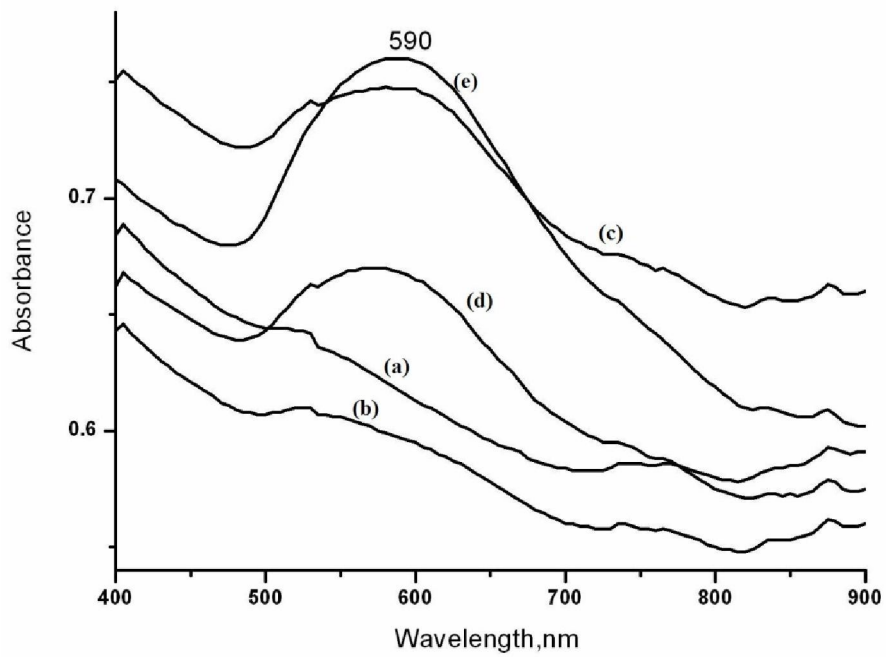


**Figure 45** UV-Vis spectra of gold modified cobalt-silica nanoparticles prepared at various Au / cobalt-silica volume ratio. APTS /TEOS volume ratio was 1 (high amine deposition) and Au / cobalt-silica volume ratio: (a) 0.1, (b) 0.25, (c) 0.5,(d) 1 and (e) 2.

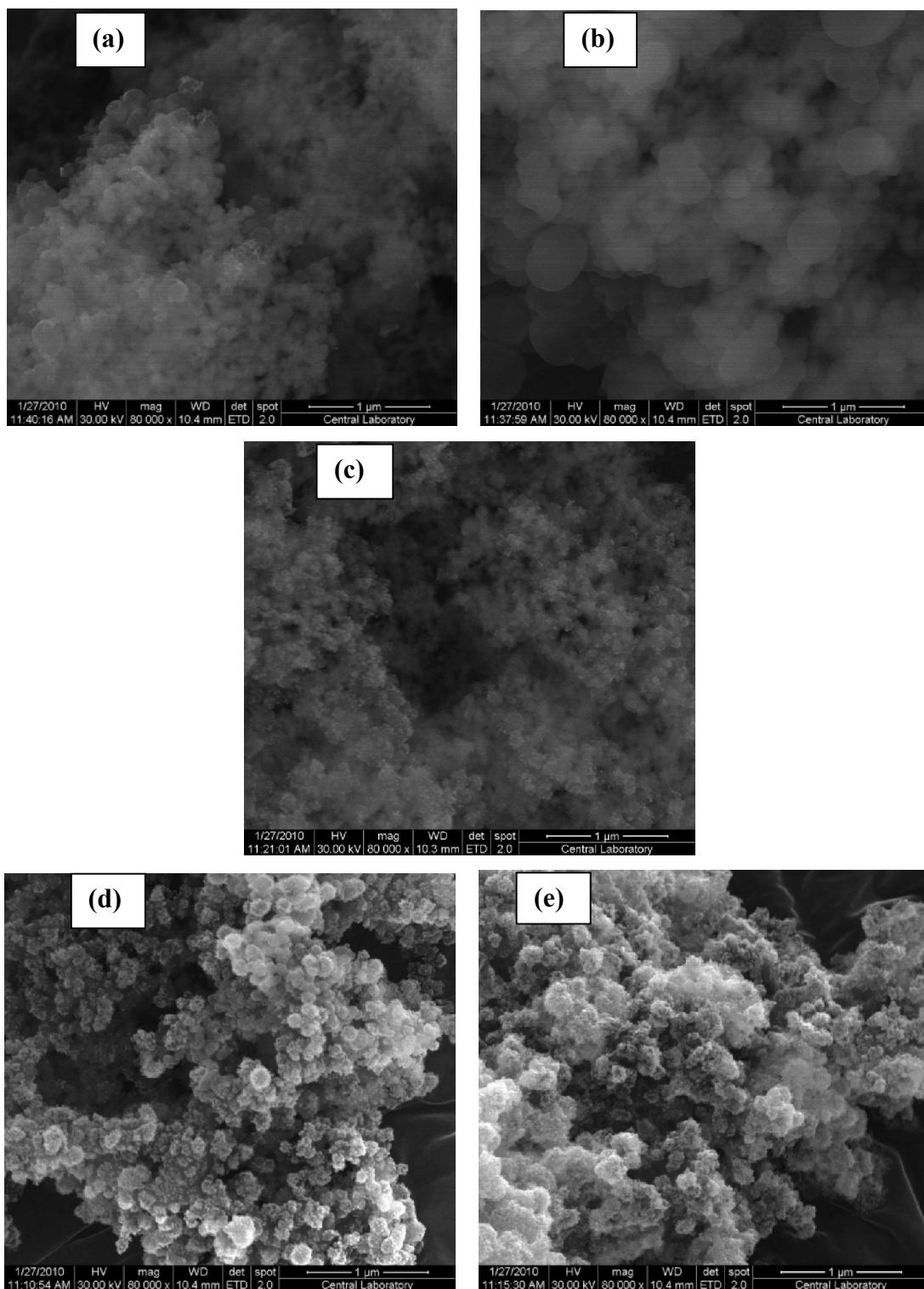


**Figure 46** FE-SEM images of gold modified cobalt-silica nanoparticles prepared at various Au / cobalt-silica volume ratio. APTS /TEOS volume ratio was 1 (High amine deposition) Au / cobalt-silica volume ratio: (a) 0.1, (b) 0.25, (c) 0.5, (d) 1 and (e) 2.

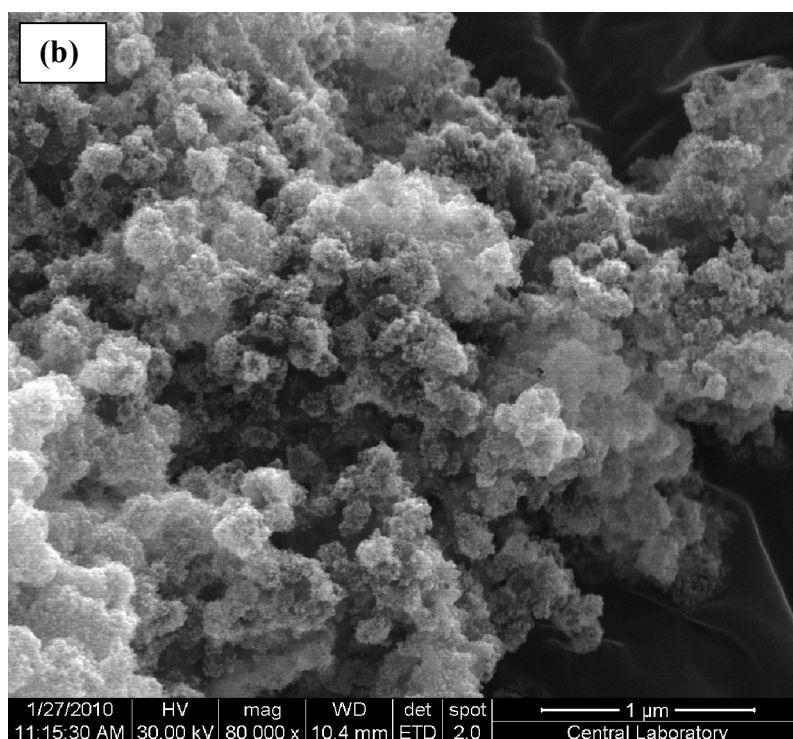
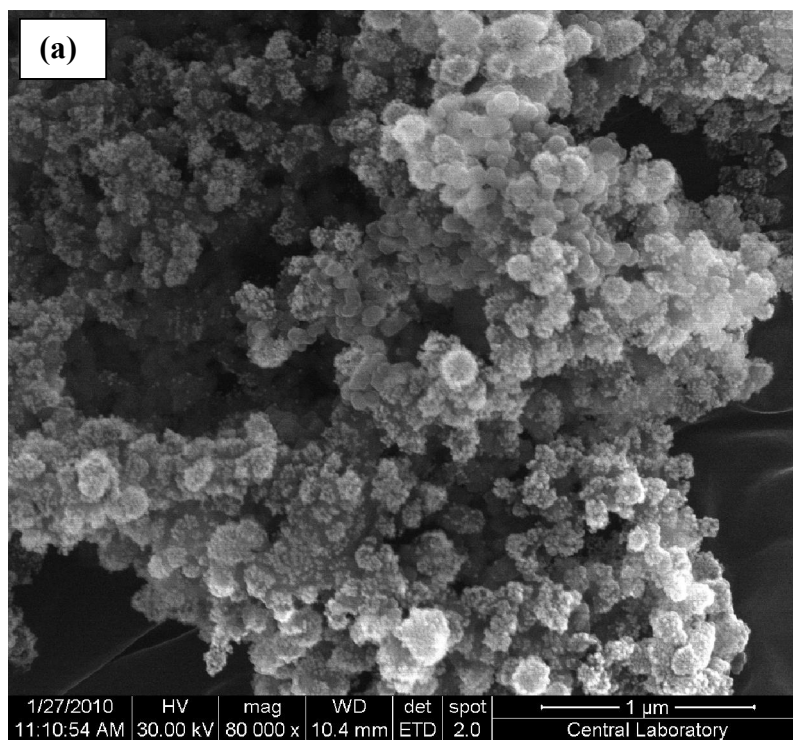


**Figure 47** Larger scale FE-SEM images of gold modified cobalt-silica nanoparticles prepared at Au / cobalt-silica volume ratio of 1 and 2 . APTS /TEOS volume ratio was 1 (high amine deposition) Au / cobalt-silica volume ratio: (a) 1, (b) 2.

In Figure 47 large aggregates of gold nanoparticles can be easily seen. The aggregate formation was correlated to the presence of the higher number of amine groups on the surface that could accommodate larger amount Au nanoparticles. However it is difficult to obtain reproducible aggregate formation. Therefore in the following SERS application studies we preferred to use gold modified cobalt-silica nanoparticles prepared with APTS /TEOS and Au /cobalt-silica volume ratios of 1/3 and 2 respectively.

### 3.2 Magnetic Behavior of the Prepared Particles

#### 3.2.1 Magnetic Behavior of Cobalt Nanoparticles

Magnetic properties of the particles were simply inspected by their collection kinetic under the influence of external magnetic field for each batch. Illustration of 5, 10 and 20 seconds of external magnetic field applications to a cobalt colloid was shown in Figure 48. As can be seen, particle collection was complete after 20s, leaving almost a clear solution.

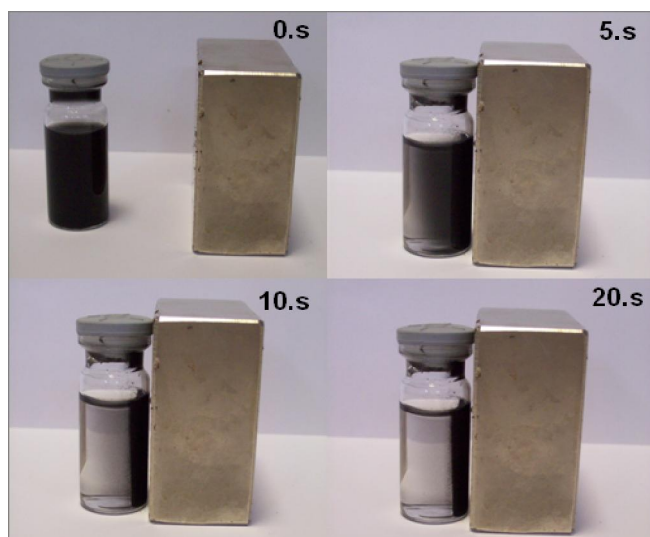


**Figure 48** The collection kinetic of Co nanoparticles under the influence of external magnetic field (1.6 T) at various time intervals (5, 10, 20 seconds).

Hysteresis curve of Co nanoparticles having size range 80-90 nm recorded at 300 K illustrated in Figure 49 shows. The coercivity value was 16.154 Oe and the saturation magnetization was 10 emu/g.

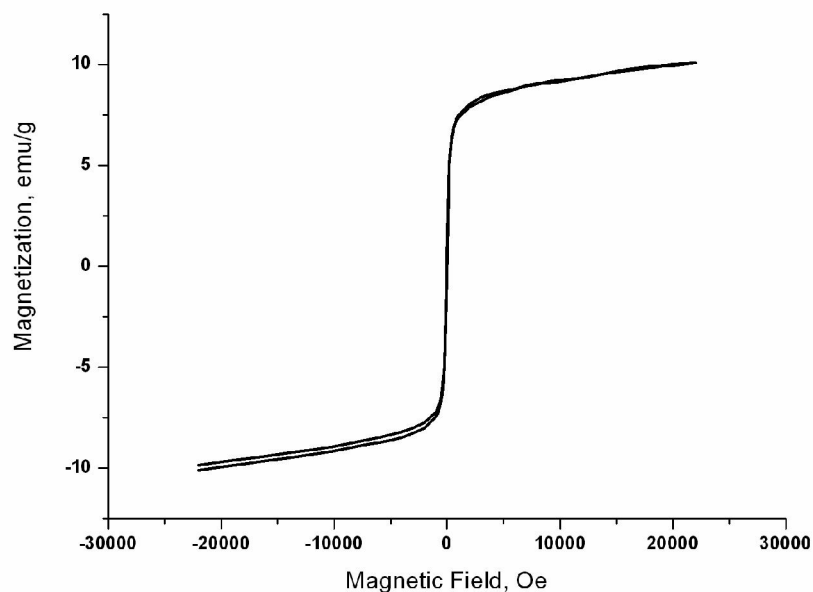


**Figure 49** Hysteresis curve of cobalt nanoparticles recorded at 300 K.

### 3.2.2 Magnetic Behavior of Cobalt-Silica Nanoparticles

To examine the change in the magnetization of Co nanoparticles after silica coating, the simple collection rate experiment under magnetic field was applied. Cobalt-silica nanoparticles were collected magnetically when external magnet is next to the solution as depicted in the Figure 50. However, the collection was not as rapid as in the case of Co nanoparticles; it takes 90 seconds to obtain clear solution behind the particles instead of 20s.

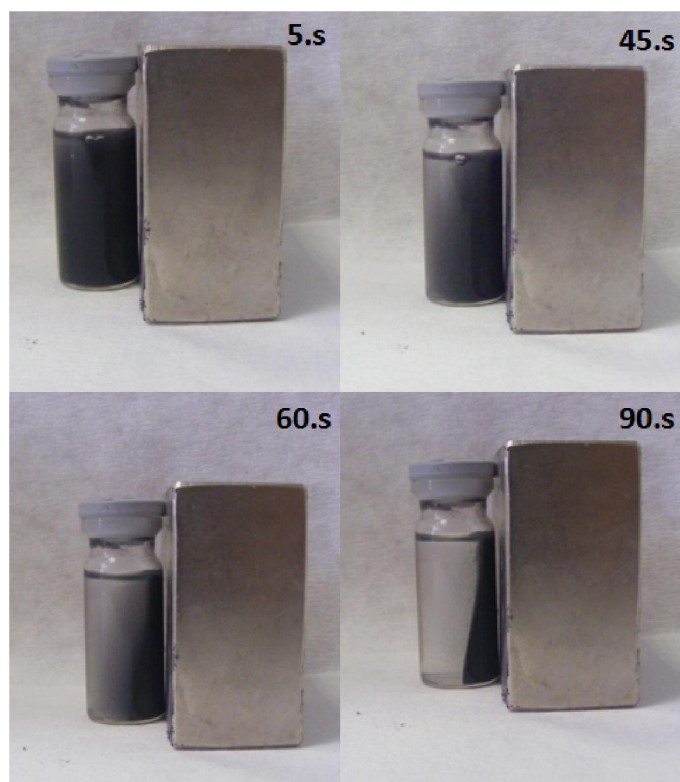


**Figure 50** Cobalt-silica nanoparticles under external magnetic field.

The hysteresis curve for cobalt-silica core-shell nanostructures is given in Figure 51. Coercivity and saturation magnetization value for the core-shell particles were 15.32 Oe and 1.5 emu/g value respectively. Compared to Co nanoparticles, magnetization value (emu/g) decreases due to the presence of nonmagnetic silica coating.

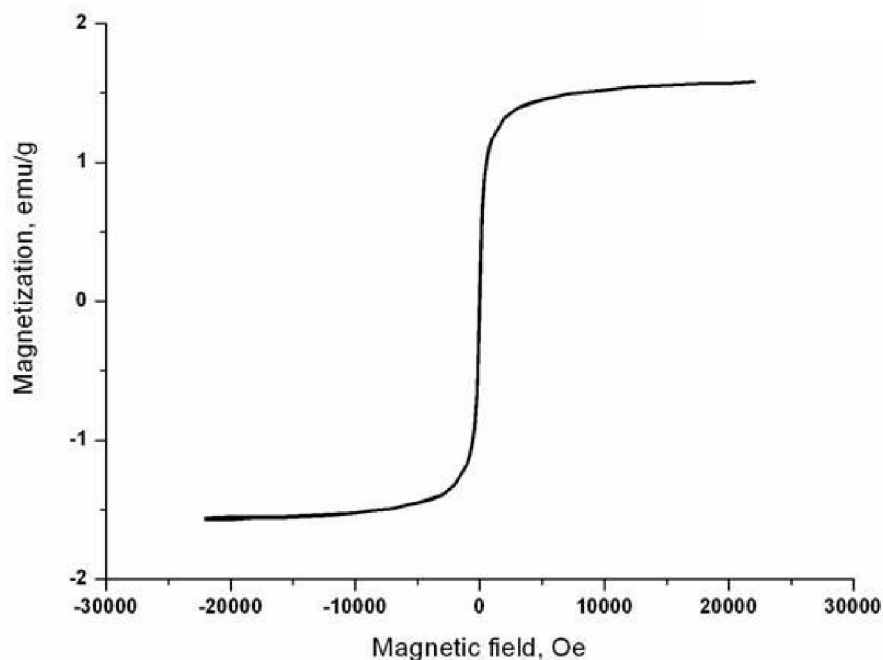


**Figure 51** The hysteresis curve for cobalt-silica core-shell nanostructures.

### **3.2.3 Magnetic Behavior of Gold Modified Cobalt-Silica Nanocomposites**

To understand magnetization of Au modified cobalt-silica nanoparticles, they were also prepared for VSM measurement, however, drying in an oven destroyed our modified particles and we could not observe the saturation magnetization of them. Magnetization behavior of Au modified cobalt-silica particles were exhibited in Figure 52 and they are magnetic. However, collection under magnet takes longer than pure Co and also cobalt-silica particles. Magnetization of cobalt-silica particles is enough for further experiment.

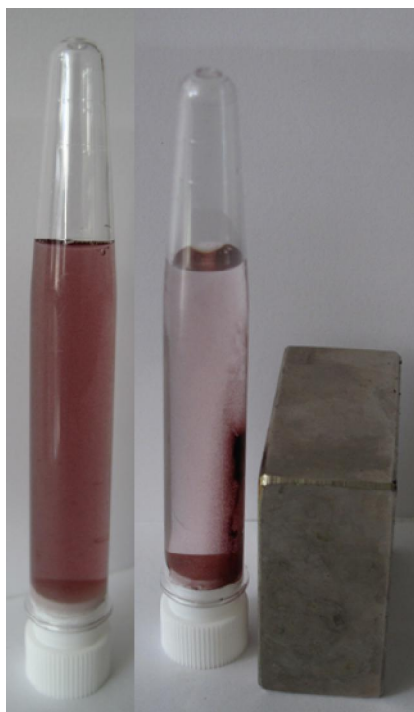


**Figure 52** Magnetization behavior of Au modified cobalt-silica nanoparticles.

### **3.3 Application of Gold Modified Cobalt-Silica as SERS Substrate**

Au modified cobalt-silica particles multicomponent is thought to be useful as SERS substrate because of the large number of irregular nanoscale gold particles arranged randomly and the gaps formed between these gold nanoparticles.

SERS technique is very popular in today's research technology; therefore there is a wide variety of SERS substrates and SERS media. Colloid of metal is important member of the substrates which can be found as nanoparticles of various sizes. Silver colloid and gold colloid are often used to produce SERS-active substrate. There are several advantages in using colloid hydrosols, such as simple preparation, simple characterization by UV-absorption.

It is reported that there are two major mechanisms that contribute to the enhancement effect: one is the electromagnetic effect associated with large local fields due to resonances occurring in the microstructures on the metal surface, the other is the chemical effect involving a scattering process associated with chemical

interaction between the molecule and the metal surface. The enhancement due to the former is believed to be a few orders of magnitude more than the latter (Zhou, Chao, Li, Xu, Wu, & Zheng, 2007).

### 3.3.1 SERS Effect of Au Modified Cobalt-Silica Nanoparticles

For SERS studies, hundred micro liters of solution of Raman dye in the range between  $10^{-2}$  and  $10^{-6}$  M was mixed with same volume of Au modified cobalt-silica nanocomposites. Then the mixtures were dropped on glass slide and dried at room temperature. SERS measurements were performed using a micro-Raman system equipped with a thermoelectrically cooled CCD detector. Raman spectra of solid BCB, R6G and 4-MBA were depicted in Figure 53, Figure 54, Figure 55 respectively.

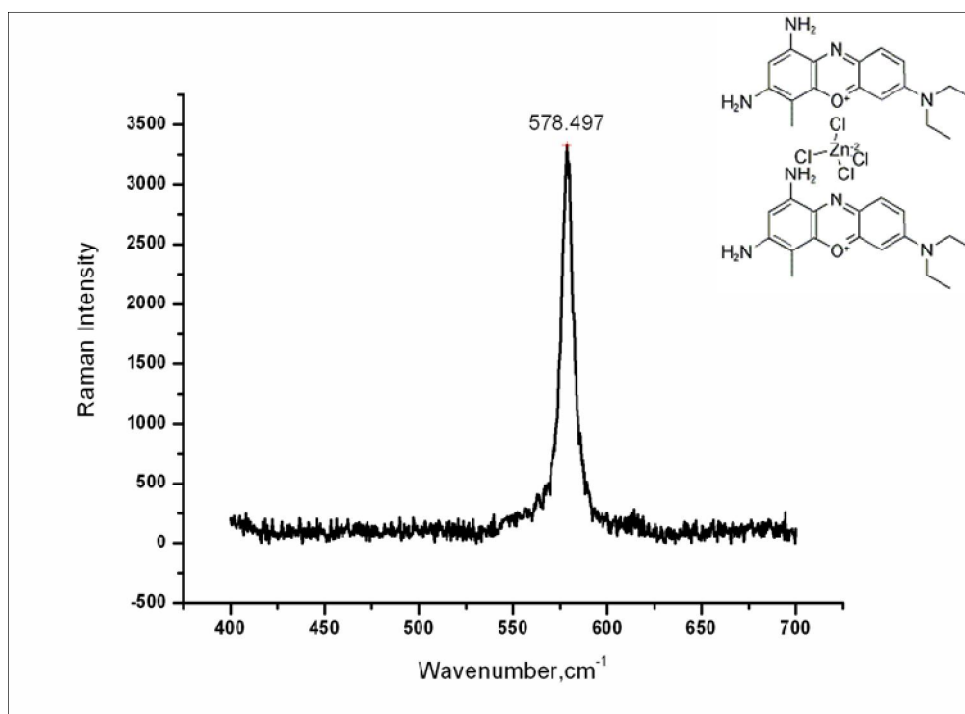


**Figure 53** Raman spectrum of solid BCB. Insert is the molecular formula of BCB.

The peak for the BCB appears clearly at  $578\text{ cm}^{-1}$ . The strong Raman band at  $580\text{ cm}^{-1}$  has been assigned to aromatic C-C bending mode (Yeo, Schmid, Zhang, & Zenobi, 2007).

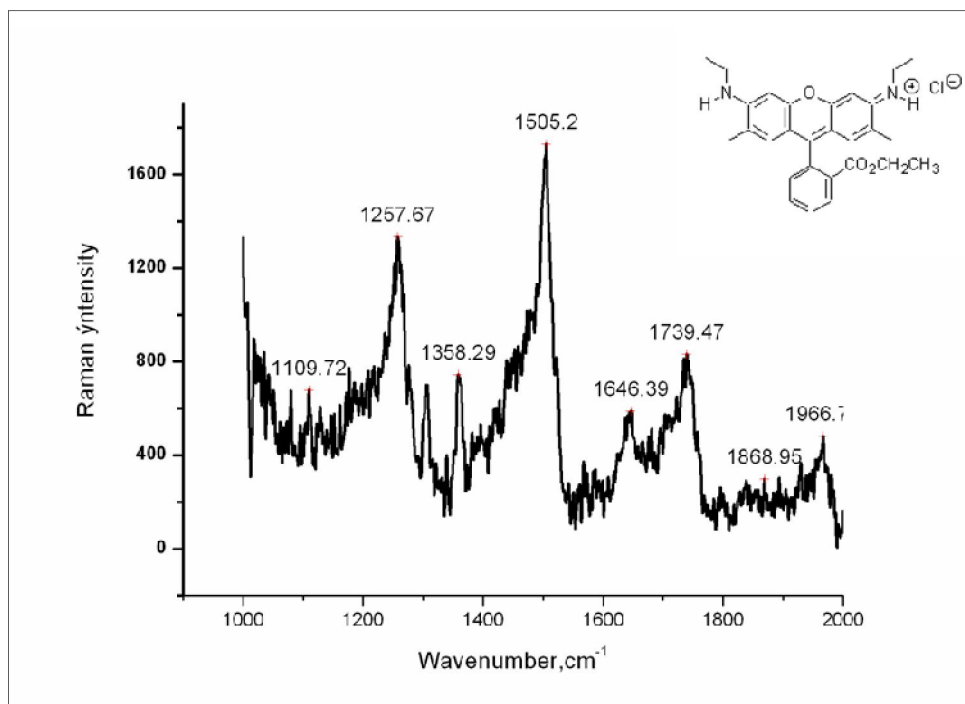


**Figure 54** Raman spectrum of solid R6G. Insert is the molecular formula of R6G.

The peak at about  $1188\text{ cm}^{-1}$  is associated with C-C stretching vibrations, while the peaks at about  $1303$ ,  $1356$ , and  $1575\text{ cm}^{-1}$  are associated with aromatic C-C stretching vibrations (Yeo, Schmid, Zhang, & Zenobi, 2007).

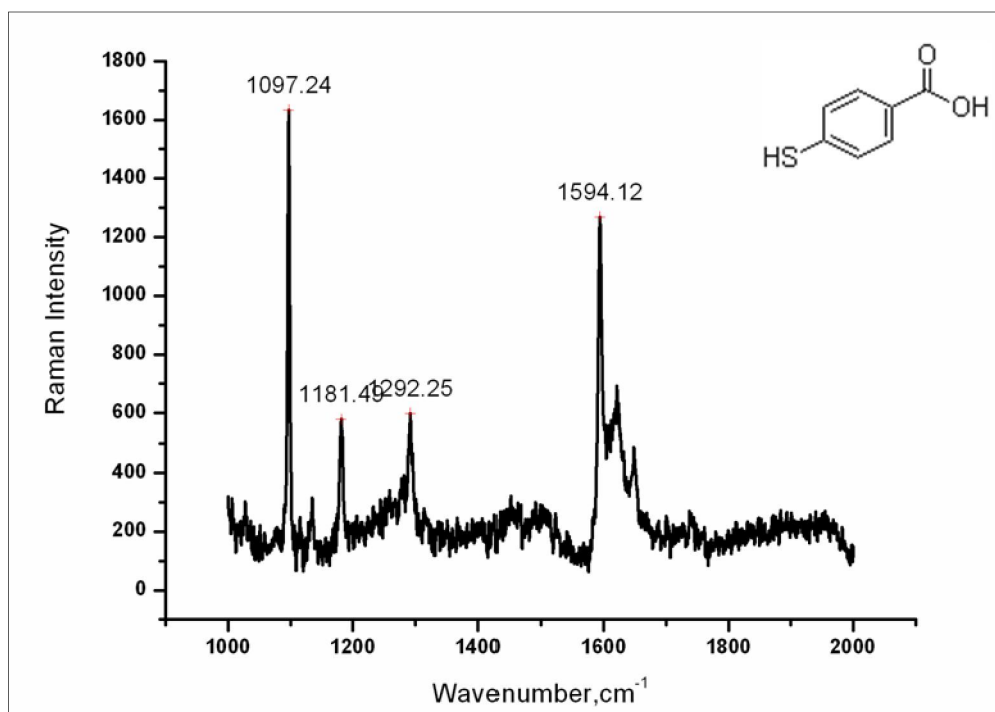


**Figure 55** Raman spectrum of solid 4-MBA. Insert is the molecular formula of 4-MBA.

The spectrum of solid 4-MBA is dominated by the strong bands at about 1590 and 1080 cm<sup>-1</sup>, which have been assigned to aromatic ring vibrations (Michota & Bukowska, 2003).

The SERS spectra of 10<sup>-5</sup>M BCB and 10<sup>-4</sup>M R6G and 4-MBA were acquired by using Au modified cobalt-silica colloid as a substrate.

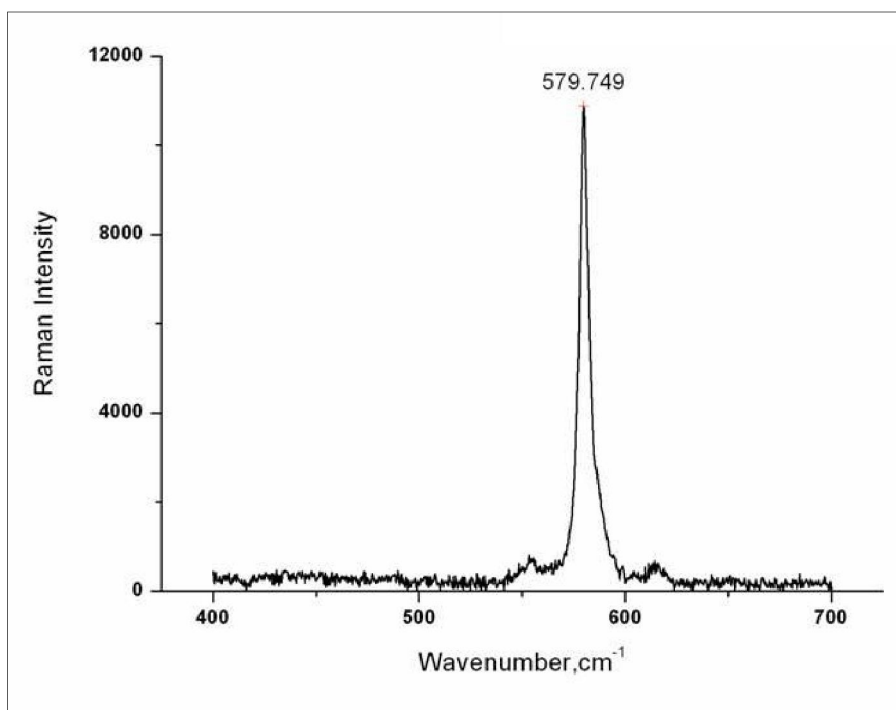


**Figure 56** SERS spectrum of  $10^{-5}$  M BCB acquired by using Au modified cobalt-silica colloid as a substrate.

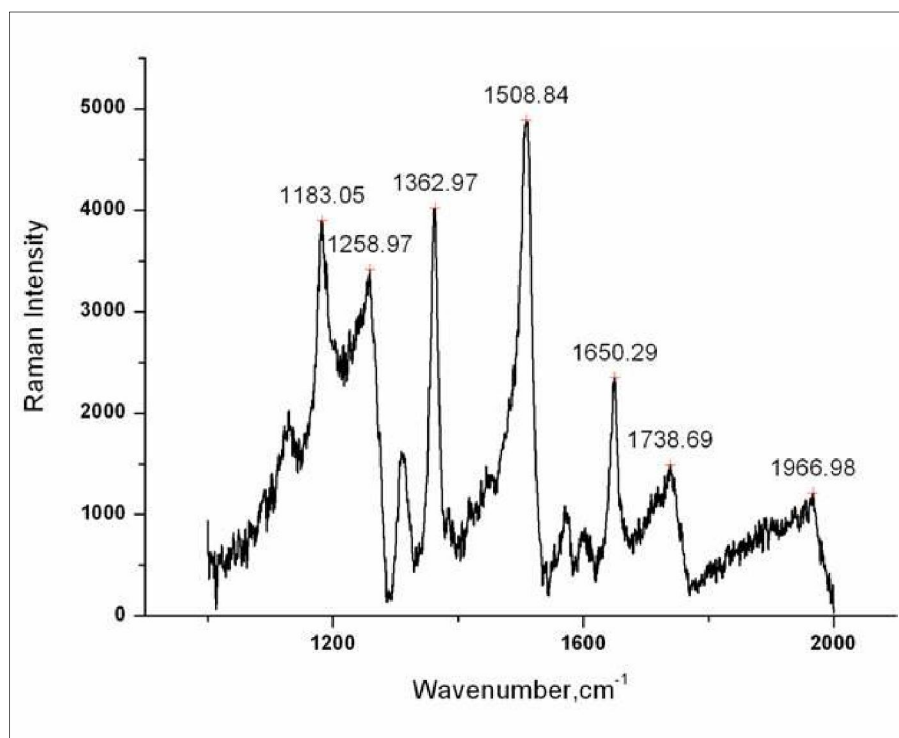


**Figure 57** SERS spectrum of  $10^{-4}$  M R6G acquired by using Au modified cobalt-silica colloid as a substrate.

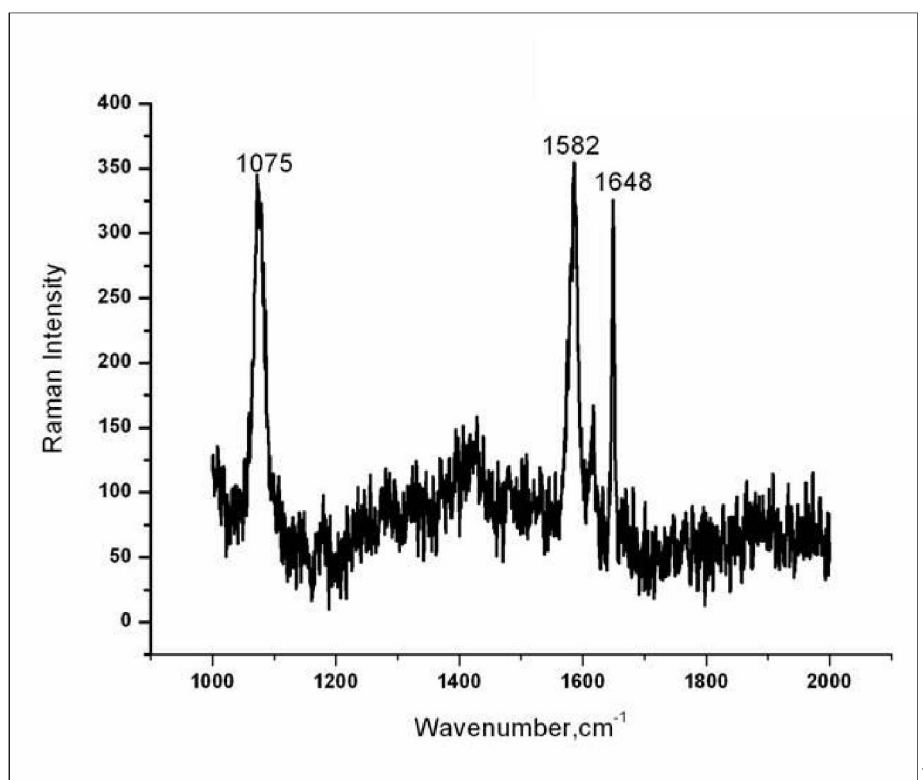


**Figure 58** SERS spectrum of  $10^{-4}$ M 4-MBA acquired by using Au modified cobalt-silica colloid as a substrate.

As can be seen from Figure 56, Figure 57, and Figure 58 intense SERS spectra were obtained for BCB, R6G and 4-MBA utilizing Au modified cobalt-silica colloids as substrate. It means that Au nanoparticles on the surface of core-shell particles provide adequate surface plasmon required for the enhancement of the Raman signal.

### **3.3.2 The Performance of the Gold Modified Cobalt-Silica Nanoparticles both as a Magnetic Separator and SERS Substrate for the Preconcentration and the Detection of 4-MBA**

Generally, magnetic separation is a process in which magnetically susceptible material is extracted from a mixture using an external magnetic field. In case of nanotechnology, magnetic separation is performed by magnetic nanoparticles in

biological or chemical solutions or suspensions. The separation method is easy, quick and efficient (Liu, 2006).

The processes of isolation and separation of specific molecules are used in almost all areas of biosciences and biotechnology. The separation process consists of two main steps: a) immobilization of a molecule on magnetic nanoparticles and b) the separation out of these immobilized entities via external magnetic field (Pankhurst, Connolly, Jones, & Dobson, 2003; Liu, 2006). In Figure 59, a schematic procedure for the magnetic separation/ purification of analyte is presented. To collect the target molecule it is sufficient to apply magnet near the reaction media and separate the sample molecules.

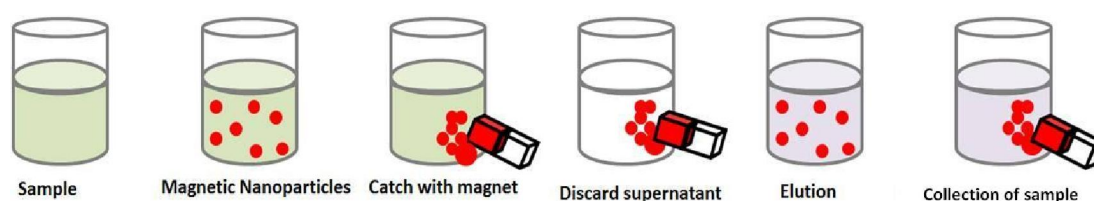


**Figure 59** Illustration of magnetic separation procedure for biological molecules (Pankhurst, Connolly, Jones, & Dobson, 2003).

Gold and thiol groups are selectively and easily recognize each other. Therefore 4-MBA which contains thiol group in its structure was selected for magnetic separation and SERS measurement studies. Taking advantage of their magnetic properties, Au modified cobalt-silica nanocomposites were used for the preconcentration of 4-MBA from its dilute aqueous solution ( $10^{-5}$  M). The particles were shaken in the presence of  $10^{-5}$  M 4-MBA for one hour. After that, by-external magnetic field particles were collected and supernatant was removed. Following the magnetic separation of the particles from the solution, 15  $\mu$ l amount was placed on the microscope glass and its SERS spectrum was acquired directly. The SERS spectra of 4-MBA on the surface of Au modified cobalt-silica nanoparticles with and without preconcentration is shown in Figure 60.

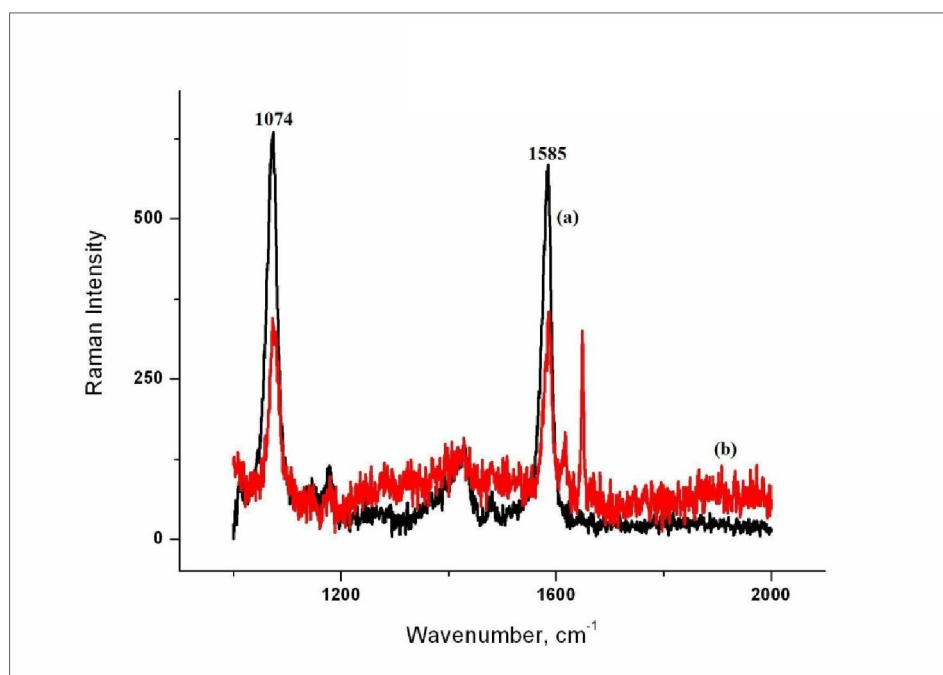


**Figure 60** SERS spectrum of (a)  $10^{-5}$ M 4-MBA 1-hour incubated with gold modified cobalt-silica and magnetically collected by an external magnet and (b)  $10^{-4}$ M 4-MBA on Au modified cobalt-silica.

As can be understood from the Figure 60, the enhancement on SERS signal is increased by applying magnetic separation due to preconcentration. Signal of  $10^{-4}$  M 4-MBA on gold modified cobalt-silica nanocomposites was hardly detected while the signal of  $10^{-5}$ M 4-MBA applied to magnetic separation and preconcentration process was detected easily. Therefore, there is an increase in sensitivity. As can be seen in the Figure 60, signal/noise(S/N) ratio of preconcentrated 4-MBA increases about 4 times whereas peak height increases 2 times. Regarding the concentration, S/N and peak height, overall enhancement factor can be estimated as 80 times.

## CHAPTER 4

### CONCLUSION

Main purpose of this study is to develop multimodality nanoparticles which are both magnetic and optically active. Hence magnetic cobalt particles decorated with gold nanoparticles were prepared and used both as a magnetic separator and SERS substrate for the preconcentration and the SERS detection of 4-MBA. To the best of our knowledge this is the first time that gold decorated cobalt-silica core-shell nanoparticles were prepared and used as a SERS substrate.

Cobalt nanoparticles were prepared by hydride reduction method under inert atmosphere in the presence of capping agent. The particles were characterized by FE-SEM and EDX. The size of the particles was arranged in the ranges of 7-90 nm by changing capping agent concentration.

Since magnetic cobalt particles are air-sensitive, a silica shell was applied onto the cobalt core to protect it from oxidation. Silica coating was based on sol-gel formation on the nanoparticles surface by addition of TEOS in ethanolic solution of the colloid. By the addition of APTS to the aged sol-gel medium, an outer layer which was rich in amine groups was created on the nanoparticle surface. Shell thickness changing from 20-30 nm to 400-500 nm was achieved by monitoring the amount of TEOS used.

Through the amine groups on the silica surface, gold nanoparticle, synthesized by citrate reduction, were attached on the core-shell structure. The size of the gold nanoparticles were in the range of 10-15 nm. For a proper gold loading on the

surface, both the amount of gold nanoparticles and the duration of interaction between cobalt- silica and gold nanoparticles were optimized.

Gold nanoparticles, due to their surface Plasmon electrons, are well known substrate for surface enhanced Raman scattering technique. Because of this special feature, gold decorated cobalt-silica nanoparticles were used as SERS substrate for the detection of BCB, R6G and 4-mercapto benzoic acid.

For magnetic separation, thiol groups containing 4-mercaptobenzoic acid were used, because of high reactivity of gold nanoparticles towards sulfur groups. The particles were shaken in the presence of  $10^{-5}$  M 4-MBA for one hour. After that, by-external magnetic field particles were collected and supernatant was removed. The collected particles were analyzed with Raman microscope. The signal of  $10^{-5}$ M 4-MBA applied to magnetic separation and preconcentration process was more easily detected than the signal of  $10^{-4}$  M 4-MBA on gold modified cobalt-silica nanocomposites. Overall enhancement factor can be estimated as 80 times for preconcentrated  $10^{-5}$  M 4-MBA with respect ot  $10^{-4}$  M 4-MBA.

To conclude, the synthesized three-layer particles were both magnetic and optically active. Therefore, this makes them attractive for magnetic separation and identification of biologically important molecules.

## REFERENCES

- Wikimedia Foundation, Inc., . (2010, Temmuz 27 ). *Wikipedia, Free Encyclopedia*. ( Wikimedia Foundation, Inc., ) Retrieved Ağustos 11, 2010, from Vibrating sample magnetometer: [http://en.wikipedia.org/wiki/Vibrating\\_sample\\_magnetometer](http://en.wikipedia.org/wiki/Vibrating_sample_magnetometer)
- An-Hui Lu, W. S. (2004). Nanoengineering of a Magnetically Separable Hydrogenation Catalyst. *Angew. Chem. Int. Ed* , 43 (33).
- Baena, J., & Lendl, B. (2004). Raman spectroscopy in chemical bioanalysis. *Curr Opin Chem Biol* , 8, 534-539.
- Bisht, S., Feldmann, G., Soni, S., Ravi, R., Karikar, C., Maitra, A., et al. (2007). Polymeric nanoparticle-encapsulated curcumin ("nanocurcumin"):a novel strategy for human cancer therapy. *Journal of Nanobiotechnology* , 5 (3).
- Britannica, I. E. ( 2010, Ağustos 12). *Encyclopædia Britannica Online*. Retrieved Ağustos 12, 2010, from Antiferromagnetism: <http://www.britannica.com/EBchecked/topic/27970/antiferromagnetism>
- Chaudret, B. (2003). Chemical Synthesis of Magnetic Metal Nanoparticles. *Magnétisme des systèmes nanoscopiques et structures hybrides*. Brasov: Ecole Franco-Roumaine.
- Chen, J., Sorensen, C., Klabunde, K., & Hadjipanayis, G. (1995). Enhanced magnetization of nanoscale colloidal cobalt particles. *Physical Review B* , 51 (17).
- Cotton, T., Kim, J., & Chumanov, G. (1991). Application of Surface-Enhanced Raman Spectroscopy to Biological Systems. *Journal of Raman Spectroscopy* , 22, 729-742.
- Ditsch, A., Laibinis, P., Wang, D., & Hatton, T. A. (2005). Controlled Clustering and Enhanced Stability of Polymer-Coated Magnetic Nanoparticles. *Langmuir* , 21 (13).
- Drexler, K. E., & Peterson, C. (1989). *Nanotechnology and Enabling Technologies* . (The Foresight Institute.) Retrieved Ağustos 10, 2010, from The foresight institue.org: <http://www.foresight.org/updates/Briefing2.html>

Edelstein, A., & Cammarata, R. (1996). *Nanomaterials: synthesis, properties, and applications*. USA: Taylor & Francis Group.

Faraji, M., Yamini, Y., & Rezaee, M. (2010). Magnetic Nanoparticles: Synthesis, Stabilization, Functionalization, Characterization, and Applications. *J. Iran. Chem. Soc.*, 7 (1).

Ferraro, J., Nakamoto, K., & Brown, C. (2003). *Introductory Raman Spectroscopy*.

Fleischmann, M., Hendra, P., & McQuillan, A. (1974). Raman spectra of pyridine adsorbed at a silver electrode. *Chemical Physics Letters*, 26 (2), 163-166.

Fu, H.-B., & Yao, J.-N. (2001). Size Effects on the Optical Properties of Organic Nanoparticles. *J. Am. Chem. Soc.*, 123 (7), 1434-1439.

*Geochemical Instrumentation and Analysis*. (2010, Haziran 15). (Science education Resource Center at Carleton College) Retrieved Temmuz 29, 2010, from Energy-Dispersive X-Ray Spectroscopy (EDX): [http://serc.carleton.edu/research\\_education/geochemsheets/eds.html](http://serc.carleton.edu/research_education/geochemsheets/eds.html)

Gubin, S. P., Yu Koksharov, Y. A., Khomutov, G., & Yu Yurkov, G. (2005). Magnetic nanoparticles: preparation, structure and properties. *Russian Chemical Reviews*, 74 (6).

Gupta, J., & Gupta, M. (200). Synthesis and surface engineering of iron oxide nanoparticles for biomedical applications. *Biomaterials* (26), 3995–4021.

*Handbook of Analytical Methods for Materials*. (2009). (Materials Evaluation and Engineering, Inc.) Retrieved Temmuz 29, 2010, from Materials Evaluation and Engineering, Inc: <http://mee-inc.com/eds.html>

Harris, P. J. (1999). Carbon nanotubes and related nanostructures. In P. J. Harris, *Carbon nanotubes and related nanostructures*. Cambridge: Cambridge university press.

Hernando, A., Crespo, P., & García, M. (2005). Metallic Magnetic Nanoparticles. *TheScientificWorldJOURNAL* (5), 972–1001.

*Horiba Scientific*. (2010). (HORIBA, Ltd.) Retrieved Ağustos 4, 2010, from Raman spectroscopy: <http://www.horiba.com/scientific/products/raman-spectroscopy/tutorial-faqs/raman-tutorial/raman-spectroscopy/>

Hyeon, T. (2003). Chemical synthesis of magnetic nanoparticles. *Chem. Commun.*, 927 - 934.

Jana, N., Gearheart, L., & Murphy, C. (2001). Wet Chemical Synthesis of High Aspect Ratio Cylindrical Gold Nanorods. *J. Phys. Chem. B*, 105 (19).

Jiles, D. (1998). *Introduction to magnetism and magnetic materials*. USA: Taylor & Francis Group.

Jun, Y. W., Huh, Y. M., Choi, J. S., Lee, J. H., Song, H. T., Kim, S., et al. (2005). Nanoscale Size Effect of Magnetic Nanocrystals and Their Utilization for Cancer Diagnosis via Magnetic Resonance Imaging. *J. Am. Chem. Soc*, 127 (16).

Kim, D. K., Zhanga, Y., Voith, W., Raob, K. V., & Muhammed, M. (2001). Synthesis and characterization of surfactant-coated superparamagnetic monodispersed iron oxide nanoparticles. *Journal of Magnetism and Magnetic Materials*, 225 (1-2), 30-36.

Kima, E., Lee, H., Kwakb, B., & Kim, B. (2005). Synthesis of ferrofluid with magnetic nanoparticles by sonochemical method for MRI contrast agent. *Journal of Magnetism and Magnetic Materials*, 289, 328-330.

Klabunde, K. (2001). *Nanoscale materials in chemistry*. Canada: John Wiley & Sons Inc.

Kobayashi, Y., Horie, M., Konno, M., Rodri'guez-Gonza'lez, B., & Liz-Marza'n, L. (2003). Preparation and Properties of Silica-Coated Cobalt Nanoparticles. *J. Phys. Chem. B*, 107, 7420-7425.

Koch, C. (2007). *Nanostructured materials; Processings, properties and applications*. USA: Wiliiam Andrew Inc.

Kouassi, G. K., & Irudayaraj, J. (2006). Magnetic and Gold-Coated Magnetic Nanoparticles as a DNA Sensor. *Analytical chemistry*, 78 (10), 3234–3241.

Lam, C., Zhang, Y. F., Tang, Y. H., Lee, C. S., Bello, I., & Lee, S. T. (2000). Large-scale synthesis of ultrafine Si nanoparticles by ball milling. *Journal of Crystal Growth*, 220 (4), 466-470.

Laurent, S., Forge, D., Port, M., Roch, A., Robic, C., Elst, L., et al. (2008). Magnetic Iron Oxide Nanoparticles: Synthesis, Stabilization, Vectorization, Physicochemical Characterizations, and Biological Applications. *Chemical Reviews*, 108 (6), 2064–2110.

Lee, W.-J., & Fang, T.-T. (1995). The effect of the molar ratio of cations and citric acid on the synthesis of barium ferrite using a citrate process. *Journal of Materials Science*, 30 (17), 4349-4354.

Li, Z., Wei, L., Gao, M., & Lei, H. (2005). One-Pot Reaction to Synthesize Biocompatible Magnetite Nanoparticles. *Advanced Materials* , 17 (8), 1001-1005.

Liu, W.-T. (2006). Nanoparticles and Their Biological and Environmental Applications. *Journal of Bioscience and Bioengineering* , 102 (1), 1-7.

Lu, Y., Yin, Y., Mayers, B. T., & Xia, Y. (2002). Modifying the surface properties of superparamagnetic iron oxide nanoparticles through a sol-gel approach. *Nano Lett.* , 2, 183-186.

Ma, M., Zhang, Y., Yu, W., Shen, H., Zhang, H., & Gu, N. (2003). Preparation and characterization of magnetite nanoparticles coated by amino silane. *Colloids and Surfaces A: Physicochemical and Engineering Aspects* , 212 (2-3), 219-226.

Ma, Z., & Liu, H. (2007). Synthesis and surface modification of magnetic particles for application in biotechnology and biomedicine. *China Particuology* , 5 (1-2), 1-10.

Majetich, S. A., Artman, J. O., McHenry, M. E., Nuhfer, N. T., & Staley, S. W. (1993). Preparation and properties of carbon-coated magnetic nanocrystallites. *Phys. Rev. B* 48 , 48 (22), 16845-16848.

Michota, A., & Bukowska, J. (2003). Surface-enhanced Raman scattering (SERS) of 4-mercaptobenzoic acid on silver and gold substrates. *Journal of Raman Spectroscopy* , 34, 21-25.

Nagarajan, R. a. (2008). *Nanoparticles: Building Blocks for Nanotechnology*. Washington, DC: ACS Symposium Series; American Chemical Society.

*Nanoparticles and their Applications*. (2007). (Present Hawk's Perch Technical Writing, LLC ) Retrieved August 9, 2010, from understandingnano.com: <http://www.understandingnano.com/nanoparticles.html>

Nave, R. (2010). *Georgia state university*. (Department of Physics and Astronomy Georgia State University) Retrieved temmuz 27, 2010, from Hyperphysics: <http://hyperphysics.phy-astr.gsu.edu/hbase/solids/hyst.html>

*NDT Resource center*. (2001-2010). (Iowa State University) Retrieved August 11, 2010, from The Hysteresis Loop and Magnetic Properties : <http://www.ndt-ed.org/EducationResources/CommunityCollege/MagParticle/Physics/HysteresisLoop.htm>

Oldenburg, S. J., Westcott, S. L., Averitt, R. D., & Halas, N. J. (1998). Nanoengineering of optical resonances. *Chemical Physics Letters* , 288 (2-4), 243-247.

Ozin, G. A., & Arsenault, A. C. (2009). *Nanochemistry; A Chemical Approach to Nanomaterials*. RCS Publishing.

Pankhurst, Q., Connolly, J., Jones, S., & Dobson, J. (2003). Applications of magnetic nanoparticles in biomedicine. *Journal of Physics D: Applied Physics* , 36, R167–R181.

Petry, R., Schmitt, M., & Popp, J. (2003). Raman Spectroscopy—A Prospective Tool in the Life Sciences. *CHEMPHYSCHEM* , 4, 14-30.

Pickett, N., & O'Brien, P. (2001). Syntheses of Semiconductor Nanoparticles Using Single-Molecular Precursors. *The Chemical Record* , 1 (6), 467–479.

Princeton Instruments. (2010). *Princeton Instruments*. Retrieved from Raman Spectroscopy Basics: [http://content.piacton.com/Uploads/Princeton/Documents/Library/UpdatedLibrary/Raman\\_Spectroscopy\\_Basics.pdf](http://content.piacton.com/Uploads/Princeton/Documents/Library/UpdatedLibrary/Raman_Spectroscopy_Basics.pdf)

Rack, P. D. (2010). *Philip D. Rack*. Retrieved Temmuz 29, 2010, from MSE 300 - Materials Laboratory Procedures: <http://web.utk.edu/~prack/MSE%20300/SEM.pdf>

Rozhkova, E., Ulasov, I., Lai, B., Dimitrijevic, N., Lesniak, M., & Rajh, T. (2009). A High-Performance Nanobio Photocatalyst for Targeted Brain Cancer Therapy. *Nano letters* , 9 (9), 3337–3342.

Safarik, I., & Safarikova, M. (2009). Magnetic nano- and microparticles in biotechnology. *Chemical Papers* , 63 (5), 497–505.

Salgueirino-Maceira, V., Correa-Duarte, M., Farle, M., López-Quintela, M., Sieradzki, K., & Diaz, R. (2006). Synthesis and Characterization of Large Colloidal Cobalt Particles. *Langmuir* , 22 (4), 1455-1458.

Salgueirino-Maceira, V., & Correa-Duarte, M. (2006). Cobalt and silica based core-shell structured nanospheres. *Journal of Materials Chemistry* , 16, 3593–3597.

*Science Encyclopedia*. (2010). Retrieved Temmuz 13, 2010, from Magnetism - History Of Magnetism, Origin Of Magnetism, Types Of Magnetism, Measurement Of Magnetic Field, Applications Of Magnetism: <http://science.jrank.org/pages/4087/Magnetism.html>

Sergeev, G. (2006). Synthesis and Stabilization of Nanoparticles. In G. B. Sergeev, *Nanochemistry*. UK: Elsevier B.V.

Skoog, D., Holler, F., & Nieman, T. (1998). *Principles of Instrumental Analysis*. USA: Harcourt Brace & Company.

Son, S., Reichel, J., He, B., Schuchman, M., & Lee, S. (2005). Magnetic Nanotubes for Magnetic-Field-Assisted Bioseparation, Biointeraction, and Drug Delivery. *J. Am. Chem. Soc.* , 17 (20), 7316–7317.

Spencer, R. (1997, Nisan 8). *Paramagnetism*. (maxwell.byu.edu) Retrieved Ağustos 9, 2010, from maxwell.byu.edu: <http://maxwell.byu.edu/~spencerr/websumm122/node79.html>

*Splung.com*. (2010). Retrieved Eylül 20, 2010, from Magnetism: <http://www.splung.com/content/sid/3/page/magnetism>

Stiles, P., Dieringer, J., Shah, N., & Van Duyne, R. (2008). Surface-Enhanced Raman Spectroscopy. *Annual Review of Analytical Chemistry* , 1, 601–626.

Stöber, W., Fink, A., & Bohn, E. (1968). Controlled growth of monodisperse silica spheres in the micron size range. *J. Colloid Interface Sci.* , 26 (1), 62-69.

Sue, K., Suzuki, M., Arai, K., Ohashi, T., Ura, H., Matsui, K., et al. (2006). Size-controlled synthesis of metal oxide nanoparticles with a flow-through supercritical water method. *Green Chem.* , 8 (7), 634–638.

Tartaj, P., Morales, M., Gonzalez-Carreno, T., Veintemillas-Verdaguer, S., & Serna, C. (2005). Advances in magnetic nanoparticles for biotechnology applications. *Journal of Magnetism and Magnetic Materials* , 290-291 (1), 28–34.

*The University of Texas at Austin*. (2008). Retrieved Eylül 20, 2010, from Texas Advanced Computing Center: <http://www.tacc.utexas.edu/research/users/features/nano.php>

*Venkata Raman - Biography*. (2010, ağustos 4). Retrieved Ağustos 4, 2010, from Nobelprize.org: [http://nobelprize.org/nobel\\_prizes/physics/laureates/1930/raman-bio.html](http://nobelprize.org/nobel_prizes/physics/laureates/1930/raman-bio.html)

Vo-Dinh, T. (1998). Surface-enhanced Raman spectroscopy using metallic nanostructures. *Trends in Analytical Chemistry* , 17 ( 8-9), 557-582.

Vollath, D. (2008). *Nanomaterials: an introduction to synthesis, properties and application* . Germany: Strauss GmbH Mörlenbach.

Wartewig, S., & Neubert, R. (2005). Pharmaceutical applications of Mid-IR and Raman spectroscopy. *Adv Drug Deliv Rev* , 57 (8), 1144-1170.

Willard, M., Kurihara, L., Carpenter, E., Calvin, S., & Harris, V. (2004). Chemically prepared magnetic nanoparticles. *International Materials Reviews* , 49 (3-4), 125-170.

Wu, W., He, Q., & Jiang, C. (2008). Magnetic Iron Oxide Nanoparticles: Synthesis and Surface Functionalization Strategies. *Nanoscale Research Letter* , 3 (11), 397–415.

Yeo, B., Schmid, T., Zhang, W., & Zenobi, R. (2007). Towards rapid nanoscale chemical analysis using tip-enhanced Raman spectroscopy with Ag-coated dielectric tips. *Anal Bioanal Chem* , 387 (8), 2655–2662.

Yoshida, T. (1996). Vapour phase deposition of cubic boron nitride. *Diamond and Related Materials* , 5 (3-5), 501-507.

Zhai, Y., Zhai, J., Wang, Y., Guo, S., Ren, W., & Dong, S. (2009). Fabrication of Iron Oxide Core/Gold Shell Submicrometer Spheres with Nanoscale Surface. *J. Phys. Chem. C* , 113 (17), 7009-7014.

Zhou, Q., Chao, Y., Li, Y., Xu, W., Wu, Y., & Zheng, J. (2007). Contribution of Charge-Transfer Mechanisms to Surface-Enhanced Raman Scattering with Near-IR Excitation. *ChemPhysChem* , 8 (6), 921 – 925.